Technische Universität München
Lehrstuhl für Technische Chemie II

Sulfur and Nitrogen Sensitivity of Supported Pt-Hydrogenation Catalysts

Maria Florencia Williams

Vollständiger Abdruck der von der Fakultät für Chemie der Technischen Universität München zur Erlangung des akademischen Grades eines

Doktors der Naturwissenschaften

genehmigten Dissertation.

Vorsitzender: Univ.-Prof. Dr. Klaus Köhler

Prüfer der Dissertation:

1. Univ.-Prof. Dr. Johannes A. Lercher
2. Univ.-Prof. Dr. Kai-Olaf Hinrichsen

Die Dissertation wurde am 02.06.05 bei der Technischen Universität München eingereicht und durch die Fakultät für Chemie am 15.06.05 angenommen.

Acknowledgements

First of all I would like to thank Johannes Lercher for giving me the opportunity to work in his group. Thank you for your guidance and support during my Ph.D. I greatly enjoyed the scientific freedom you granted me, still watching carefully the steps leading to the final success. I was always enlightened to hear your point of view, be it on the deeper insights of chemistry, be it on the more technical side of the work, be it on matters not related to any of the above.

I am grateful for the financial support provided by Shell Chemicals. I am very much indebt with Rob van Veen and Wim Stork who cooperated in this project. Thanks Rob for your fruitful discussions and for your always very good mood. From the Shell team I would also like to thank Arend-Jar for his advice concerning the hydrogenation set-up and also for introducing me to the synthesis of the catalysts used in this work.

Thanks Andy for the help and discussion with the XAFS data, Marianne for introducing me in the use of the electron-microscope and Jeroen for the interesting NMR discussions

Thanks Xaver, Martin and Andreas for your help with measurements and troubleshooting

Thanks to all the TC2 people, it was really nice working with all of you. Thanks for being so cool and friendly. I am very glad that I had the chance to meet you, this was a wonderful experience and I will never forget you!

Last but not least, I would like to thank my family and my friends outside TC2

Chapter 1
General introduction

Chapter 2
Characterization of ASA-supported platinum catalysts by ^{27}Al (3Q) MAS NMR, ^{1}H MAS NMR, FTIR, TPD, TEM, and EXAFS

Chapter 3
Metal-support interaction: influence of the support on the catalytic activity of platinum for deep hydrotreating

Chapter 4
Mechanistic aspects of tetralin hydrogenation in the presence of poisons

Chapter 5
Summary

Chapter 1

Introduction

This chapter introduces to the importance of Diesel fuel, presents catalytic routes to high quality Diesel and highlights the motivation for the research conducted. Finally, the milestones of the work presented in the subsequent chapters are highlighted.

1 Motivation

1.1 Economic significance of diesel fuel

Diesel and jet fuel are the fastest growing segments of the refined products market. Passenger cars powered by diesel engines are becoming increasingly more common in Europe and Japan (10 - 25 %), whereas in North America the percentage of diesel-fuel passenger cars is about 1 - 2 %, with a slightly decreasing tendency. Global Diesel demand is likely to continue to grow at around 3 % per year while demand for certain other refined products is likely to flatten and even decline [1] (Figure 1).

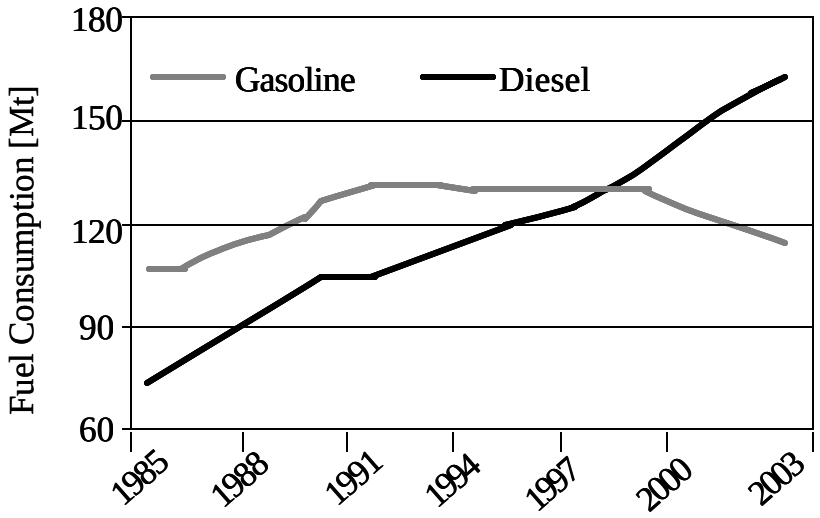

Figure 1. Consumption of road transport fuel in Europe (i.e. E.U. + Switzerland + Norway + Turkey + Iceland).

Based on its 2001 forecasts, the European Commission expects road transport fuel consumption to reach 325 Mt by 2020.

1.2 Emissions from diesel engines

Typically, Diesel fuel is a complex mixture of alkanes (C9 to C30 of normal, branched, and cyclic ones, 60 to 90 vol. %); aromatics (e.g., alkylbenzenes; 5 to 40 vol. %), and small amounts of alkenes (0 to 10 vol. %) [2]. When hydrocarbon fuel is burned with the correct amount of air in a diesel engine, the gases that are left are predominately water vapor, carbon dioxide and nitrogen – all of which are benign, although carbon dioxide is a greenhouse gas. However deviations from this ideal combustion lead to the production of some volatile organic compounds (VOCs), CO, NOx, SO_2, and particulate matter

(PM). Diesel engines are substantial emitters of PM and NOx, but since diesel engines are designed to run lean, i.e., with excess of oxygen, they do not emit much CO or unburned hydrocarbons. And because diesel fuel has a much higher boiling range than gasoline (and consequently a much lower volatility), evaporative VOC emissions are not a problem. PM emissions are mainly the result of the heterogeneous nature of diesel combustion. These high temperature cracking reactions (pyrolysis) lead to the formation of carbonaceous soot particles. Unburned or partially burned fuel can condense on these particles, increasing their size and mass. Finally, these particles can stick together (agglomerate) to create visible smoke. Diesel exhaust NOx and PM are linked by the nature of diesel combustion. Efforts to reduce PM by increasing combustion efficiency lead to higher combustion temperatures and, thus, higher NOx emissions. Lowering NOx formation by lowering combustion temperature leads to less complete combustion and, thus, higher PM emissions. One of the most important fuel parameters in this regard is cetane number. Increasing the cetane number improves fuel combustion and tends to reduce NOx and PM emissions (Figure 2). NOx seems to be reduced in all engines, while PM10 (particle size less than or equal to 10 microns) reductions are more engine-dependent. These cetane number effects also tend to be non-linear in the sense that increasing the cetane number does the most good when starting with a relatively low cetane number fuel. Reducing the aromatics content of diesel fuel reduces NOx and PM10 in some engines. Recent studies indicate that polynucleararomatics content is the key to the reduction of PM (the concentration of single-ring aromatics is not important). Thus, one way to improve the fuel's cetane number parameters is to reduce the content of aromatics in the fuel (Figure 3).

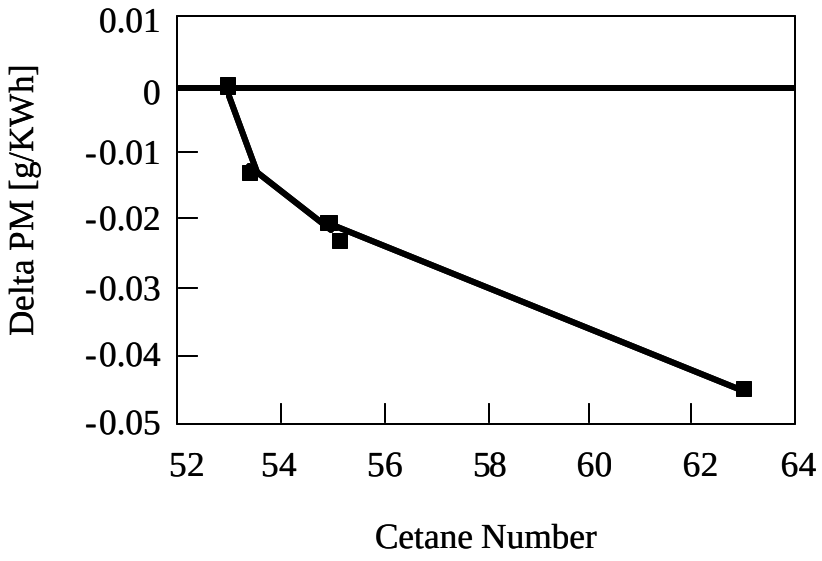

Figure 2. Cetane number reduces particulate matter (without sulfates).

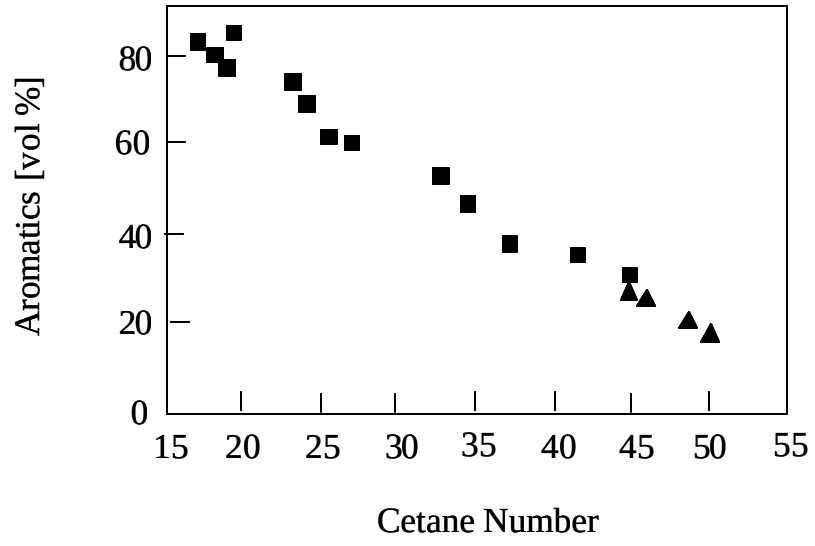

Figure 3. Cetane number vs. aromatic content: (¦) LCO and SR distillate; (?) Diesel fuel.

1.3 Environmental legislation on diesel fuel

Environmental specifications aim on reduction of pollutant emissions from motor emission. The European Union Directive 98/70 [3] as amended by Directive 2003/17/EC [4] contains the environmental fuel quality specifications for petrol and diesel fuels in the community with the main focus on sulfur and for petrol on lead in aromatics. There are

three distinct specifications. The first entered into effect on 1st January 2000. The second entered into force on 1st January 2005 and sets limits for the sulfur content of petrol and diesel (50 ppm) and the aromatics content of petrol (35 % by volume). The third (as amended by Directive 2003/17/EC), starting from 1st January 2005 as well, requires to phase in diesel and petrol with a sulfur content of 10 ppm. Member States may also impose more stringent standards on fuels marketed on their territory in order to protect the environment or public health. High aromatic content in diesel fuel lowers fuel quality and contributes significantly to the formation of undesired emissions in exhaust gases. Because of health hazards associated with these emissions, environmental regulations governing the composition of diesel fuels are tightening in Europe and the U.S. There is, however a large span in the stipulated maximum level of aromatics being in Sweden and California [5] more strict than in the rest of Europe and US, respectively.

Table 1. Diesel fuel specifications in Europe.

Parameter	1996	2000	2005	2005 - 2010
Sulfur Content [ppm]	500	350	50	10 – 30
Polyaromatics [%]	-	11	2 – 11	1 – 2
Density [$kg \cdot m^{-3}$]	860	845	845 – 820	< 840
Cetane No.	49	51	51 – 58	53 - 55

2 Catalytic hydrotreating

Hydrotreating (or hydroprocessing) refers to a variety of hydrogenation processes which lead to saturation of aromatics, olefins, etc. and to removal of sulfur- (i.e., hydrodesulfurization or HDS), nitrogen- (hydrodenitrogenation or HDN), oxygen- (hydrodeoxygenation or HDO) compounds and metals (hydrodemetallization or HDM) from different petroleum streams in a refinery. The main aim of hydrotreating is to diminish air pollution emissions, to avoid poisoning of noble metals and acid catalysts used in catalytic reforming and cracking and to improve the fuel quality [6].

2.1 Saturation of aromatic hydrocarbons

Hydrogenation of aromatic hydrocarbons are reversible, with equilibrium conversions of hydrocarbons often being less than 100% under practical processing conditions. These reactions are exothermic; the extent of reaction at equilibrium decreases with increasing temperature. Thus increasing the temperature to give higher rates of other reactions results in lower equilibrium conversions in aromatic hydrogenations and-because the hydrogenations are often fast enough to be nearly equilibrated-lower actual conversions as well. In practice, the lower equilibrium conversions are especially significant at lower pressures.

Quantitative reaction networks have been reported for naphthalene hydrogenation. The hydrogenation is sequential, with the rate of tetralin hydrogenation being an order of magnitude less than that of naphthalene hydrogenation. Tetralin is a typical molecule targeted in deep hydrotreating (DHT). Under high hydrogen pressures and low temperatures, the formation of the hydrogenated products (i.e., *cis*- and *trans*-decalins) is thermodynamically strongly favorable [7]. The hydrogenation of C=C double bonds on metals should be intrinsically *cis* in character [8]; however, the formation of *trans*-decalin is always observable [9].

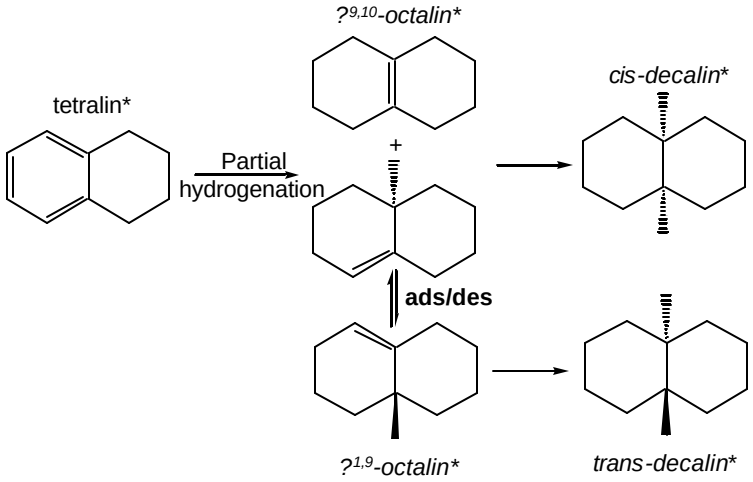

Figure 4. Step-hydrogenation of an adsorbed tetralin molecule to *cis*- and *trans*-decalin.

2.2 Hydrodesulfurization (HDS)

The HDS of organosulfur compounds is exothermic and essentially irreversible under the reaction conditions employed industrially. Sulfur removal occurs either with or without hydrogenation of the heterocyclic ring. The pathways involving prior hydrogenation of the ring can be affected by thermodynamics because hydrogenation of the sulfur-containing rings of organosulfur compounds is equilibrium-limited at practical HDS temperatures. Thus, sulfur-removal pathways via hydrogenated organosulfur intermediates may be inhibited at low pressures and high temperatures because of the low equilibrium concentrations of the latter species.

HDS rates are functions of several variables including concentrations of organic reactants and products, hydrogen, and hydrogen sulfide. Comparison of reactivities should thus be made when inhibition by other organic compounds is weak and when concentrations of hydrogen and hydrogen sulfide are similar to those used commercially. Dibenzothiophene (DBT) is one of the compounds most representative of the unreactive organosulfur compounds in higher boiling fractions of fossil fuels.

Houalla et al. [10] proposed a detailed network for dibenzothiophene HDS (Figure 5).

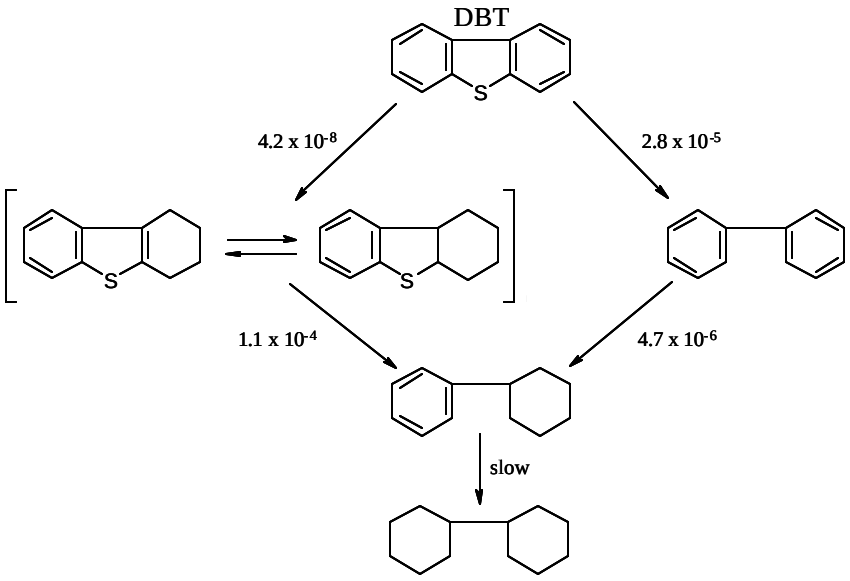

Figure 5. Reaction network for dibenzothiophene with pseudo-first-order rate constants in L/(g of cata1yst s) at 573 K.

Dibenzothiophene conversion proceeds selectively via the path of least hydrogen consumption and hydrogenation of biphenyl and cyclohexylbenzene is comparatively slow. The selectivity to the hydrogenated dibenzothiophenes is higher when the hydrogen sulfide concentration is higher. The latter selectivity also depends on the catalyst composition. Both, hydrogenation and hydrogenolysis of DBT, take place on separate kinds of catalytic sites [11].

2.3 Hydrodenitrogenation (HDN)

The increasing interest in converting petroleum residum, coal, and shale to liquid fuels has spurred research in the chemistry of HDN. Nitrogen in these feedstocks is present predominantly in heterocyclic aromatic compounds. Nonheterocyclic organonitrogen compounds such as aliphatic amines and nitriles are also present, but in considerably smaller amounts, and they are denitrogenated much more rapidly than the heterocyclic compounds. Consequently, nonheterocyclic organonitrogen compounds are less important for purposes of elucidating the nitrogen-removal chemistry occurring in the hydroprocessing of heavy feeds. The nitrogen heterocyclic compounds in these feeds are classed as basic and nonbasic. In the latter (e.g., indole and carbazole), the lone-pair electrons on the nitrogen atom are delocalized around the aromatic ring and are unavailable for donation to a Lewis acid. The opposite is true for basic heterocyclic compounds such as quinoline and acridine.

Nitrogen removal from heterocyclic organonitrogen compounds requires hydrogenation of the ring containing the nitrogen atom before hydrogenolysis of the carbon-nitrogen bond occurs. Hydrogenation of the heteroring is required to reduce the relatively large energy of the carbon-nitrogen bonds in such rings and thus permit more facile carbon-nitrogen bond scission. The energies of carbon-nitrogen double bonds and single bonds are 147 and 73 kcal/mol, respectively. If the carbon-nitrogen bond energy in a typical heterocyclic compound is close to that of a carbon-nitrogen double bond, a reaction breaking the carbon-nitrogen bond is expected to have a high activation energy.

The requirement that ring hydrogenation occur before nitrogen removal also implies that the position of the equilibrium of the hydrogenation reactions can affect nitrogen-removal rates if the rates of the hydrogenolysis reactions are significantly lower than the rates of

hydrogenation. An unfavorable hydrogenation equilibrium would result in low concentrations of hydrogenated nitrogen compounds undergoing hydrogenolysis; HDN rates, at least at low surface coverages of organonitrogen compounds, could thus be lowered. High hydrogen partial pressures can be used to increase the equilibrium concentrations of saturated heteroring compounds to obtain larger HDN rates.

Because nitrogen heterocyclic compounds must first be hydrogenated before the nitrogen is removed, there are numerous intermediate products that contain nitrogen. Therefore, the conversion of a nitrogen- containing compound must be distinguished from its HDN conversion (i.e., that giving hydrocarbon products and ammonia).

The complex reaction network of quinoline is representative of those of higher molecular weight organonitrogen compounds found in heavier hydroprocessing feeds (Figure 6).

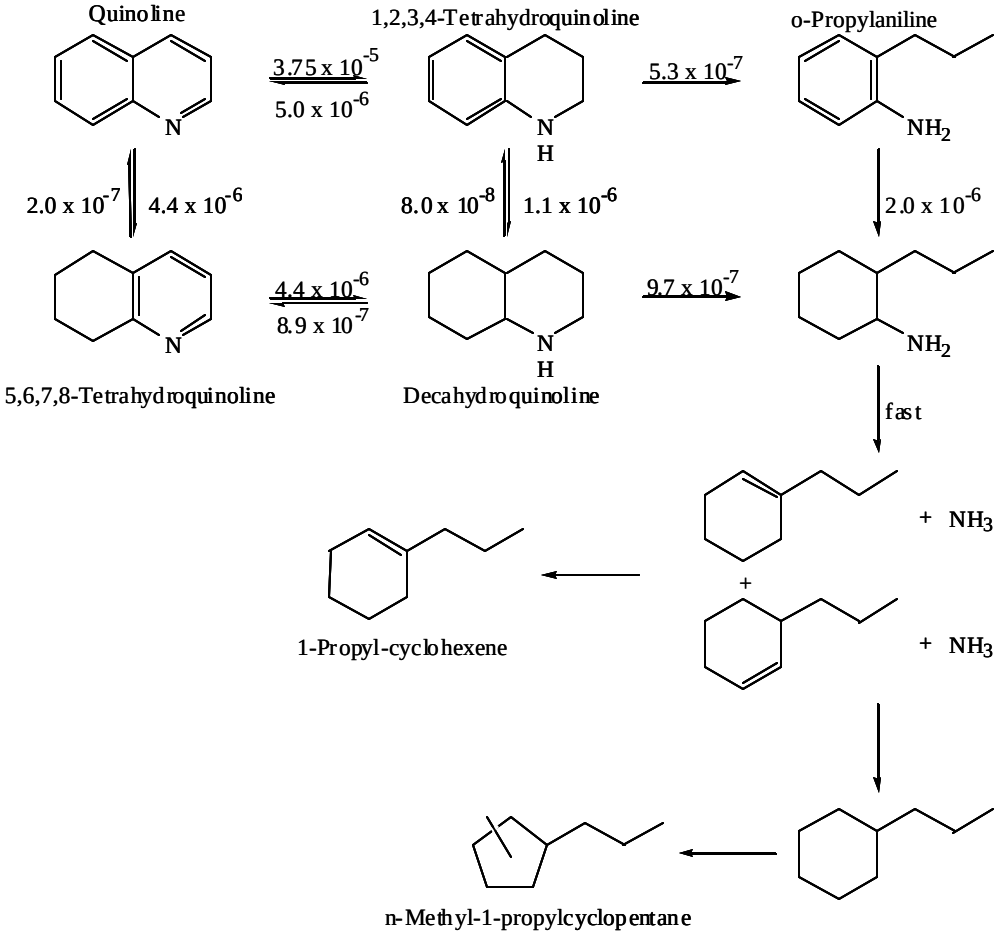

Figure 6. Reaction network for quinoline HDN proposed by Satterfield and Yang [12]. The numbers next to the arrows are pseudo-rate constants at 648 K in units of mol/(g of cata1yst·s).

Quinoline HDN requires the prior hydrogenation of one or both rings. Quinoline hydrogenation to give 1,2,3,4-tetrahydroquinoline is much more rapid than that giving 5,6,7,8-tetrahydroquinoline and approaches equilibrium at lower quinoline conversions. The rapidity of 1,2,3,4-tetrahydroquinoline formation is associated with the higher-electron density of the quinoline heteroring. Hydrogenolysis of 1,2,3,4-tetrahydroquinoline to give o-propylaniline is slower than its hydrogenation to give decahydroquinoline. The slow hydrogenolysis of 1,2,3,4-tetrahydroquinoline could be due to the resonance interaction between the benzenoid ring and the nitrogen-lone-pair electrons; this interaction "ties up" the lone-pair electrons that may be involved in adsorption of 1,2,3,4-tetrahydroquinoline. Most of the nitrogen removal therefore proceeds via decahydroquinoline, with the pathway through 5,6,7,8-tetrahydroquinoline dominating. The path of high hydrogen consumption is thus favored kinetically.

2.4 Hydrotreating in refining

A schematic layout of a modern, fully integrated refinery is shown in Figure 7.

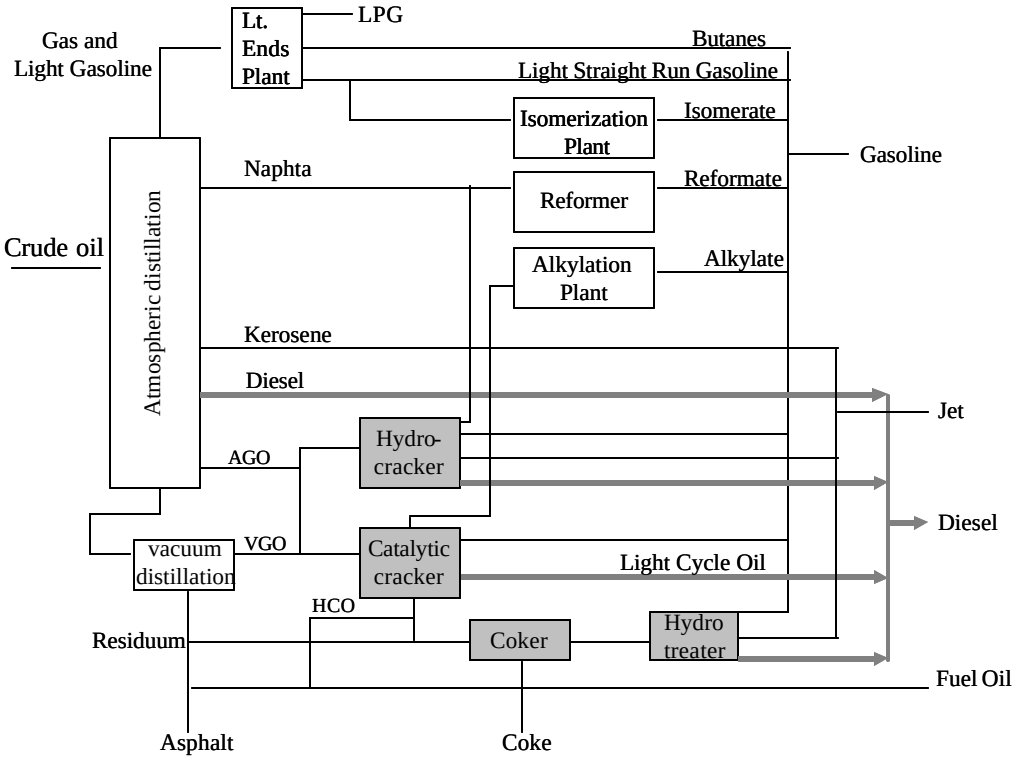

Figure 7. Schematic layout of a fully integrated refinery.

The resulting straight-run fractions are characterized by their boiling point range. Atmospheric distillation usually ends around 360 °C. The remaining fraction (atmospheric residue) is often separated by further vacuum distillation into vacuum gas oil (VGO) and vacuum residue. The atmospheric residue fraction may be the dominant fraction for some heavy crude, in such cases conversion into lighter products becomes especially important. The type and concentration of heteroatom compounds vary significantly between the fractions as do the demands for hydrotreating. Different reactions are used for treating different refinery streams depending on the main purpose and the properties of the feed. For instance HDS is used before catalytic reforming, HDN before hydrocracking to avoid catalyst poisoning and HDM is used before fluid catalytic cracking (FCC) to avoid metal deposition.

Diesel Fuel is formed from straight run diesel, light cycle oil from the FCC unit and, hydrocracker diesel and coker diesel. Nowadays, diesel is desulfurized by hydrotreating all blended refinery streams. To get diesel with less sulfur content, the hydrotreating operation has to be more severe. For straight run diesel, sulfur removal is the only point of concern in hydrotreating since the other diesel specifications (e.g. cetane number, density, and polyaromatics content) are satisfactorily met. Hydrocracker diesel is usually relatively high in quality and does not require additional treatment to reduce the sulfur content. As with gasoline, the diesel produced by the FCC and coker units contains up to 2.5 wt. % sulfur. Both, the FCC and coker diesel products have very low diesel number cetane numbers (slightly above 20), high densities, and high aromatics and polyaromatics content (about 80-90 %). In addition to being desulfurized, these streams must be upgraded by high pressure and temperature process requiring expensive catalysts. Another problem is that at high temperature hydrogenation- dehydrogenation equilibrium shifts towards aromatics.

2.5 Deep catalytic hydrotreating

In order to meet the gradually strict diesel fue1 standards, refiners have been developing new catalysts systems and hydrotreating processes to meet the challenge. One group of candidates for the catalysts in the hydrogenation of aromatics consists of conventional hydrotreating catalysts, such as sulfided NiMo and NiW on Al_2O_3. Such catalysts have

the advantage of high tolerance to sulfur in the feedstock. However, the activity of a metal sulfide catalyst is not sufficient, so severe operating conditions, such as high hydrogen pressure and high temperature, are required. As the reaction is exothermic, high temperature is thermodynamically unfavorable for the hydrogenation of aromatics.

The most widespread method of producing low aromatic diesel is a two-stage process based on a NiMo on alumina catalyst in the first stage and a sulfur-tolerant noble metal catalyst in the second stage. Several two-stage processes like this have been proposed by Shell, IFP, Amoco, Topsoe, Criterion/Lummus, Akzo and UOP [13, 14, 15]. The process consists of four main sections: initial hydrotreating, intermediate stripping, final hydrotreating and product stripping. In the initial hydrotreating section, the sulfur and nitrogen contents are reduced to levels that allow the catalyst in the final hydrotreater to achieve the required degree of aromatic saturation. Some aromatic conversion might be achieved in this section but, for the most part, conversion of di- and triaromatics to monoaromatics will occur. The process layout is the same as that of a conventional diesel hydrotreater unit. The reactor will normally contain a high activity NiMo catalyst. The reactor effluent is cooled and the gas and liquid are separated. The liquid goes to the intermediate stripper where dissolved H_2S and NH_3 are stripped off using either steam or recycle hydrogen. The final hydrotreating is performed using a process layout similar to that of the initial hydrotreater. The reactor contains several beds of the sulfur- and nitrogen-tolerant noble metal catalyst. Temperature control in the final hydrotreater can be achieved using interbed quenching by cold hydrogen or feed oil. Make-up hydrogen is normally added to the final reactor. The product stripper column removes H_2S, dissolved gases and the small amount of naphtha formed in the process. The exit gas from the second reactor contains only minor amounts of H_2S and can be recycled to the first section without scrubbing. The catalyst types used in the second stage normally consist of noble metal on an acidic carrier. These catalysts show low sensitivity to sulfur and nitrogen [16, 17], and the various vendors claim that up to 1000 ppm sulfur and 50 ppm nitrogen can be tolerated in the feedstock. In point of fact, as shown for sulfur [18], there is no sharp limit for the amount of sulfur or nitrogen that can be tolerated. The limit is in practice set by process design considerations. The loss of hydrogenation activity at high sulfur and/or nitrogen levels can be compensated by operating at a higher temperature

but, at some point, thermodynamic equilibrium will be reached. Loss of yield owing to higher selectivity towards cracking reactions at higher temperatures can also determine the maximum operating temperature. Activity loss can be countered by decreasing LHSV, but owing to the higher cost of the noble metal catalyst it may be better to increase the amount of the pretreatment catalyst.

Conventionally used hydrotreating reactors are fixed beds with co-current supply of oil streams and hydrogen, resulting in unfavorable H_2 and H_2S concentration profiles through the reactor. Due to high H_2S concentration at the reactor outlet, the removal of the last ppm of sulfur in inhibited. Counter-current reactor operation can provide a more preferable concentration profile. In counter-current reactor operation mode, the oil feed is introduced into the reactor at the top and hydrogen is introduced at the bottom of the reactor, in the place where its presence is most desired. H_2S is removed from the reactor at the top, avoiding possible recombination of H_2S and olefins at the reactor outlet. A commercial example of this approach is the hydrotreating process based on SynSat Technology, which combines Criterion's SynSat catalysts and ABB Lummus' reactor technologies [19, 20]. The general process scheme is shown in Figure 8.

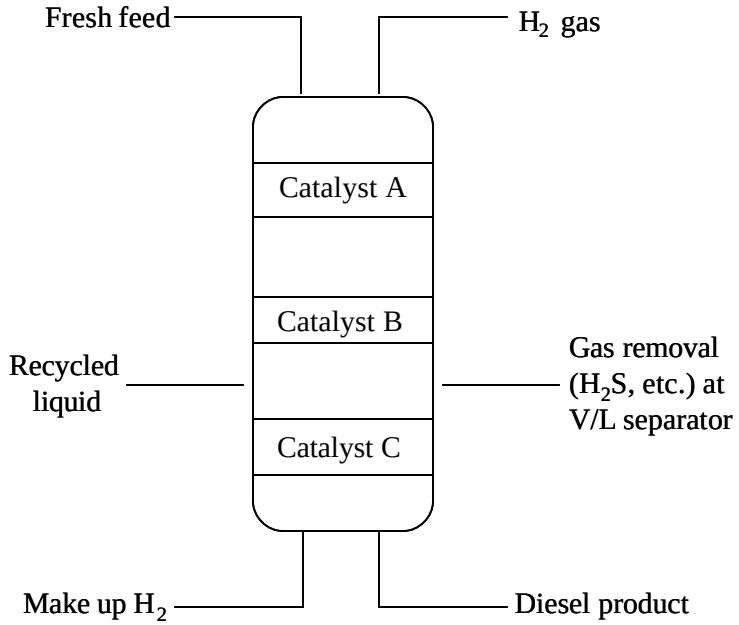

Figure 8. SynSat process with Criterion/Lummus catalytic hydrotreating reactor technology. The process uses intermediate byproduct gas removal and optional countercurrent gas flow.

The SynSat process is an innovation that merges the fields of catalysis and reactor engineering [21, 22, 23]. SynSat uses several different catalyst beds within a single reactor shell with intermediate removal of byproduct gas (e.g., H_2S), and optional countercurrent gas flow. Catalysts A and B in Figure 8 are metal sulfide catalysts such as sulfided Ni-Mo. Catalyst C is noble metal loaded on an acidic support. There is an intermediate gas removal step after the beds of catalysts A and B. Nearly all the sulfur compounds must be converted and removed as H_2S on beds A and B before the fuel feed reaches noble-metal catalyst bed C.

3 Mechanistic aspects in the catalytic hydrogenation of aromatics

3.1 Sulfur tolerance of noble metals.

It is often taken as a fact that the catalytic properties of noble metals are drastically reduced by even a few ppm of sulfur. Two deactivation routes of noble metals by sulfur have been proposed: (i) a direct poisoning of the metal surface due to the high affinity of sulfur for noble metals and (ii) a migration of the small metal particles resulting in the formation of large metal clusters. The high stability of the metal sulfide species results in a rapid deactivation of the metallic function even at a very low sulfur concentration in the feedstock [17,24, 25]. The larger concentration of adsorbed sulfur species on the metal surface has been shown to adsorb irreversibly, decreasing the number of metal active sites for the main reaction.

Acidic supports have been shown to have a significant influence on the sulfur sensitivity of noble metals. Noble-metal catalysts loaded on zeolites or other acidic supports will provide higher hydrogenation activity and better sulfur resistance than Al_2O_3 or TiO_2 supports [26]. It was observed that trend for aromatic hydrogenation over microporous zeolites [27, 28, 29] and mesoporous aluminosilicate molecular sieves [30].

The enhancement of activity has been explained by the presence of additional hydrogenation sites in the metal-acid interfacial region, which contributed to the overall rate of hydrogenation. In addition to the conventional metal catalyzed aromatic hydrogenation, Wang et al. [31] also suggested a second pathway of hydrogenation of

benzene involving acid sites of the support close to the metal particles and proposed a spillover of hydrogen from the Pt particles. In this mechanism carbenium ions adsorbed on acid sites could react with the spillover hydrogen, which is delivered through interparticle migration from the metal phase.

Another explanation for the higher resistance towards sulfur poisoning may be also attributable partly to the electron deficiency of metals when supported on acidic materials. The latter concept was first proposed by Dalla Betta and Boudart [32]. A lower electron densitiy on the metal weakens the metal–sulfur bond strength. As a result a significant change in turnover frequency of the hydrogenation reaction can be observed [33, 34, 35, 36, 37].

4 Scope of the thesis

The research presented in the thesis was conducted in a close collaboration with Shell International Chemicals B.V. The aim was to understand mechanistic aspects of sulfur and nitrogen poisoning of supported platinum catalysts in the dependence on acid-base properties of the amorphous silica-alumina carriers. This knowledge would lay groundwork for developing highly active hydrogenation catalysts operating under S- and N-poison conditions. Dibenzothiophene was chosen as the model compound for sulfur poisoning because (1) it is one of the sulfur compounds in diesel and (2) its catalytic chemistry is understood. Quinoline was selected as a typical nitrogen poison heteropolyaromatic compound.

In Chapter 2 the detailed characterization study of the supported platinum catalysts is presented. The aim was to qualify and quantify the different phases present in the amorphous carriers. Multinuclear Nuclear Magnetic Resonance (^{27}Al (MQ) MAS and ^{1}H MAS NMR), Fourier Transformed Infrared (FTIR), Temperature Programmed Desorption (TPD), Transmission Electron Microscopy (TEM), and X-ray Absorption Spectroscopy (EXAFS) were employed for that purpose. ^{27}Al (3Q) MAS NMR allowed determining the concentration of pure alumina domains and quantifying the aluminosilicate phase, where aluminum tetrahedral species are separated by silica ones. The quantification of Brønsted acid sites by ^{1}H MAS NMR agreed with the determination of surface-acidity (i.e., pyridine adsorption) and could be correlated with the development

of the aluminosilicate phase. The Pt particles anchored by wet impregnation were exceptionally small and uniform, i.e., between 0.6 and 0.8 nm on all aluminum containing supports.

In Chapter 3 the catalyst activity was tested in the hydrogenation of tetralin. The hydrogenolysis of neopentane was carried out to probe metal-support interaction. The activity of the nanosized Pt particles was influenced by the electronegativity of the supports with an exception of the neutral silica support. In parallel a compensation effect was observed in both reactions (e.g. $\ln(A(exp) = m \bullet Ea(exp) + c$). This phenomenon was explained assuming a metal-support interaction affecting the adsorption of the reactants. The ratio of Brønsted acid sites (BAS) to Lewis acid sites (LAS) is proposed to govern the sorption properties of the nanosized platinum particles. Furthermore, the electronic structure of the platinum particles was affected by the support as shown by the changes in the X-ray absorption near-edge structure (XANES).

In Chapter 4 the study of the catalytic performance in the hydrogenation of tetralin in the presence of either quinoline or DBT is presented. The former poison neutralized every acid site and competed with tetralin for the adsorption sites on platinum, while DBT poisoned the metal sites. As a result, the observed catalytic activity was significantly reduced. The mechanistic aspects of the residual catalytic activity are discussed and a novel model for the hydrogenation of tetralin in the presence of poisons is proposed.

In Chapter 5 the main results and conclusions of this thesis are summarized.

Acknowledgment

Shell International Chemicals B.V. is gratefully thanked for the generous financial support through the experimental phase of the project.

5 References

1 B. Bensaïd, IFP paper, Panorama 2005, *Road Transport Fuels in Europe: the Explosion of Demand for Diesel Fuel.*

2 Diesel Fuel and exhaust emission report sponsored by United Nations Environment Programme, Internation Labour Organization, World Health Organization (http://www.inchem.org/documents/ehc/ehc/ehc171.htm).

3 http://europa.eu.int; Official Journal of the European Union L 350 , 28/12/1998 P. 0058 – 0068.

4 http://europa.eu.int; Official Journal of the European Union L 076 , 22/03/2003 P. 0010 – 0019.

5 http://www.arb.ca.gov; The California Diesel Fuel Regulations in the California Code of Regulations, Title 13, Section 2281-2285 and Title 17, Section 93114.

6 R.R. Chianelli, M. Daage, M.J. Ledoux, Adv. Catal. 40 (1994) 177.

7 Thermodynamic Calculation was performed in HSC Chemistry for Windows 5.1, Outokumpu Research Oy, P.O. Box 60, FIN – 28101 Pori, Finland.

8 K. Schrage, R. L. Burwell, J. Am. Chem. Soc. 88 (1966) 4555.

9 E. P. Martins, D. A. G. Aranda, F. L. P. Pessoa, J. L. Zotin, Braz. J. Chem. Eng. 17 (2000) 1603.

10 M. Houalla, D. H. Broderick, A. V. Sapre, N. K. Nag, V. J. H. de Beer, B. C. Gates, H. Kwart, J. Catal. 61 (1980) 523.

11 M. J. Girgis, B. C. Gates, Industrial and Engineering Chemistry Research 30 (1991) 2021.

12 C. N. Satterfield, S. H Yang, Ind. Eng. Chem. Process Des. Dev 23 (1984) 11.

13 B.H.C. Winquist, S.N. Milam, B.D. Murray and R.C. Ryan, Eur. Patent Appl. 0519 573.

14 S.G. Kukes, F.T. Clark, D. Hopkins, US Patent 5 151 172 (1991) to Amoco Corp.

15 P.Sogaard-Andersen, B.H. Cooper, P.N. Hannerup, AM-92-50, NPRA Annual Meeting, March 1992.

16 C.H . Bartholomew, P.K Agarwal and J.R Katzer , Adv. Catal. 31 (1982) 135.

17 J. Barbier, E. Lamy-Pitara, P. Marecot, J . P Boitiaux, J. Cosyns, F. Verna , Adv. Catal. 37 (1990) 279.

18 N. Marchal, S. Kasztelan and S. Mignard, Catalyst Hydroprocessing of Petroleum and Distillates, Marcel Dekker, New York (1994) 315.

19 B. van der Linde, R. Menon, D. Dave, S. Gustas, Asian Refining Technology Conference, DD-ARTC-99 (1999) 24.

20 J. Langston, L. Allen, D. Dave, Petr. Tech. Quart. (1999) 2:65.

21 I.E. Maxwell, CATTECH 1 (1997) 5.

22 W.H.J. Stork, Am. Chem. Soc. Sym. Ser. 634 (1996) 379.

23 A. Suchanek, Am. Chem. Soc. Div. Petrol. Chem. Prepr. 41 (1996) 583.

24 J. Oudar, Catal. Rev-Sci. Eng 22(2) (1980) 171.

25 J. Oudart, Stud. Surf. Sci. Catal. 11 (1982) 258.

26 C. Song, CHEMTECH 29 (1999) 26.

27 C. Song; A.D. Schmitz, Energy Fuels 11 (1997) 656.

28 S.D. Lin, C. Song, Catal. Today 31 (1996) 93.

29 A.D. Schmitz, C. Song, Catal. Today 31 (1996) 45.

30 K.M. Reddy, C. Song, Mat. Res. Soc. Sym. Proc. Ser. 454 (1997) 125.

31 J. Wang, Q. Li, J. Yao, Applied Catal. A: General 175 (1998) 191.

32 R.A. Dalla Betta, M. Boudart, Proc. 5th Int. Congr. Catal. 1972, p. 1329.

33 P. Gallezot, Catalysis by Zeolites (B. Imelik, C. Naccache, Y. Ben Taarit, J. C. Vedrine, G. Coudurier, H. Praliaud, Eds.), Vol. 5, Elsevier Science, Amsterdam (1980) 227.

34 M. T. Tri, J. Massardier, P. Gallezot, B. Imelik,B , Metal-support and Metal Additives Effects in Catalysis (B. Imelik, C. Naccache, G.Coudurier, H. Praliaud, M. Meriaudeau, P. Gallezot, G. A. Martin,and J. C. Vedrine, Eds.), Vol. 11, Elsevier, Amsterdam (1982) 141.

35 F. Figueras, R. Gomez, M. Primet, Adv. Chem. Ser. 121, (1973) 480.

36 T. T: Phuong, J. Massardier, P. Gallezot, J. Catal. 102 (1986) 456.

37 R. Szymanski, H. Charcosset, P. Gallezot, J. Massardier, J, L.Tournayan, J. Catal. 97 (1986) 366.

Chapter 2

Characterization of ASA-supported platinum catalysts by ^{27}Al (3Q) MAS NMR, ^{1}H MAS NMR, FTIR, TPD, TEM, and EXAFS

A series of catalysts based on platinum nanoparticles supported on amorphous silica-alumina (ASA) with varying amount of alumina (100, 55, 20, 5 and 0 %), were prepared by incipient wetness impregnation. Detailed characterization of the Pt-catalysts was carried out by means of Nuclear Magnetic Resonance (^{27}Al (MQ) MAS and ^{1}H MAS NMR), Fourier Transformed Infrared Spectroscopy (FTIR), Temperature Programmed Desorption (TPD), Transmission Electron Microscopy (TEM), and X-ray Absorption Spectroscopy (EXAFS). The structural characterization with ^{27}Al (3Q) MAS NMR allowed determining the concentration of pure alumina domains and quantifying the aluminosilicate phase, where aluminum tetrahedral species are separated by silica ones. The quantification of Brønsted acid sites by ^{1}H MAS NMR agreed with the determination of surface-acidity (i.e., pyridine adsorption) and could be correlated with the development of the aluminosilicate phase. The Pt particles anchored by wet impregnation were exceptionally small and uniform, between 0.6 and 0.8 nm on all aluminum containing supports.

1 Introduction

The interest in the acidic behavior of amorphous silica-aluminas (ASA) and related materials originates in their use in catalytic processes of significant industrial importance [1, 2]. Because of the acidic properties of ASAs, they have been employed in such catalytic transformations like isomerization of olefins, paraffins and alkyl aromatics, alkylation of aromatics with alcohols and olefins, and olefin oligomerization and cracking. Similar to crystalline silica-aluminas, the ASAs can also serve as a support that increases the resistance of a metal catalyst towards sulfur poisoning in deep hydrotreatment of diesel fuels [3, 4]. ASA carriers have one important advantage related to their mesoporous that prevent diffusion limitations even when employing bulky organic molecules. Further, the ASAs usually exhibit more moderate acid sites than those usually present in the crystalline material. Strongly acidic supports cause excessive coke formation and hydrocracking of the feedstock that lead to a decrease in the middle-distillate yields. Therefore, the potential of ASA-supported noble metal was targeted as a promising alternative.

It has been reported that the properties of the support (i.e., Si to Al ratio; type, strength and concentration of acid sites) can modify the catalytic activity of platinum catalysts. However, only a systematic study of Pt/ASA catalysts exhibiting: (i) small Pt particles within a narrow size distribution and (ii) a gradual change in the acidic composition of the ASA support, could be used to correlate the acidity, metal-support interactions and catalytic activity for the hydrogenation of aromatics in the presence of S-poisons.

In this paper we report a comprehensive characterization of alumina-, ASA-, and silica-supported Pt-catalyst in view of elucidating the structural origin of the different kinds of acid sites in the amorphous ASA carriers. To directly probe the local configuration of the supports, solid-state magic angle spinning (MAS) NMR study was performed [5, 6, 7]. For the aluminosilicates (ASA, zeolites, etc.), the ^{27}Al NMR provides useful information on the Al-O environments since chemical shifts strongly depends on the coordination number of aluminum. An insight into the flexibility of the aluminum environment and the acidity was gained from a study of ammonia treated samples. It has been suggested that such a treatment can restore the tetrahedral coordination of octahedral alumina species if they are still connected to the framework via an oxygen atom [8, 9]. The application of

^{1}H MAS NMR and IR enabled to examine the hydroxyl groups that originate Brønsted acidity. Proton NMR spectra of solids provide simple and quantitative measurements of acidic and non-acidic protons [10, 11]. Furthermore, different sorts of OH groups were observed by means of IR spectroscopy. An additional IR study was carried out using pyridine as a probe molecule, which interacts with the acidic oxides of the Pt-catalyst supports. The surface PyL and PyB species with characteristic bands at 1447 to 1464 and 1535 to 1550 cm^{-1}, respectively, were quantified and cross-validated with the data obtained in the temperature programmed desorption study of pyridine (Py-TPD). The Py-TPD experiment permitted to follow desorption of chemisorbed pyridine species according to their binding energies [12]. The platinum particle size distribution was estimated by combining the results obtained with transmission electron microscopy (TEM) and hydrogen chemisorption. Analysis of (high-resolution) transmission electron micrographs is unique in providing directly the particle size distribution of supported metal. However, to accurately determine the size of Pt-nanoparticles, X-ray absorption fine structure (EXAFS) data and particle size modeling were used [13].

2 Experimental

2.1 Preparation and chemical composition of supported Pt-catalysts

A series of Pt-based catalysts supported on silica-alumina (ASA 5/95, 20/80 and 55/45 containing 5, 20 and 55% of alumina in silica, respectively) as well as on pure alumina and silica, were prepared at the Shell Research and Technology Center. The ASA supports were produced from a gel formed at pH = 7.5 by mixing (i) acetic acid with $AlCl_3 \cdot 6H_2O$ in distilled water (pH = 1.5) and (ii) sodium silicate with NH_4OH (pH = 12). Subsequently, the gel was washed with a solution of ammonium acetate to eliminate sodium and heated. Finally, the samples were calcined at 949 K for 2 hours. The supports were impregnated with an aqueous solution of $Pt(NH_3)_4(OH)_2$ (1h), calcined at 573 K (5 h), and reduced at 623 K in a flow of hydrogen (2 h).

Chemical compositions of carriers and supported catalyst were determined with atomic absorption spectroscopy (AAS) using a UNICAM 939 spectrometer. The amount of leftover sodium for ASA carriers was 5, 33 and 5 ? $mol \cdot g^{-1}$, for the (55/45), (20/80) and (5/95) samples, respectively. The concentration of every element was calculated on a water-free basis.

2.2 Specific surface area and porosity

Surface area and pore diameters were calculated from nitrogen adsorption measurements carried out at 77.4 K using a PMI-automated BET-sorptometer. Prior to the measurements, samples were degassed at 523 K over 20 hours. The surface area and micro- and mesopore distributions were calculated using the BET and BJH theories [14, 15].

2.3 Nuclear magnetic resonance spectroscopy

For the ^{27}Al (MQ) MAS NMR experiments the catalyst samples were packed at ambient conditions into 4-mm ZrO_2 rotors. For the ammonia treatment, the samples were heated and contacted with a flow of NH_3 at 393 K for 6 h before being packed in the rotors. The spectra were obtained on a Bruker Avance AMX 400 NMR spectrometer operating at 104.263 MHz for aluminium. Magic angle spinning was carried out at a rotational rate of

12 kHz. Chemical shifts were referenced to solid $(NH_4)Al(SO_4)_2$ ($?_{Al}$ = - 0.59 ppm). For the MQ MAS NMR experiments, a three-pulse sequence, including z-filtering and States acquisition method, was applied [16]. After Fourier transformation, the 2D spectra were sheared [17], so that the orthogonal projection on the isotropic axis gives the 1D spectrum free of any anisotropic broadening. The quantification of different ^{27}Al species was performed by fitting the corresponding MAS spectra using the parameters determined in the 3Q MAS experiments [18]. For the fitting, a custom-made program by the group of Prof. Kentgens, University of Nijmegen, was used. This program used Gaussian distributions for the quadrupolar coupling constant and for the isotropic shift $?_{iso}$.

^1H MAS NMR measurements were carried out using a Bruker AV-500 NMR spectrometer in a magnetic field of 11.7 T and at a spinning rate of 15 kHz. The pre-reduced, dry samples (activated in vacuum over 1 h at 673 K) were pressed into 4 mm ZrO_2-rotors under dry nitrogen. The ^1H chemical shifts were referenced to adamantine (?=2.0ppm).

2.4 Infrared spectroscopy

A Perkin Elmer 2000 spectrometer operating at a 4 cm^{-1} resolution was used in the IR studies. Prior to the IR investigation the catalyst samples were activated in vacuum (p = 10^{-6} mbar) at 673 K over 1 h. The surface hydroxyl groups were examined in the stretching region of the OH (3000 – 4000 cm^{-1}).

Activated catalyst samples were exposed to pyridine (p(Py) = 10^{-2} mbar) at 423 K for 0.5 h. After removing the excess of the adsorbate (i.e., outgassing at 423 K over 1 h) the spectrum was recorded. Subsequently, each sample was heated up to 673 K, kept at this temperature for 1 h, and cooled down to 423 K. Then, the second spectrum was recorded. A comparison of the spectra obtained before and after thermal treatment gave the amount of strongly adsorbed pyridine. The concentration of different Py-species on the surface was determined by a method based on the molar extinction coefficients [19].

2.5 Temperature programmed desorption

A sample of ca. 20 mg was outgassed ($p = 10^{-3}$ mbar) while heating at 10 $K \cdot min^{-1}$ and kept at 673 K for 1 h. After cooling down to 423 K, the sample was equilibrated with pyridine within 1 h (p(Py) = 0.3 mbar) and outgassed for another 3 h. Finally, the sample was heated (10 $K \cdot min^{-1}$) and desorption of pyridine was followed with mass spectrometry (MS) using the $m/z^+ = 52$ signal. Gaussian deconvolution was used for the quantitative comparison of catalyst acidities [20].

2.6 Transmission electron microscopy

The pre-reduced catalysts samples, stored under air, were grinded, suspended in ethanol and ultrasonically dispersed. Drops of the dispersions were applied on a copper grid-supported carbon film. A JEM-2010 Jeol transmission electron microscope operating at 120 kV was used for these purposes. Transmission electron micrographs were recorded at a magnification of 54,000.

2.7 H_2 Chemisorption

Formation of chemisorbed monolayer is the most frequently used method for characterization of metallic catalysts. Generally, hydrogen adsorbs dissociatively on metals. From the volume of chemisorbed hydrogen required for the formation of a monolayer, the metal dispersion D is directly obtained. The hydrogen uptake was measured at SRTC Amsterdam, Netherlands. The Pt-catalyst was activated at T = 588 K for 1 h in vacuum. The sample was then equilibrated at 298 K and successive doses of hydrogen were admitted. The amount of adsorbed hydrogen was determined by measuring the pressure after a time delay which was needed for reaching the adsorption equilibrium. In order to account for the H_2 adsorbed on the support, the sample was outgassed and another isotherm was measured. The chemisorbed hydrogen on the metal is calculated by subtracting the first isotherm (e.g Hydrogen adsorbed on the metal and support) to the second one (e.g. hydrogen adsorbed on the support).

2.8 Extended X-ray absorption fine structure

EXAFS spectra were collected on the beamline X1 at HASYLAB, DESY, Hamburg, Germany. The storage ring was operated with an electron energy of 4.5 GeV and an average current of 100 mA. The Si (311) double crystal monochromator was detuned to 60% of the maximum intensity to minimize the intensity of higher harmonics in the X-ray beam. Fresh catalysts prepared as self-supporting wafers were reduced in situ with H_2 at 315°C for 2 h. X-ray absorption spectra were collected at the Pt L_{III} edge (11564 eV), at liquid N_2 temperature, and analyzed with the Viper software [21]. For EXAFS analysis the scattering contributions of the background were removed from the X-ray absorption with a third order polynomial function. The oscillations were weighted with k^2 and Fourier transformed within the limits k = 3 – 14 Å $^{-1}$. The local environment of the Pt atoms was determined from the EXAFS using the phase-shift and amplitude function for Pt-Pt calculated assuming multiple scattering processes (FEFF Version 8.10) [22,23].

3 Results

3.1 Chemical composition, textural properties and bulk structure of the catalysts

Chemical compositions of the Pt-catalysts obtained in the AAS measurements are summarized in Table 1. The platinum content was very uniform among the samples, i.e., 1 wt. % for Pt/SiO_2 and approximately 0.8 wt. % for all other catalysts. The nitrogen adsorption-desorption isotherms of the catalyst samples were comparable to those of the parent materials. The ASA carriers had specific surface areas comprised between 360 and 400 $m^2 \cdot g^{-1}$, higher than those of pure silica and alumina (64 and 310 $m^2 \cdot g^{-1}$, respectively). Mesopores were present in every carrier.

Catalyst	Composition [wt. %]			Surface Area [$m^2 \cdot g^{-1}$]		Pore Diameter [nm]
	Pt	SiO_2	Al_2O_3	BET	t-plot	
Pt/Al_2O_3	0.78	0.0	99.3	307	305	8.7
Pt/ASA (55/45)	0.82	46.1	52.9	376	375	7.8
Pt/ASA (20/80)	0.81	78.7	20.4	363	363	9.4
Pt/ASA (5/95)	0.78	94.9	4.3	396	396	9.2
Pt/SiO_2	1.03	99.1	0.0	64	64	22

Table 1. Chemical composition and textural properties of the calcined catalysts.

^{27}Al 3Q MAS NMR spectroscopy was used to probe the chemical environment and determine the coordination flexibility of aluminum species in the Pt-catalysts on alumina-containing carriers. The quantification of the computed 1D ^{27}Al MAS NMR spectra provided information on the amounts of 4-, 5- and 6-coordinated Al atoms in the samples, based on the quadrupolar and isotropic parameters derived from the 3Q MAS NMR data. The results are presented in Figure 1 and Table 2.

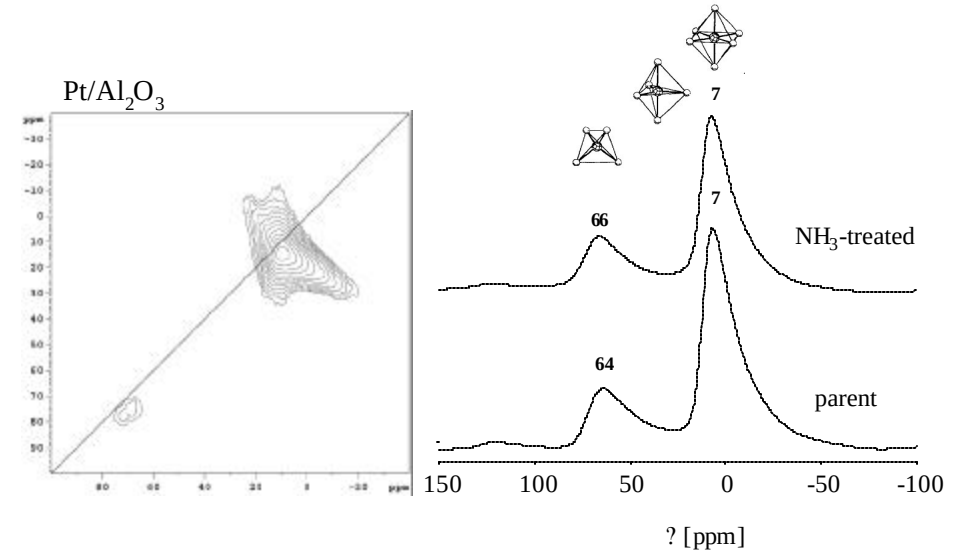
Pt/Al2O3
7
7
66
NH3-treated
64
parent
150
100
50
0
-50
-100
? [ppm]

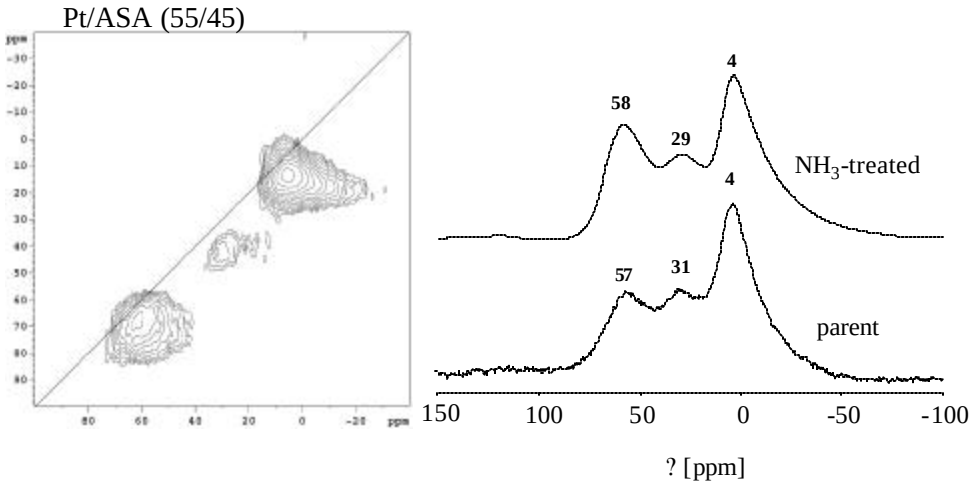
Pt/ASA (55/45)
4
58
29
NH3-treated
4
57
31
parent
150
100
50
0
-50
-100
? [ppm]

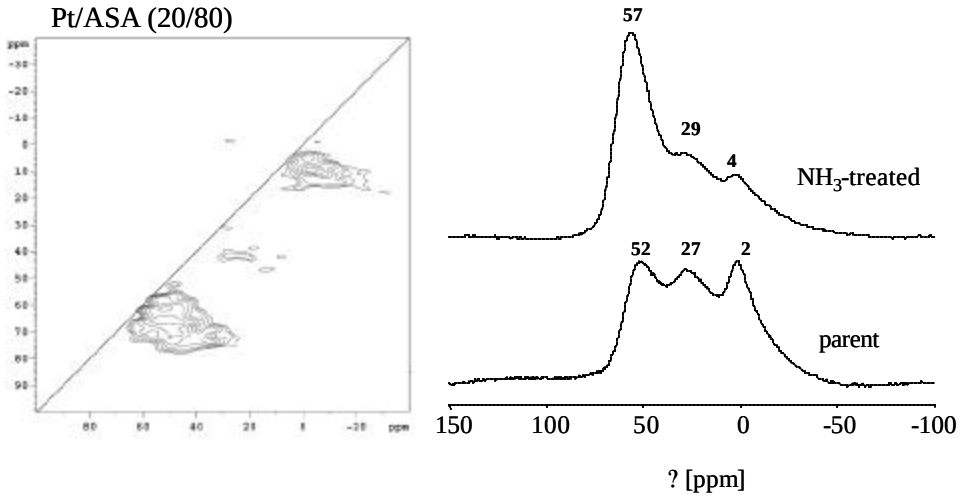
Pt/ASA (20/80)
57
29
4
NH3-treated
52
27
2
parent
150
100
50
0
-50
-100
? [ppm]

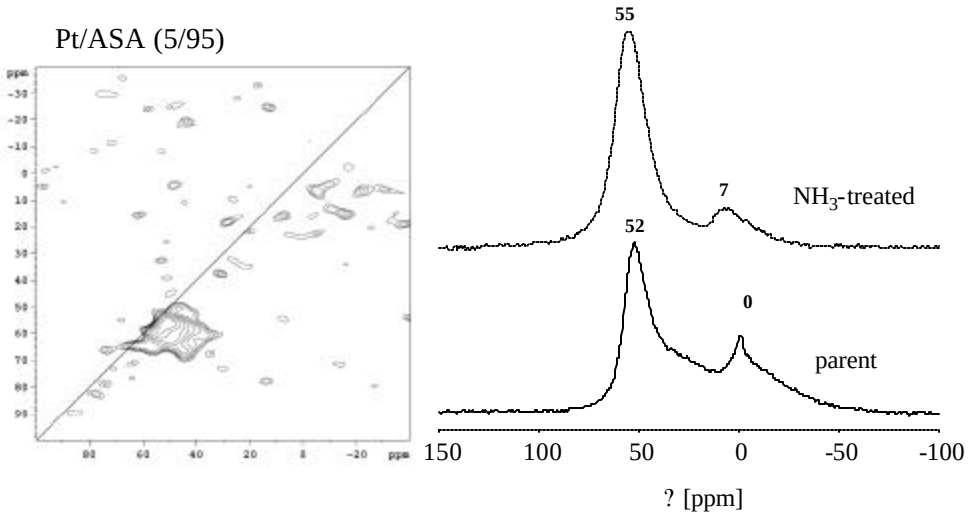

Figure 1. ^{27}Al (MQ) MAS NMR study of Pt-catalysts supported on alumina, ASAs and silica carriers. Left side: ^{27}Al 3Q MAS NMR spectra recorded at 104.263 MHz using a spinning rate of 12 kHz. Right side: the corresponding 1D ^{27}Al MAS NMR calculated on the basis of quadrupolar parameters derived from the 3Q MAS NMR data; the bottom spectrum represents that of the parent sample; the upper one corresponds to the catalyst sample treated with ammonia.

Catalyst	Aluminum species [mol %]					
	Th-Al		penta-Al		Oh-Al	
	parent	NH_3-treated	parent	NH_3-treated	parent	NH_3-treated
Pt/Al_2O_3	30	33	0	0	70	67
Pt/ASA (55/45)	25	34	26	26	49	40
Pt/ASA (20/80)	46	60	24	29	30	11
Pt/ASA (5/95)	69	87	0.0	0.0	31	13

Table 2. The amount of different types of structural aluminum in alumina and in ASA-supported Pt-catalysts.

The ^{27}Al 3Q MAS NMR spectrum of Pt/Al_2O_3 showed signals at 66 and 7 ppm that arise from tetrahedral (Th) and octahedral (Oh) aluminum, respectively [24]. Both peaks consisted of a sharp component and a rather broad signal. The narrow resonance of Th-Al was centered close to the diagonal, indicating that the corresponding aluminum species experienced a relatively small quadrupolar interaction (i.e., $?_{iso}$? $?_{F2}$), issuing from their location in a rather symmetric environment. The signal attributed to Oh-Al, stretched in F_1 and F_2, resulted from a large distribution in isotropic chemical shifts and quadrupolar

interactions. This indicates a broad distribution of the electron density and the degree of distortion. The simulation of 1D ^{27}Al MAS NMR spectrum required for both 4- and 6-coordinated Al species two different QCC parameters (i.e., the tailing of the peaks). Fractions of Th and Oh aluminum were approximately 30 and 70 %, respectively. The comparison with the 1D ^{27}Al MAS NMR spectrum of the ammonia-treated sample showed hardly any change in the position or in the overall intensity of the peaks. Remarkably, the 1D fitting was performed only with one QCC parameter for either Oh or Th contributions.

The resonance of Th-Al was much stronger in the ^{27}Al 3Q MAS NMR spectrum of Pt/ASA (55/45) than in Pt/Al_2O_3. However, the signal was less resolved and its center downshifted to about 57 ppm. Furthermore, a new resonance signal at about 30 ppm was observed. The latter was attributed to five-coordinated aluminum (i.e., penta-Al). The aluminum species in an octahedral environment were detected at 4 ppm. Note, that every one of the resonance signals in the Pt/ASA (55/45) spectrum was broadened in the isotropic and anisotropic dimensions. This reflected the topological distribution of aluminum atoms in the amorphous sample with bond angles that are not well defined. While the Th-Al signal was fitted with one value of QCC, both broad and sharp features were resolved for the Oh-Al species in the 1D spectrum. Ammonia treatment reduced the amount of Oh-Al (mainly the narrow-QCC contribution) and increased that of Th-Al by the same value (i.e., 9 %). Evidently, surface-adsorbed ammonia generated aluminum species with lower coordination. Reversible coordination of aluminum species is a general property of alumino-silicate structures and was previously reported for zeolites and mesoporous materials as well as for ASAs [25 and references therein]. It has been proposed that reversibility of the Al coordination is associated with coordination of water molecules upon partial hydrolysis of the structure of ASA that being amorphous (metastable) is more susceptible to hydrolysis. It is interesting to observe that the signal at 30 ppm did not change its intensity.

The NMR spectra of Pt/ASA (20/80) showed a remarkable downfield shift of the peak attributed to Th-Al, which was observed at 52 ppm. This downfield shift was assigned to a significant dilution of aluminum in the neighborhood of a central Al-atom. Some geometric factors (e.g., disordered Al-O-Si angles [26]) and the composition of the

further coordination shells could influence the resonance of Th-Al [27]. The other aluminum species were found in six- and five-coordination states (resonance signals at 2 and 27 ppm, respectively). The relative amount of Th-Al was higher than that of the Oh-Al (46 to 30 %, respectively). Upon ammonia adsorption, the intensity of the signal attributed to tetrahedral aluminum was increased significantly, which correlated with a loss in the intensity of the octahedral aluminum. It is interesting to note that the narrow octahedral signal disappeared entirely while only small changes were observed for the broad one. In addition, the Th-Al peak was shifted slightly upfield to 57 ppm. Minor changes were observed for the penta-Al signal.

The NMR spectra of the Pt/ASA (5/95) showed a substantial contribution of the four-coordinated aluminum (at 52 ppm) and only minor resonance signals of five- and six-coordinated aluminum. Apparently, the majority of the aluminum atoms adopted tetrahedral coordination. The ammonia-treated sample showed a further increase of the fraction of four-coordinated aluminum (to ca. 87 %) with a loss of the six-coordinated Al. As for Pt/ASA (20/80) the changes are dominantly attributed to the narrow octahedral feature.

3.2 Surface structure of the Pt-catalysts

Qualitative and quantitative studies of acid sites, related to the presence and concentration of different OH groups in the Pt-catalysts activated at 673 K, were performed by means of ^{1}H MAS NMR. Since a rather narrow range of chemical shifts is considered, deconvolution was necessary to show the contributions of various sorts of OH groups. The results are presented in Figure 2.

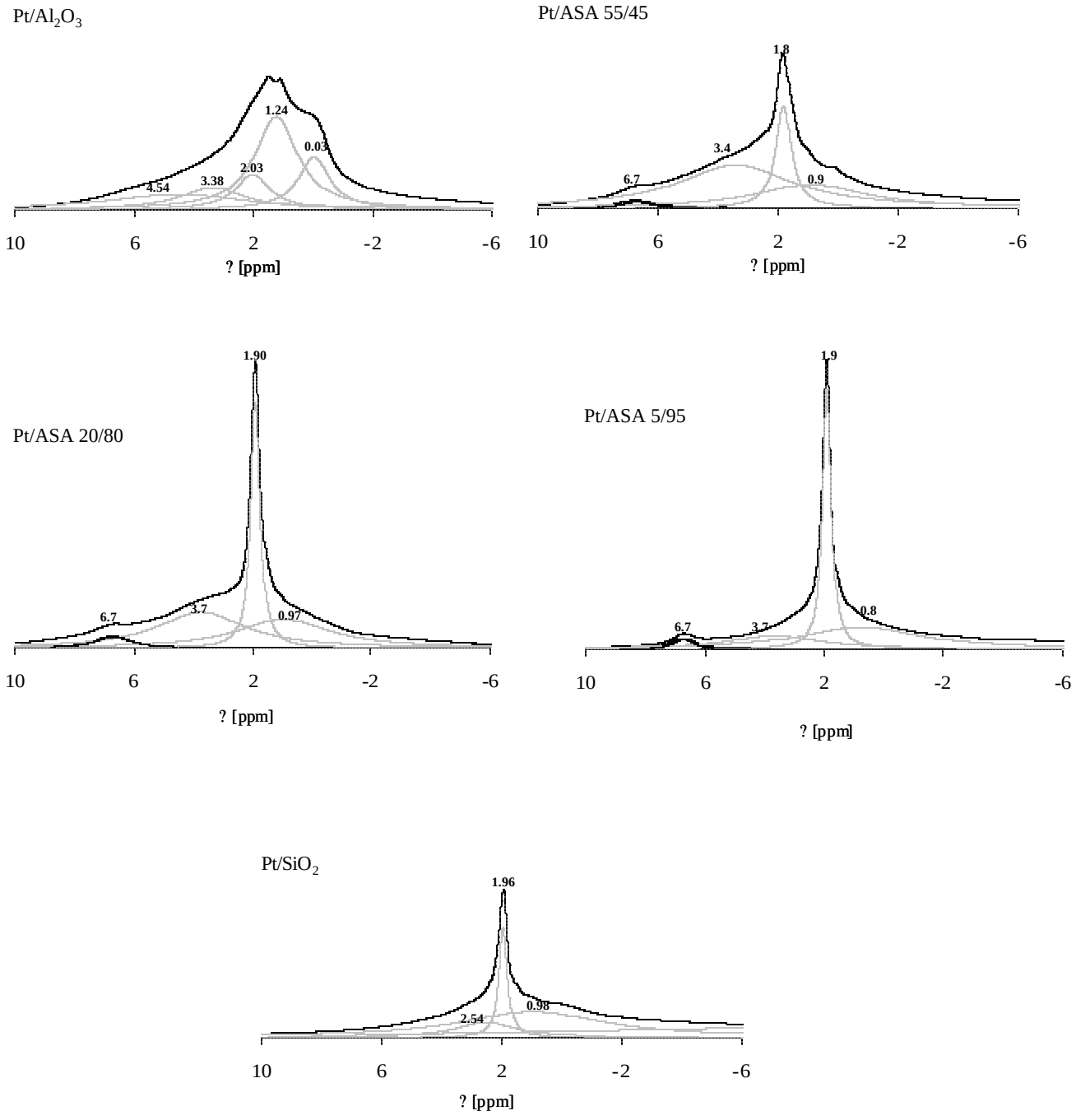

Figure 2. ^{1}H MAS NMR spectra of Pt-catalysts supported on alumina, ASAs and silica carriers. Deconvolution with lorentzian-shape peaks shows the contributions of various sorts of OH groups.

In the ^{1}H MAS NMR spectrum of the Pt/Al_2O_3 catalyst a number of overlapping peaks was detected at 0.0, 1.2, 2.0, 3.4, and 4.5 ppm. The array of distinct signals resulted from the fact that the OH group can bond to one, two or three aluminum atoms located in different coordination environments [28]. The low-field signals (i.e., 0 and 1.2 ppm) indicated a basic character of the hydroxyl group attached to a single aluminum atom. The signals at 2.0 and 3.4 ppm could be attributed to bridging OH groups. Finally, the chemical shift at 4.5 ppm was assigned to a fairly acidic hydrogen of an OH group in a three-fold binding structure with aluminum [29].

In the ^{1}H MAS NMR spectra of the platinum catalysts supported on ASAs and silica carriers a well resolved singlet at 1.8 – 1.9 ppm was found. The signal was attributed to the presence of silanol groups. The low-field component of every ASA spectrum was asymmetric due to some minor contributions that were less significant as the concentration of alumina in the supports decreased. In the ^{1}H MAS NMR spectrum of the Pt/SiO_2 catalyst, the Si-OH signal was asymmetric in the high-field region due to the presence of various types of silanol groups.

In contrast to the NMR spectra of Pt/Al_2O_3 and Pt/SiO_2 catalysts, the spectra of the ASA-supported samples always showed an additional signal at 6.7 ppm. This resonance could indicate the presence of structural OH groups compensating for the charge deficiency in a new phase where silica and alumina tetrahedra form structures similar to those of H-type zeolites (i.e., Si-O(H)-Al) [30].

An IR investigation of hydroxyl groups present in the platinum catalysts was also carried out. IR spectra in the region of the stretching vibration of OH groups are presented in Figure 3.

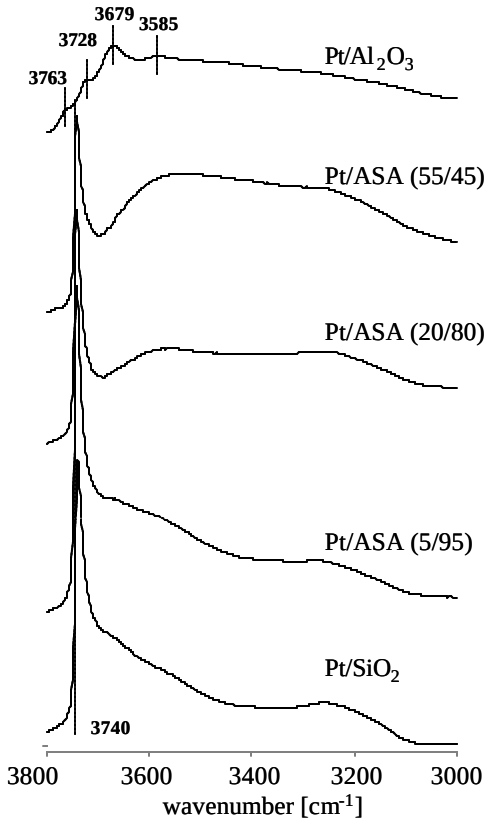

Figure 3. IR spectra of Pt-catalysts supported on alumina, ASAs and silica carriers.

The IR spectra exhibited the presence of a broad band in the 3000 to 3800 cm^{-1} region. Apparently, a number of OH groups interacted mutually through hydrogen bonding. Nevertheless, for the Pt/Al_2O_3 catalyst at least three major bands could be detected at 3763, 3728 and 3679 cm^{-1}. As the OH vibrational frequency decreases with increasing number of coordinating Al atoms, the bands reflected single-bonded (1 Al), bridging (2 Al) and capping (3 Al) OH groups, respectively [31]. The ASA and silica supported catalysts showed one sharp peak at 3740 cm^{-1} and a broader band at lower wavenumbers. The sharp peak can be attributed to the presence of terminal Si-OH groups while the broader band is assigned to vicinal hydroxyl groups showing internal hydrogen bonding. However, hydroxyls groups within the bulk of the structure (i.e., closed cavities) rather than those on the silica surface might contribute to the broad band in the IR spectrum [32]. A correlation of various sorts of surface OH groups observed in IR and ^1H MAS NMR spectra of Pt/Al_2O_3 followed a linear interdependence between the $?_{OH}$ and $?_H$ (Equation 1) [see also 33 and 34]. According to Equation 1, the signal at 0.0 ppm would

give a stretching frequency at 3810 cm^{-1}. The anion OH^- has a fundamental stretching frequency at about 3839 cm^{-1}, while that of neutral OH neutral lies at about 3735 cm^{-1} [35].

$$\nu_{OH}\,/\,cm^{-1} = 3810 - 40.46\,\delta_H\,/\,ppm \quad (R^2 = 0.998) \qquad (1)$$

The acidic properties of the catalyst surface were further investigated in a series of pyridine adsorption experiments. The results of the Py-IR and Py-TPD study are presented in Figure 4 and Figure 5, respectively.

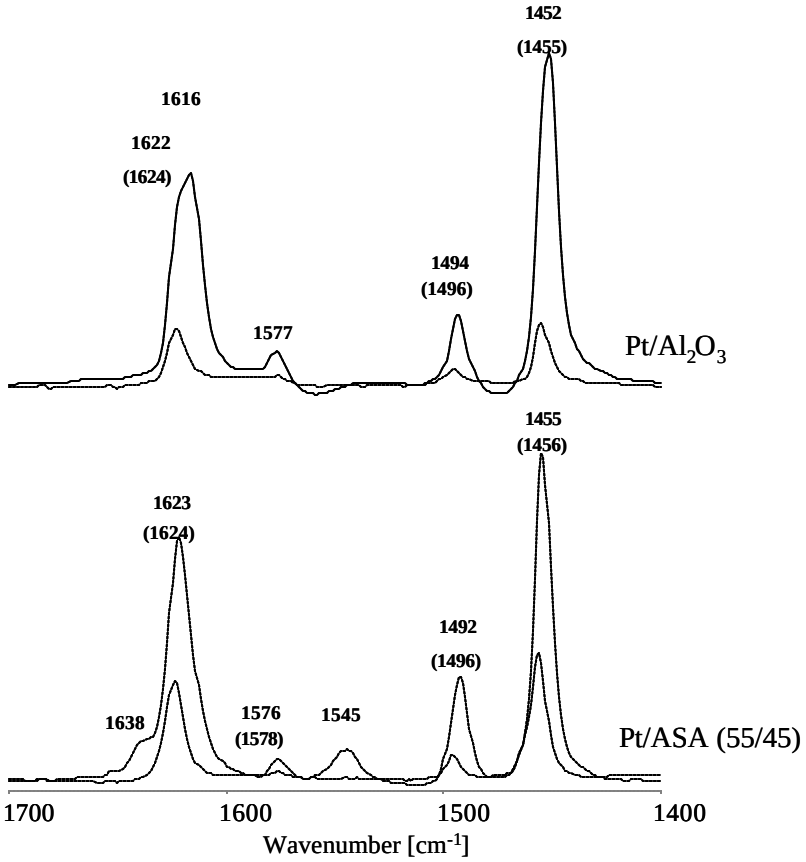

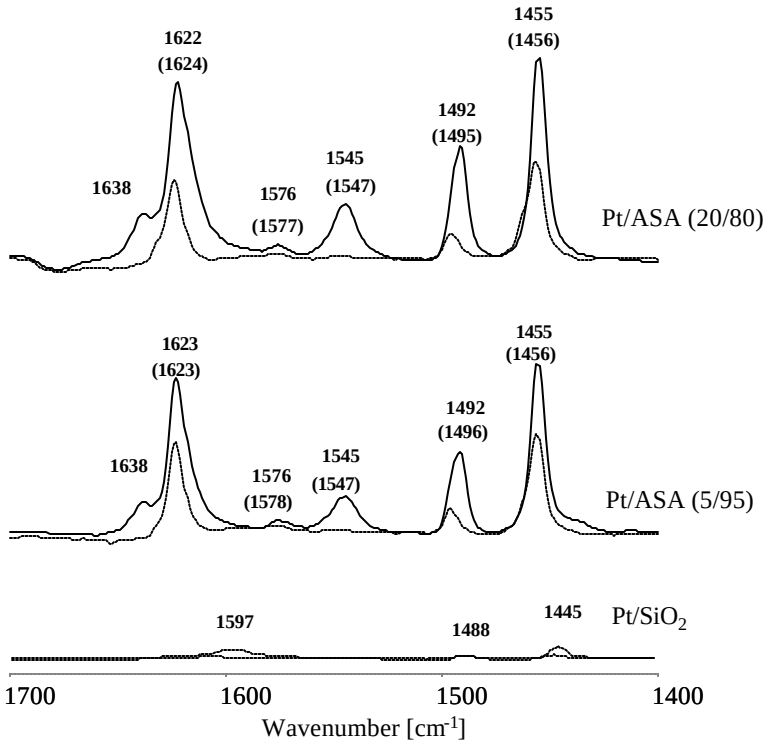

Figure 4. IR study of pyridine adsorbed on the series of alumina, ASA and silica supported Pt-catalysts at T = 423 K, p(Py) = $2 \cdot 10^{-2}$ mbar (continuous lines). Spectra recorded upon temperature treatment (i.e., after degassing at 673 K over 1 h) are also included (dashed lines, band values in brackets).

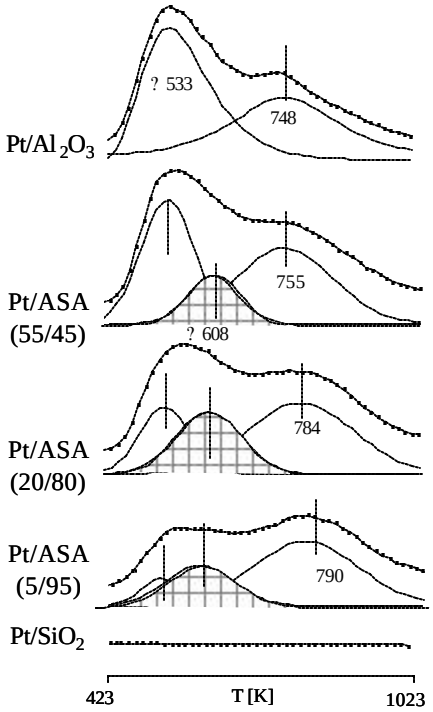

Figure 5. TPD study of pyridine adsorbed on the series of alumina, ASA and silica supported Pt-catalysts.

Pyridine adsorbed at 423 K on Pt/Al_2O_3 showed bands at ca. 1452, 1494, 1577 and 1616 cm^{-1} with a shoulder at 1622 cm^{-1}. Their presence indicated the formation of PyL species. The retention of pyridine after evacuation at 673 K, was evidenced by the bands at 1455, 1496 and 1624 cm^{-1}. Apparently, alumina exhibited strong Lewis acidity. However, a decrease in intensity and a slight increase in the frequency of the maxima was observed. Probably, there were at least two groups of Lewis sites on the surface (i.e., weak and strong ones).

In the spectra of Pt/ASAs samples, apart from the bands indicating the PyL species, an additional band at 1545 cm^{-1} and a broad shoulder at 1638 cm^{-1} were detected. This suggests the formation of pyridinium ions on the surface. After the thermal treatment the intensity of the spectra decreased. In particular, the additional peak at 1545 and the shoulder at 1638 cm^{-1} disappeared almost completely indicating the presence of weak Brønsted acid sites in the material. On the Pt/SiO_2 sample with pyridine only three small peaks were found at 1445, 1488 and 1597 cm^{-1} indicating weak adsorption (e.g. hydrogen-bonded pyridine) [36]. After outgassing at 673 K, the weakly adsorbed PyH completely disappeared.

The deconvoluted Py-TPD profiles (Figure 5) disclosed the presence of two and three pyridine desorption peaks from Pt/Al_2O_3 and Pt/ASAs catalysts, respectively. No peak was observed during temperature programmed desorption of Py from Pt/SiO_2. For the alumina-supported sample, the peak temperatures were estimated at 533(±10) and 748(±10) K. As Al_2O_3 exhibits only Lewis acidity, apparently two types of Lewis acid sites were present. Silica-alumina supports showed similar low- and high- temperature desorption peaks at roughly 530 and 776 K, respectively. The concentration of desorbing species associated with the high- temperature desorption peak was similar for all the samples. However, the relative strength of adsorption increased as the alumina concentration decreased (i.e., peak temperature shifting from 755K to 790 K). However, in contrast to the pure alumina support, an additional medium-temperature peak (at approximately 610 K) was observed upon Py desorption from ASAs-supported samples. Thus, in agreement with the IR data, Brønsted acid sites were detected in the ASA carriers.

Table 3 summarizes the quantification of the Lewis (LAS) and Brønsted (BAS) acid sites arising from Py-adsorption studies.

Catalyst	Concentration of LAS [mmol·g^{-1}]		Concentration of BAS [mmol·g^{-1}]	
	IR	TPD	IR	TPD
Pt/Al_2O_3	0.14	0.13	0.00	0.00
Pt/ASA (55/45)	0.13	0.13	0.02	0.02
Pt/ASA (20/80)	0.09	0.09	0.04	0.04
Pt/ASA (5/95)	0.07	0.08	0.03	0.03
Pt/SiO_2	0.00	0.00	0.00	0.00

Table 3. Concentration of BAS and LAS calculated from Py-IR and Py-TPD.

Py-IR and Py-TPD experiments gave similar concentrations of the different types of acid sites (differences were less than 10 %). The concentration of Lewis acid sites was highest for the Pt/Al_2O_3 catalyst and decreased when the concentration of alumina decreased in the Pt/ASA samples. In contrast, Brønsted acidity was not observed for the Pt/Al_2O_3 catalyst and passed through the maximum concentration of 0.036 mmol·g^{-1} at 20 % concentration of alumina in the ASA-supported catalyst.

3.3 Characterization of platinum nanoclusters

The size histogram, corresponding to about 50 analyzed particles in the TEM micrographs, for the alumina, ASAs, and silica supported Pt-catalyst is reported in Figure 6, which also includes the calculated Pt dispersion obtained by H_2-chemisorption.

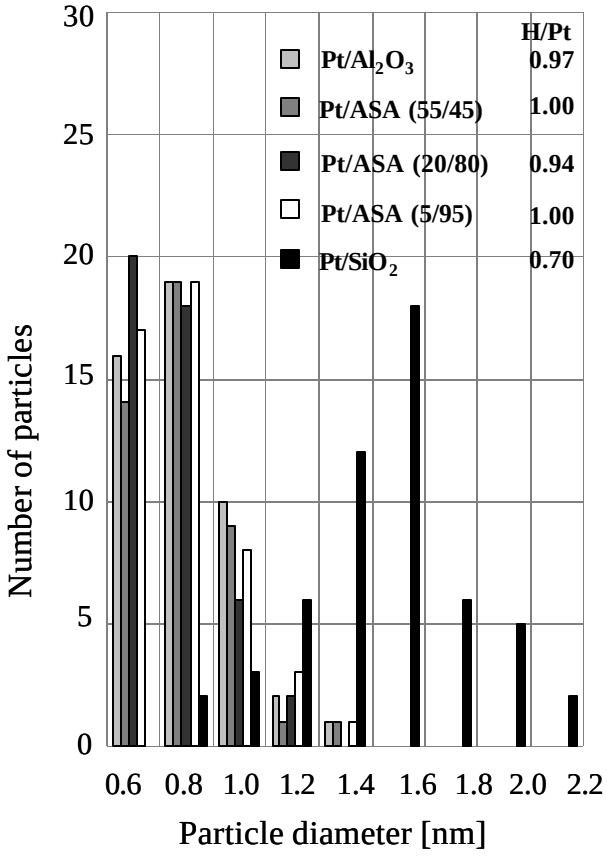

Figure 6. Size histograms corresponding to about 50 analyzed particles, for the alumina, ASAs, and silica supported Pt-catalysts.

For Pt on alumina and ASAs the mean cluster size was about 0.8 nm with a standard deviation of 0.2 nm. Thus, a very narrow particle size distribution was observed. On the other hand, Pt/SiO_2 catalysts exhibited bigger metal clusters (1.5 nm) again with a narrow size distribution (0.3 nm). The metal dispersion obtained from H_2 chemisorption measurements was consistent with the TEM data, indicating a high dispersion of platinum in the case of alumina and amorphous silica-alumina and somehow lower dispersions on the silica support.

In order to calculate the Pt-particle size more accurately, the analysis of the EXAFS measurements was performed based on a particle size modeling.

The Fourier transformed EXAFS of the Pt/ASA catalysts after reduction are plotted in Figure 7. Results of the EXAFS analysis of the reduced samples are reported in Table 4.

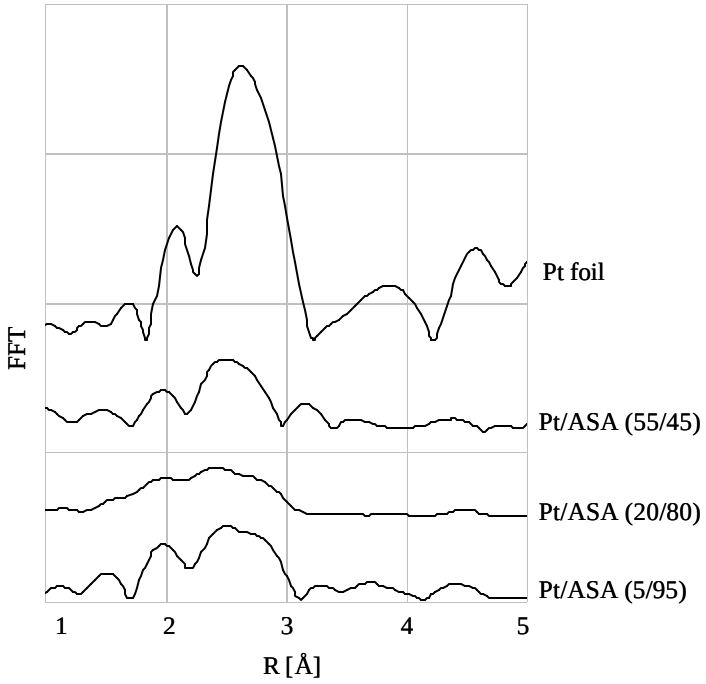

Figure 7. Magnitude of the Fourier transformed oscillations (k2 -weighted) after in-situ H_2 reduction at 588 K.

Catalyst	[1]Particle size [nm]	[2]H/Pt ratio	N_{Pt-Pt}	r_{Pt-Pt} [Å]	$10^3 \cdot ? s^2_{Pt-Pt}$ [Å^2]	? E0 [eV]
Pt/Al_2O_3	0.8 (0.6-1.3)	0.97	4.49	2.59	9.2	-6.17
Pt/ASA (55/45)	0.8 (0.6-1.4)	1.00	3.33	2.66	9.0	5.77
Pt/ASA (20/80)	0.75 (0.5-1.2)	0.94	5.03	2.68	8.7	6.18
Pt/ASA (5/95)	0.8 (0.5-1.3)	1.00	5.75	2.70	8.2	9.27
Pt/SiO_2	1.6 (0.8-2.2)	0.70	8.17	2.75	6.6	9.68

1. TEM measurement; in brackets min – max value
2. Hydrogen chemisorption

Table 4. Results of the EXAFS analysis of the reduced Pt-catalysts.

The small particle size was apparent from the low height of the Pt-Pt first shell (N_1) contribution and the absence of peaks due to a contribution of further shells. The main contribution in the EXAFS resulted from platinum neighbors. The Pt/Al_2O_3, Pt/ASA (55/45), Pt/ASA (20/80), Pt/ASA (5/95) and Pt/SiO_2 showed contributions from the Pt-Pt

coordinations at 2.59, 2.68, 2.66, 2.70 and 2.75 Å corresponding to the coordination numbers of 4.49, 3.33, 5.03, 5.75 and 8.17 respectively. A decrease in the particle size is accompanied by a decrease of the Pt-Pt distance and by an increase in the Debye-Waller factor. The interatomic distance is reduced due to a stronger interaction between the atoms when compared with bulk Pt [37, 38]. The Debye-Waller factor accounts for the disorder in the solid and therefore smaller particles are less ordered and present a higher value of this factor. Assuming a cubooctahedral shape for the platinum particle, it was possible to generate metal clusters by means of a computer program (CERIUS, [39]) and calculate the average coordination number, the metal dispersion and the particle size (Figure 8).

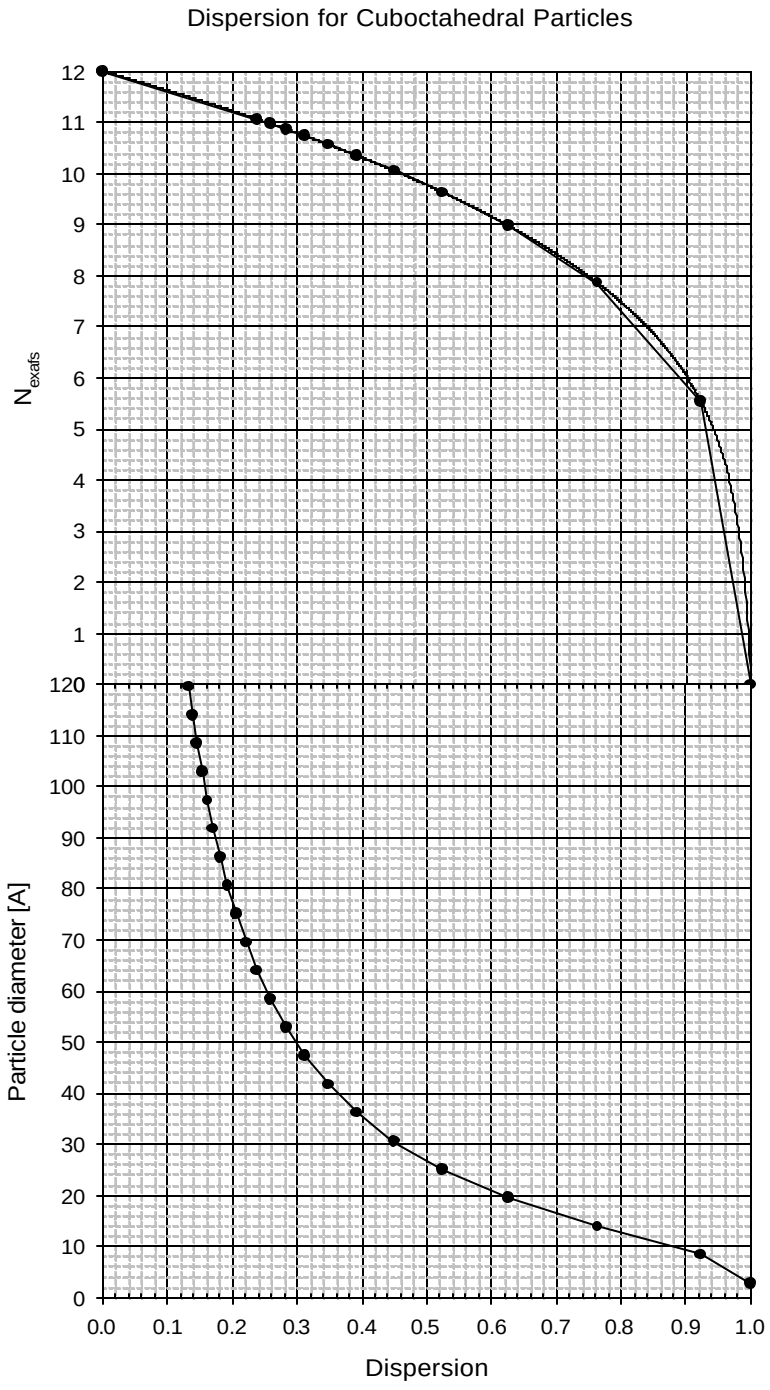

Figure 8. Determination of the platinum particle size based on cubooctahedral morphology.

The calculated Pt particle size for Pt/Al_2O_3, Pt/ASA (55/45), Pt/ASA (20/80), Pt/ASA (5/95) and Pt/SiO_2 is 0.6, 0.5, 0.7, 0.8 and 1.5 nm, respectively.

4 Discussion

The most important characteristics of the amorphous silica-aluminas are related to the concentration and relative ratios of the different kinds of acid sites.

The silica parts of the ASA support have a uniform composition with hydrogen atoms that exhibit hardly any acidic properties. The ASA-supported samples show also Lewis acidity which has been attributed to the presence of alumina patches. Based on the bulk structure of alumina, surface exposed tetra- and octahedral aluminum species would be devoid of one and two oxygen atoms, respectively, to give 3- and 4-coordinated aluminum atoms. Oxygen vacancies in the environment of Al atoms present in the surface lead to weak (a vacancy in the octahedral environment) and strong (a vacancy in the tetrahedral environment) Lewis acid sites as it is observed with the pyridine adsorption experiment.

On the other hand, it is generally accepted that in amorphous silica-alumina the Brønsted acid centers are formed by an isomorphous substitution of Si^{4+} by Al^{3+} ions in the silica lattice (i.e., the aluminosilicate phase). This leads to a net unit negative charge on the alumina tetrahedra, requiring neutralization by a cation, e.g., a proton. Possible structures include aluminum tetrahedra sharing corners or edges with silicon tetrahedra. Alternatively, aluminum octahedra can share corners with the SiO_2 tetrahedra [40]. To better characterize the aluminosilicate phase it is necessary first to analyze pure alumina and silica phases. In the case of alumina, within the restrictions imposed by the spinel lattice and the Al_2O_3 stoichiometry, the fraction of the Al in tetrahedral coordination must be comprised in the range of 25 to 37.5 %. The quantitative 1D ^{27}Al MAS NMR data showed that four-coordinated aluminum accounted for 30 % of total Al and the rest is assigned to six-coordinated Al atoms. Furthermore, ammonia treatment of the Pt/Al_2O_3 sample hardly transforms any Oh-Al into Th-Al species as the pure alumina phase does not exhibit aluminum atoms with flexible coordination. Assuming that the alumina preserves the tetrahedral to octahedral ratio as established for the Al_2O_3-supported catalyst, a direct measurement of the amount of the pure alumina phase within ASA-supported samples can be obtained [25].

4.1 The formation of brønsted acid sites in the ASA-supported platinum catalysts

A dilution of the aluminum content in the ASAs lowers the probability of formation of pure alumina domains. At the same time, the development of the aluminosilicate phase is promoted, in which alumina tetrahedra are separated by silica tetrahedra. Following the center of the chemical shift for four-coordinated aluminum in the ^{27}Al MAS NMR, it can be concluded that most of the tetrahedral aluminum does not interact with neighboring Al atoms at about 20 % concentration of Al_2O_3 in ASA, as revealed by the signal at 52 ppm, compared with the chemical shift of Th-Al in pure alumina at 64 ppm. Interesting structural features for the ASA-supported catalysts could be postulated from the presence of six- and five-coordinated aluminum. Because of homonucleation during the ASA synthesis process it is unrealistic to anticipate a perfect amorphous mixture of alumina and silica tetrahedra on the atomic scale [41]. Indeed, alumina clusters bearing the structural fingerprint of octahedral aluminum are detected with ^{27}Al MAS NMR. However, only a fraction of Oh-Al species can be recognized as a pure alumina phase because some of it undergoes reduction in the coordination number upon ammonia adsorption. The quantification of the aluminosilicate in the ASAs-supported samples has been calculated and is reported in Table 5.

Pt/ASA Catalyst	Concentration of aluminum species [mmol·g^{-1}] (Share of the total aluminum present [%]) in					
	alumina patches		amorphous silica-alumina			total
	Oh-Al	Th-Al	penta-Al	Oh-Al	Th-Al	
55/45	4.84 (47)	2.25 (22)	2.66 (26)	0.29 (3)	0.35 (3)	10.39
20/80	0.44 (11)	0.20 (5)	0.96 (24)	0.76 (19)	1.64 (41)	4.00
5/95	0.11 (13)	0.05 (6)	0.00 (0)	0.15 (18)	0.53 (63)	0.84

Table 5. Distribution of the aluminum species in the Pt/ASA catalysts.

The pentacoordinated aluminum can be tentatively attributed to a highly disordered interphase that connects the alumina patches within the silica/silica-alumina matrix. The

rest of the amorphous silica-alumina is characterized by the presence of: (i) surface-exposed Oh-Al with flexible coordination environment and (ii) Th-Al that can generate Brønsted acid sites. Note that the quantification of the Brønsted acid sites by ^{1}H MAS NMR ($?_{H}$ = 6.7 ppm) is in agreement with the other surface-probing measurements (i.e., Py-IR and Py-TPD). It is probable, that both Oh and Th aluminum species are generated by the aluminosilicate phase. The Oh-Al present in the surface can be coordinated by some extra OH groups or water molecules. On the other hand, aluminum atoms in the tetrahedral species can generate Brønsted acid sites. Interestingly, although every structural AlO_4^- of the aluminosilicate has to be compensated for the charge deficiency, the phase generates very few strong Brønsted acid sites. Also, the ion exchange capacity of the amorphous silica alumina is very low. Therefore, it can be proposed that cationic alumina species compensate in part the negatively charged tetrahedral Al. Isolated Si-O(H)-Al tetrahedra originate stronger Brønsted sites. In contrast, clusters of these tetrahedra that can interact with one another, form rather weak acid sites. Within the domains of high concentrations of tetrahedral aluminum, hydrogen bonding causes polarization of the OH groups. As a consequence a broadening of the ^{1}H NMR signal and the ?(OH) region in the IR spectra (2.5 – 7 ppm and 3200 – 3600 cm^{-1}, respectively) is detected. In fact, even the latter type of Brønsted acid sites corresponds to a relatively mild acid since thermal treatment at 673 K completely removed the pre-adsorbed pyridine species.

4.2 Characterization of platinum phase in the ASA-supported platinum catalysts

For very small Pt-nanoclusters the coordinatively unsaturated (cus) atoms from edges, corners and surfaces represent a significant fraction of the Pt atoms, and consequently, their average coordination number is smaller than in the bulk metal. Hydrogen chemisorption provides a rough estimation of the number of these sites. However, complex phenomena, such as SMSI (i.e., Strong Metal-Support Interaction) or hydrogen spillover can cause a drastic decrease in the chemisorption capacity of the supported metal [42, 43]. Therefore, TEM is needed to confirm information about the size distribution of metal clusters [44]. However, very small metal clusters are damaged by TEM fixing a detection limit of about 0.8 nm. For this reason it is necessary to validate

the results obtained by TEM measurements using EXAFS. This technique provides information on the average atom coordination number and on the particle size when supported by particle modeling computation studies.

For Pt/Al_2O_3, Pt/ASA (55/45) and Pt/ASA (20/80) catalysts, the particle sizes observed by TEM are larger than the ones calculated from EXAFS. A possible reason for this discrepancy can be ascribed to the lower detection limit of TEM that makes it difficult to detect particles smaller than 0.8 nm. For Pt/SiO_2 catalysts presenting higher coordination numbers, there is a very good correlation between TEM and EXAFS data.

The number of Pt-atoms on the surface of the cubooctahedral cluster can be further used in kinetic studies and in the calculation of Turn over frequency (TOF). Finally, as the metal is dispersed into small clusters a possible interaction between the support and the metal can be analyzed. According to Anderson's theoretical calculations [45], this interaction can only occur for particles smaller than 1 nm.

5 Conclusions

Platinum catalysts supported on amorphous silica-aluminas were characterized with a variety of experimental techniques, focusing on the presence of different phases and domains in the amorphous material and the various types of acid sites. The structural information will be correlated with the catalytic activity in hydrogenation reactions. ASA supports can be synthesized with desired concentrations of silica, alumina and aluminosilicate phases. Every phase contributes with a different type of acidity. Weak and strong Lewis acid sites are originated in the alumina clusters while Brønsted acid sites are generated in the aluminosilicate phase. Four types of aluminum-containing species were identified: aluminum (tetrahedral and octahedral) in the form of a separate alumina phase, tetrahedral aluminum in the aluminosilicate phase, surface exposed octahedral aluminum with flexible coordination connected to the aluminosilicate phase and pentacoordinated aluminum connecting the alumina clusters within the silica/silica-alumina matrix.

The concentrations of each type of aluminum could be quantified by ^{27}Al MAS NMR. Up to 40 % of aluminum atoms in Pt/ASA (20/80) were incorporated into the aluminosilicate phase, but this phase was not the only aluminum-containing phase present in these materials. A small fraction of the negatively charged Al-O tetrahedra are compensated by protons leading to the formation of strong Brønsted acid sites. However, some of them are compensated by cationic alumina species. ^{1}H MAS NMR experiments suggest that a smaller concentration of weak Brønsted acid sites exists that may result from domains of high concentrations of tetrahedrally-coordinated aluminum. The different types of acid sites in the materials were characterized and cross-validated by means of 3 different characterization techniques (Pyd-IR, Pyd-TPD and ^{1}H NMR). The Pt particles anchored by wet impregnation were exceptionally small and uniform, i.e., between 0.6 and 0.8 nm on every aluminum containing support.

Acknowledgments

Financial support of S.R.T.C. Amsterdam is gratefully acknowledged. The authors are also grateful to Dr. W. Stork for critical discussions. Martin Neukamm and Xavier Hecht (TUM, TC2) are gratefully thanked for the AAS and BET measurements, respectively. HASYLAB, DESY is acknowledged for the beam time at the X1 experimental station.

6 References

1 J. Scherzer and A.J. Gruia, in 'Hydrocracking Science and Technology', Chapter 12, Dekker, New York, 1996, p. 215.

2 J. Ward, Fuel Process. Technol. 35 (1993) 55.

3 J.A.R. van Veen and S.T. Sie, Fuel Process. Technol., 61 (1999) 1.

4 W.R.A.M Robinson, J.A.R. van Veen, V.H.J. de Beer; R.A.van Santen, Fuel Process. Technol., 61 (1999) 61.

5 J. Klinowski, Progress in NMR Spectroscopy, 16 (1984) 237.

6 A. P.M. Kentgens, Geoderma, 80 (1997) 271.

7 D. D. Laws, H.-M.L. Bitter, and A. Jerschow, Angew. Chem. Int. Ed., 41 (2002) 3096.

8 J.A. van Bokhoven, D.C. Koningsberger, P. Kunkeler, H. van Bekkum, and A.P.M. Kentgens, J. Am. Chem. Soc., 122 (2000) 12842.

9 E. Bourgeat-Lami, P. Massiani, F. Di Renzo, P. Espiau, F. Fajula, Appl. Catal. A-Gen., 72 (1991) 139.

10 M. Hunger, D. Freude, H. Pfeifer, H. Bremer, M. Jynik and K.P. Wendlandt, Chem. Phys. Lett., 100 (1983) 29.

11 D. Freude, Chem. Phys. Lett., 235 (1995) 69.

12 A. W. Czanderna, J. R. Biegen, W. Kollen, J. Colloid Interface Sci., 34 (1970) 406

13 A. Jentys, Phys. Chem. Chem. Phys., 1 (1999) 4059.

14 D. Cook, Can. J. Chem. 39 (1961) 2009.

15 G. Zerbi, B. Crawford and J.Overend, J. Chem. Phys., 38 (1963) 127.

16 J. P. Amoureux, C. Fernandez and S. Steuernagel, J. Magn. Reson. Ser. A, 123 (1996) 116.

17 R. Ernst, G. Bodenhausen and A. Wokaun, Principles of Nuclear Magnetic Resonance in One and Two Dimensions, Oxford University Press, New York, 1987.

18 J. A. van Bokhoven, A.L. Roest, D.C. Koningsberger, J.T. Miller, G.H. Nachtegaal and A. P.M. Kentgens, J. Phys. Chem. B, 104 (2000) 6743.

19 C.A. Emeis, J. Catal., 141 (1993) 347.

20 GRAMS/32 Spectral Notebase Version 4.01 (1991 – 1996), Galactic Industries Corporation.

21 K.V. Klementiv, VIPER for Windows, freeware: http://www.desy.de/~klmn/viper.html.

22 A.L. Ankudinov, J.J. Rehr, Phys. Rev. B 62 (2000) 2437.

23 A.L. Ankudinov, B. Ravel, J.J. Rehr, S.D. Conradson, Phys. Rev. B 58 (1998) 7565.

24 M.-H. Lee, C.-F. Cheng, V. Heine and J. Klinowski, Chem. Phys. Lett., 265 (1997) 673.

25 A. Omegna, J.A. van Bokhoven, and R. Prins, J. Phys. Chem. B, 107 (2003) 8854.

26 H. Koller, E.L. Meijer, RA. van Santen, Solid State Nuclear Magnetic Resonance, 9 (1997) 165.

27 D. Freude, T. Fröhlich, H. Pfeifer and G. Scheeler, Second Workshop on the Adsorption of Hydrocarbons in Microporous Sorbents, Eberswalde, GDR, November 1982, vol. 2, p. 9.

28 K. Sohlberg, S.J. Pennycook, and S.T. Pantelides, Chem. Eng. Comm., 181 (2000) 107.

29 V. M. Mastikihin, I.L. Mudrakovsky and A.V. Nosov, Progress in NMR Spectroscopy (1991) 23: Part 3 259.

30 M. Hunger, D. Freude, H. Pfeifer, H. Bremer, M. Jynik and K.P. Wendlandt, Chem. Phys. Lett., 100 (1983) 29.

31 X. Liu and R.E. Truitt, J. Am. Chem. Soc., 119 (1997) 9856.

32 J. W. Geus, J. A. R. Van Veen in 'Catalysis: An Integrated Approach', Chapter 10, Elsevier Science B. V., The Netherlands, 1999, p. 459.

33 Pfeifer, NMR Basic Principles and Progress, Springer-Verlag, Berlin – Heidelberg, 1994, 31.

34 M. Hunger, Catal. Rev.-Sci. Eng. 39 (1997) 345.

35 L.H. Johnes, J. Chem. Phys., 22 (1954) 217.

36 T.R. Hughes and H.M. White, J. Phys. Chem., 71 (1967) 2192.

37 B. Moraweck, G. Clugnet, A.J. Renouprez, Surf. Sci. 81 (1979) L631.

38 B. Delley, D.E. Ellis, A.J. Freeman, E.J. Baerends, D. Post, Phys. Rev. B 27 (1983) 2132.

39 Cerius2 program suite (Accelrys Inc, 2001).

40 Tanabe, Solid Acid and Bases, Academic Press, New York – London, 1970, p. 58 – 66.

41 Y. Kato, K. Shimizu, N. Matsushita, T. Yoshida, H. Yoshida, A. Satsuma, T. Hattori, Phys. Chem. Chem. Phys., 3 (2001) 1925.

42 S. T. Tauster, S. C. Fung, R. L. Garten, J. Am. Chem. Soc. 100 (1978) 170.

43 P. J. Levy, M. Primet, Appl. Catal. 1 (1981) 31.

44 K. Heinemann, F. Soria, Ultramicroscopy 20 (1986) 1.

45 K. E. Foger, J. R. Anderson, J. Catal. 54 (1978) 318.

Chapter 3

Metal-support interaction: influence of the support on the catalytic activity of platinum for deep hydrotreating

A series of platinum catalysts supported on amorphous silica-alumina (ASA) with varying amounts of alumina (100, 55, 20, 5 and 0 %) were tested in the hydrogenation of tetralin. The hydrogenolysis of neopentane was carried out to probe metal-support interaction. The activity of the nanosized Pt particles was influenced by the electronegativity of the supports with an exception of the neutral silica support. In parallel a compensation effect was observed in both reactions (e.g. ln(A(exp) = m•Ea(exp) + c). This phenomenon was explained assuming a metal-support interaction affecting the adsorption of the reactants. The ratio of Brønsted acid sites (BAS) to Lewis acid sites (LAS) is proposed to govern the sorption properties of the nanosized platinum particles. Furthermore, the electronic structure of the platinum particles was affected by the support as shown by the changes in the X-ray absorption near-edge structure (XANES).

1 Introduction

The formation of diesel particulates in automobile exhaust gases depends on the content of aromatic hydrocarbons. In consequence, the projected environmental regulations strictly limit their maximum level in diesel fuel [1]. Hydrogenation is one of the most promising potential routes to reduce the aromatics concentration leading to fuel components with high cetane numbers. Conventional diesel hydrotreating units based on sulfided NiMo, CoMo, NiW/Al_2O_3 catalysts are effective in decreasing the concentration of S- and N-compounds. However, insufficient reduction levels of diesel aromatics are obtained unless severe operating conditions are applied (i.e., high T and p_{H2}, low space velocities) [2, 3, 4]. To make the economics of the hydrotreating more rational, a follow-up process based on noble metal catalysts (deep catalytic hydrotreatment or DHT) is carried out [5, 6, 7]. Unfortunately, as far as the catalysts are very active in the hydrogenation of aromatics, noble metals are also very sensitive for the residual amounts of sulfur and nitrogen compounds present in the feedstock. It has been shown that the use of acidic supports increases the catalyst resistance towards sulfur poisoning [8, 9, 10]. However, the function of different kinds of acid sites (Brønsted vs. Lewis acidity) and their optimal concentration and strength is still unclear. An unambiguous picture of that phenomenon requires a thorough description of the structural relationship between the support and the platinum particle.

For the hydrogenation of aromatic molecules in the absence of poisons, the support acidity was shown to have a significant influence on the activity of metal-supported catalysts. The rate of benzene hydrogenation was reported to increase with increasing acid site concentration, which was generally explained by an increase of the metal electron deficiency [11]. However, Vannice and co-workers [12, 13] explained the increase in aromatic hydrogenation activity of Pt and Pd supported on acidic supports compared to catalysts on inert supports by the presence of additional hydrogenation sites in the metal–acid interfacial region, contributing to the overall rate of aromatic hydrogenation.

In this contribution different explanations accounting for the increase in activity are explored by studying a series of platinum nanoparticles supported on amorphous silica-alumina (ASA) with varying amounts of alumina (100, 55, 20, 5 and 0 %), in relation to the acidity and electronegativity of the support without any poison in the feed.

The hydrogenation of tetralin and the hydrogenolysis of neo-pentane were carried out as probe reactions. Tetralin is a typical molecule targeted in DHT. Under the reaction conditions studied (p_{H2} = 50 bar, T < 473 K), the formation of the hydrogenated products (i.e., *cis*- and *trans*-decalins) is thermodynamically strongly favorable [14]. The hydrogenation of C=C double bonds on metals should be intrinsically *cis* in character [15]; however, the formation of *trans*- decalin is always observable [16]. According to Weitkamp [17], it depends on the consecutive desorption and re-adsorption of a partially hydrogenated intermediate, ? ^{1,9} – octalin, as shown in Figure 1.

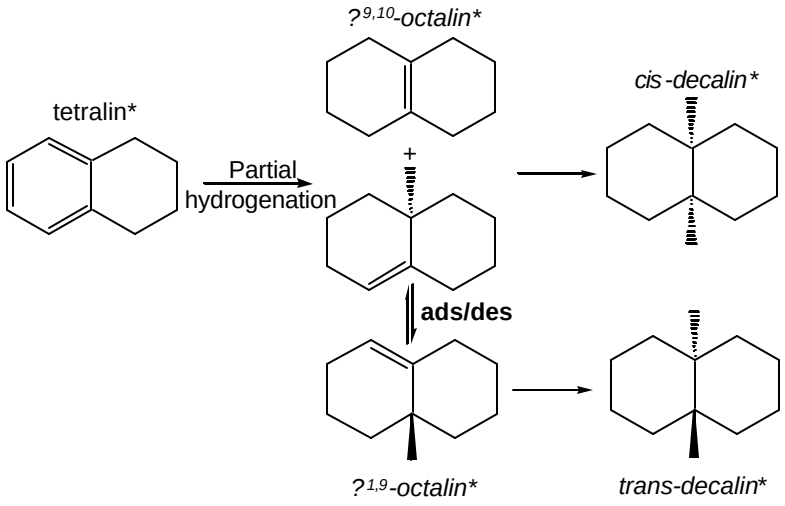

Figure 1. Step-hydrogenation of an adsorbed tetralin molecule to *cis*- and *trans*-decalin.

Any factors that reduce the strength of interaction of the olefinic intermediate with the surface will also favor the selectivity for the *trans* isomer. Therefore, the *cis* to *trans* selectivity could be considered as an indication of electronic effects in catalysis on metals [18,19]. Further, the activity of platinum nanoclusters was observed in the hydrogenolysis of neopentane. The reaction depends exclusively on the catalytic activity of platinum. The path is intrinsically monofunctional since neopentane cannot form an alkene intermediate and below 573 K no protolytic cracking of neopentane is observed. Figure 2 depicts the possible reaction products associated with either hydrogenolysis (i.e., methane and iso-butane) or isomerisation (i.e., isopentane).

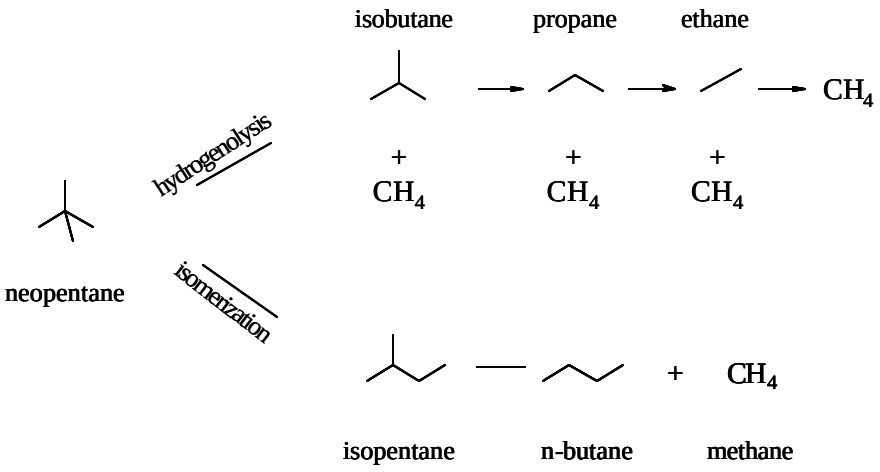

Figure 2. The hydrogenolysis of neopentane. Consecutive reaction taking place only on the metal sites.

In the present study, no products obtained from the neopentane isomerization were observed.

In order to determine the electronic properties of platinum particles on the different ASA-carriers, X-ray absorption spectroscopy was carried out. The interpretation of changes in the intensity of the XANES spectra is fairly complex because a number of factors may play a role. It has been reported that the white line intensity is affected by the metal, the chemical state of the atoms, the measuring temperature, the presence of an adsorbate on the surface of the metal particle, the size of the metal clusters and the support [20, 21, 22, 23]. In the present study the investigation of the effect of the support on the electronic properties of the Pt-nanoclusters will be analyzed.

2 Experimental

2.1 Catalytic testing

All chemicals used in the study were obtained from commercial suppliers and used as provided: tetralin (Aldrich, 99 % GC assay), hexadecane (Merck, > 99 % GC assay), n-tetradecane (Aldrich, > 99 % GC assay), *cis*- and *trans*-decalin (Aldrich, 99 % GC assay), hydrogen (Linde AG) and neopentane (Messer Griesheim GmbH, 5 vol % in hydrogen).

The hydrogenation of tetralin (20 wt. % in a mixture with hexadecane and n-tetradecane) was carried out in a trickle-bed reactor operated in continuous down-flow mode (Figure 3).

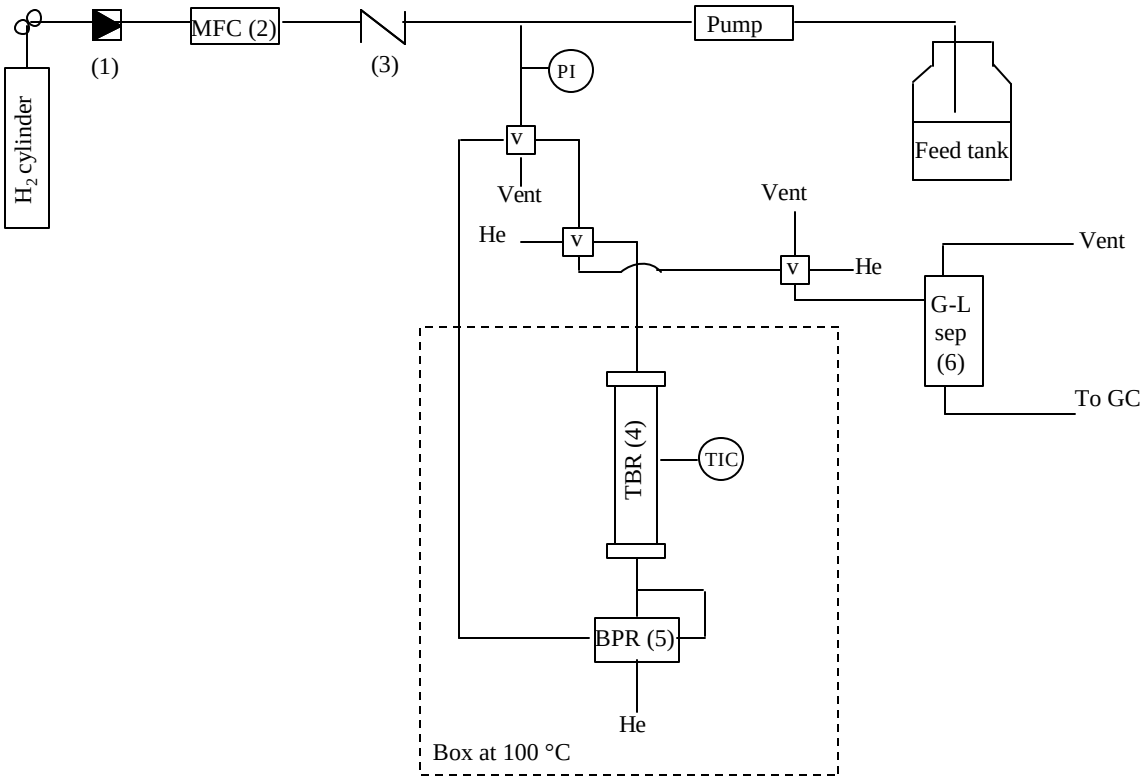

Figure 3. Simplified flow diagram of continuous hydrogenation test unit. (1) pressure reducer, (2) mass flow controller; (3) check valve; (4) trickle bed reactor; (5) back pressure regulator; (6) gas-liquid separator.

The reactor was filled with catalyst (particle size 300-600 µm) diluted with silicon carbide to ensure a homogenous thermal distribution. As an extra precaution, two inert layers (i.e., SiC and glass wool) were placed on the top of the catalyst bed to

avoid any entrance effects. The liquid feed and hydrogen was dosed by an HPLC Gilson pump (model 5cc) and a Bronkhorst EL-FLOW mass flow controller, respectively. Both reactants were mixed before entering the reactor. The variation of the amount of catalyst and the total flow rate, maintaining constant the space velocity, led to unmodified conversion values (i.e., negligible external transport limitations). The catalytic behavior was found to be independent of the particle diameter (i.e., no intraparticle gradients). The performance of the reactor and the accuracy of the analytical method were studied by feeding the organic solution to the reactor filled with SiC, operating at 463 K under 50 bar hydrogen pressure. No formation of unexpected products was detected with a recovery percentage of the tetralin of 99%.

During the experiment, a number of samples were taken for off-line GC-analyses. The analyses were carried out on an HP Gas Chromatograph 6890 equipped with an Agilent DB-1701 column. n-Tetradecane (1.5 wt. % in the feed) was used as the internal standard. Prior to the activity test, the catalysts were reduced *in situ* in hydrogen (p = 1 bar, flow rate 30 $cm^3 \cdot min^{-1}$, 2 h at 588 K). To preserve the high metal dispersion a very slow heating rate of 0.41 $K \cdot min^{-1}$ was applied to reach the temperature of reduction. The catalyst testing was carried out at 453 K and 50 bar hydrogen pressure in a weight hourly space velocity (WHSV) range varying between 90 and 250 h^{-1}. A shift in space velocity was achieved by a change in the amount of catalyst and/or the flow rate (a constant molar ratio of H_2 to the feed of 20.5 was maintained). In order to determine the apparent energy of activation ($E_{a(exp)}$) the hydrogenation was carried out at 433, 443, 453 and 463 K and at constant WHSV and hydrogen pressure of 125 h^{-1} and 50 bar, respectively.

The neopentane hydrogenolysis was studied in a set of 20 parallel reactors controlled by individual digital mass flowmeters and pressure regulators. The catalyst sample diluted with SiC, was pre-reduced *in situ* according to the procedure described above, and the neopentane/hydrogen blend was fed to the system. Temperature was varied in the range 563 to 588 K and the total gas flow in the range 5 to 25 $cm^3 \cdot min^{-1}$, while pressure was set at 1 bar. To analyze the products of hydrogenolysis, an HP-MicroGC (GC M200) chromatographic system with a very fast analysis rate (< 2 min for the C1 – C6 products) was used.

X-ray absorption spectra were collected on beamline X1 at HASYLAB, DESY, Hamburg, Germany. The storage ring was operated with an electron energy of 4.5 GeV and an average current of 100 mA. The Si (311) double crystal monochromator

was detuned to 60 % of the maximum intensity to minimize the intensity of higher harmonics in the X-ray beam. Fresh catalysts were prepared as self-supporting wafers reduced in situ (H_2, T = 588 K over 2 h). X-ray absorption spectra were collected at the Pt L_{III} edge (11564 eV) (T = 323 K) and analyzed with the Viper software [24]. White lines were broadened by hydrogen adsorption in relation to the metal foil and, therefore, the intensity of the Pt/ASA white lines was obtained from the integration of the peak areas (using a baseline of 1 in all the cases).

3 Results and discussion

3.1 Characterization of the supported Pt-catalysts

A detailed study of the nature, concentration, strength and origin of different types of acid sites present in these catalysts has been reported elsewhere [25]. The bulk and surface characterization of the supported platinum catalysts together with the particle size of the Pt clusters are summarized in Table 1.

Catalyst	Composition [wt. %]			Acidity [mmol·g^{-1}]		EXAFS particle model. Pt-size [nm]	S_{int}
	Pt	SiO_2	Al_2O_3	BAS	LAS		
Pt/Al_2O_3	0.78	0.0	99.3	0.00	0.14	0.6	2.70
Pt/ASA (55/45)	0.82	46.1	52.9	0.02	0.13	0.5	2.86
Pt/ASA (20/80)	0.81	78.7	20.4	0.04	0.09	0.7	2.98
Pt/ASA (5/95)	0.78	94.9	4.3	0.03	0.07	0.8	3.04
Pt/SiO_2	1.03	99.1	0.0	0.00	0.00	1.5	3.05

Table 1. Characterization of the supported Pt-catalysts: chemical composition, textural properties and intermediate electronegativity of the support according to Sanderson.

All the supports had mesoporous structure, thus, no diffusion limitations of the bulky aromatic molecules were expected. Note, that the set of catalyst studied showed a progressive modification of the acidic properties with respect to Lewis and Brønsted acidity. The silica-supported Pt-catalyst was used as a neutral reference material. Average sizes of metal clusters were small and similar for the different catalysts (except for Pt/SiO_2). Moreover, the particle size distribution was narrow as confirmed by TEM. As a result, the localized effect of the acid sites on the catalytic properties of the Pt-nanoclusters could be investigated. Further, the intermediate electronegativity of the support (i.e., the Sanderson electronegativity [26]) changed progressively among the series of catalysts and could be used to correlate its value with the catalytic behavior of Pt-nanoclusters.

3.2 Hydrogenation of tetralin

The hydrogenation of tetralin was used as a test reaction to compare the catalytic activity of Pt-catalysts on different supports. For every catalyst tetralin hydrogenation was the predominant reaction (Figure 1). Hardly any secondary reactions that could be expected for catalysts exhibiting acid sites were observed (e.g., isomerization, hydrocraking). Apparently, up to 463 K, the acid sites found in the support could not catalyze any by-product formation. It was further observed that the carbon mass balance in the liquid phase was close to 100 %. Thus, no reaction products were present in the gas phase. A typical conversion profile vs. time on stream (TOS) is shown in Figure 4.

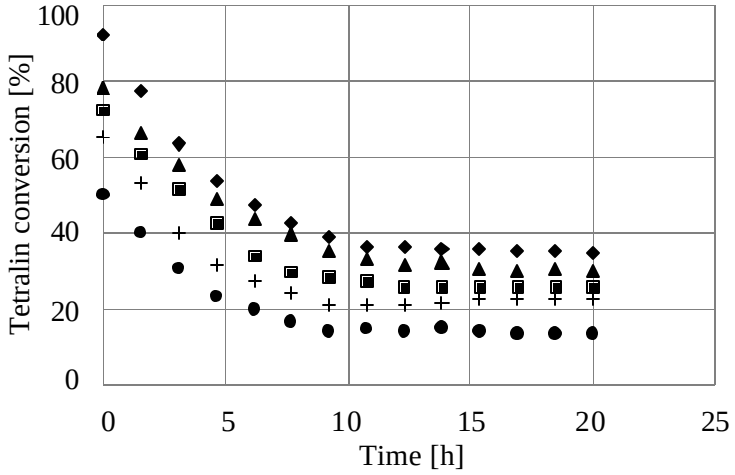

Figure 4. The hydrogenation of tetralin over Pt/ASA (20/80) at 453 K and WHSV= 90 h^{-1} (?), 115.4 h^{-1} (?), 123.8 h^{-1} (¦), 141.7 h^{-1} (+) and 249.9 h^{-1} (?).

The initial conversion of tetralin decreased within the first 15 h. At higher TOS, a constant conversion level was maintained. Based on a Langmuir–Hinshelwood (LH) model a first order dependence on the hydrocarbon reactant was found to describe the kinetics of the hydrogenation of tetralin at the steady-state reaction conditions (Equation 1, where X_{tet} is the conversion of tetralin under steady state and k is the product of the surface reaction rate constant and the reactants adsorption constant) [see also 27, 28, 29, 30]. A typical fitting procedure is reported in Figure 5.

$$? \ln ?1 ? X_{tet} ? ? \frac{k}{WHSV} \qquad (1)$$

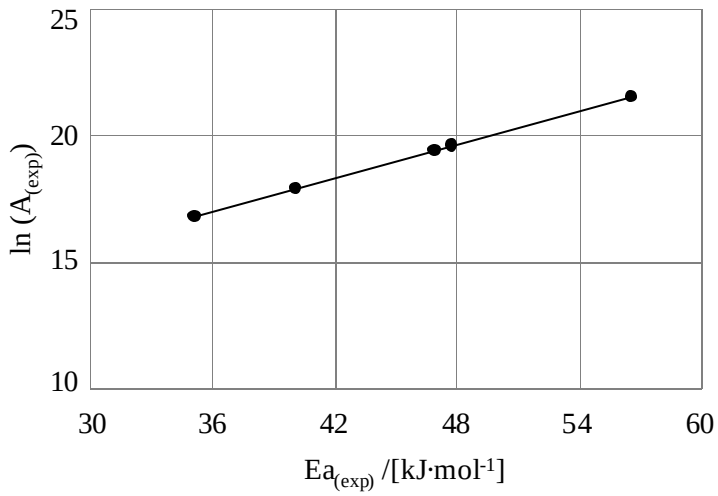

Figure 7. Constable plot of the ln (A_{exp}) vs. E_{exp} found for the hydrogenation of tetralin over a series of Pt-catalysts supported on alumina, ASA and silica carriers.

From the results presented so far it is established that the Pt-clusters are more active on more electronegative supports.

The occurrence of compensation behavior is a direct result of experimental or apparent kinetic measurements of a reaction that proceed at comparable rates over the same temperature range wherein the concentration of surface reactive species is not constant. Thus, the compensation relation points to a possibility of a correlation of the apparent values for ln($A_{(exp)}$) and $Ea_{(exp)}$ with the intrinsic kinetic parameters via the thermodynamic properties of the sorption of reactants. Bond et al. discussed extensively the compensation phenomena in heterogeneous catalysis [31]. In general terms, the apparent activation energy is the sum of the true activation energy (Ea) and the enthalpy of adsorption ($?H_{ads}$) (Equation 2).

$$E_a \; ? \; E_{a\,?\exp ?} \; ? \; ? \; n_i ? H_i \qquad (2)$$

For the hydrogenation of tetralin, the decrease in the Ea(exp) calculated for the more active Pt nanoclusters can be explained by an increased heat of adsorption of tetralin on the more electron-deficient metal. On the other hand, increasing the strength of adsorption reduces translation and rotational motions. So a loss of entropy is expected, that is present in the experimentally derived pre-exponential factor (A (exp)).

Furthermore, the hydrogenation of tetralin was dependent on the intermediate electronegativity of the support at any temperature conditions (Figure 8).

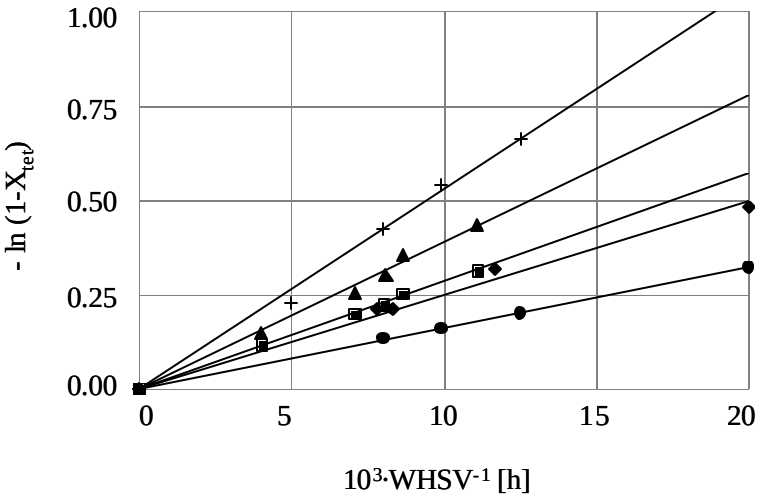

Figure 5. Pseudo-first order kinetic fitting of the hydrogenation of tetralin over Pt/Al_2O_3 (?), Pt/ASA (55/45) (¦), Pt/ASA (20/80) (?), Pt/ASA (5/95) (+), and Pt/SiO_2 (•) at 453 K.

The Arrhenius plot (Figure 6) was used to derive the apparent energy of activation ($Ea_{(exp)}$) in the hydrogenation of tetralin over different ASA-supported Pt catalysts.

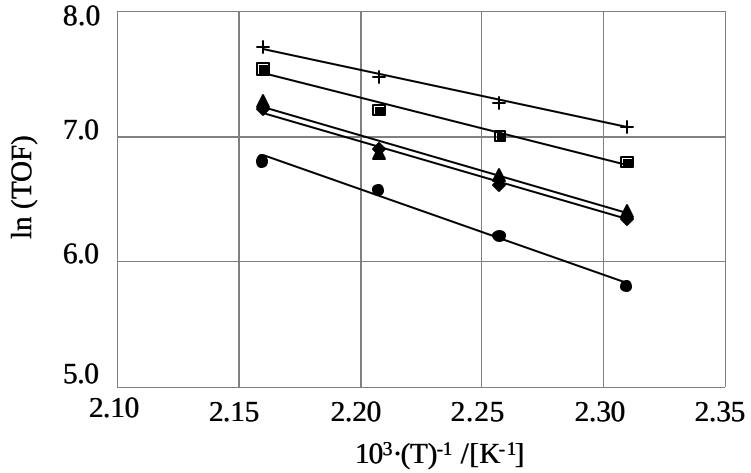

Figure 6. Arrhenius plot over Pt/Al_2O_3 (?), Pt/ASA (55/45) (¦), Pt/ASA (20/80) (?), Pt/ASA (5/95) (+), and Pt/SiO_2 (•) in the temperature range from 433 K to 463 K.

The $Ea_{(exp)}$ over Pt/Al_2O_3, Pt/ASA (55/45), Pt/ASA (20/80) and Pt/ASA (5/95) was calculated as 48, 47, 40 and 35 $kJ \cdot mol^{-1}$, respectively. Apparently, a decrease in the $Ea_{(exp)}$ followed a decrease in the nominal concentration of alumina in the supports. In contrast, over the Pt/SiO_2 catalyst the $Ea_{(exp)}$ was 57 $kJ \cdot mol^{-1}$. Further, a compensation behavior was detected that indicated a linear correlation in the increase in $Ea_{(exp)}$ compensated by the increase in $A_{(exp)}$ (Figure 7).

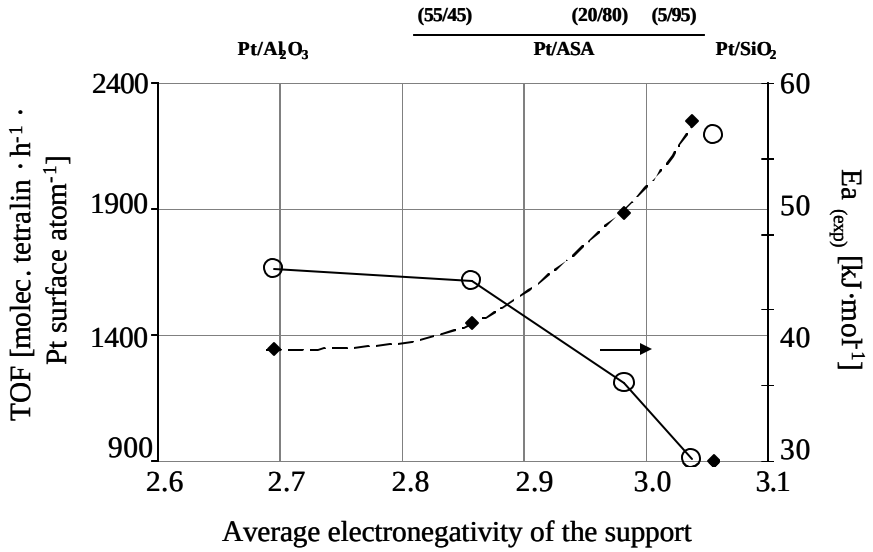

Figure 8. Changes in the apparent energy of activation in the rate of tetralin hydrogenation (463 K) over Pt catalysts supported on carriers exhibiting different average electronegativities (Sanderson electronegativity).

A higher intermediate electronegativity of the support resulted in lowering the apparent energy of activation of the reaction. In line with the previous observations, the Pt/SiO_2 was again outside the correlation. The trend can again be explained by higher heats of adsorption of tetralin onto progressively more electron-deficient platinum nanoparticles.

Further insight into the electron deficiency of Pt-nanoparticles was obtained from the *cis* / *trans* selectivity of the final hydrogenation product (Figure 9).

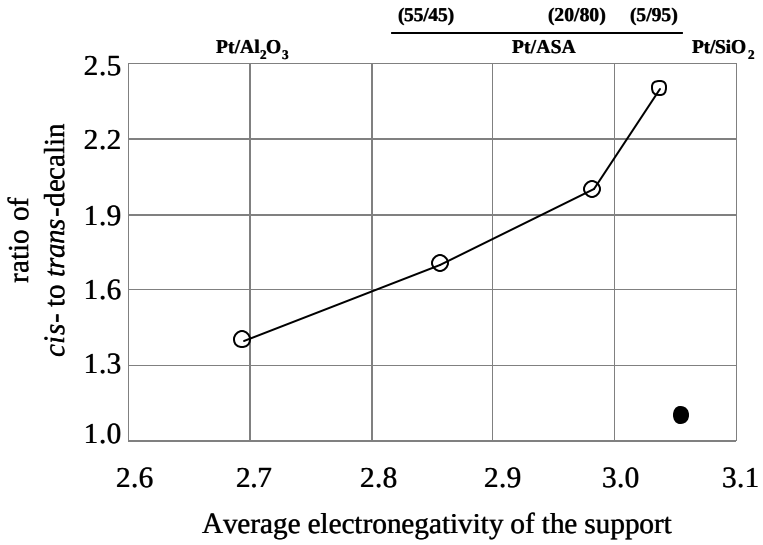

Figure 9. Dependence of cis- to trans-decalin selectivity on the intermediate support electronegativity of the Pt-catalysts at approximately 21 % conversion level of tetralin (T = 453 K, 50 bar).

To exclude the change of the isomer ratio upon the thermodynamically driven shift of the *cis* to the *trans* product after secondary re-adsorption of decalines, a blank experiment was performed. As the isomerization of decalins was kinetically retarded it was concluded that the comparison was valid. The fraction of the *cis*- to the *trans*-isomer increased as the intermediate electronegativity of the support increased with higher Si to Al ratios. Apparently, a weaker adsorption of tetralin on the metal favors the formation of the *trans* isomer while a stronger adsorption will lead directly to the formation of *cis-decalin*. This further confirms an effect induced by the support on the nano-size platinum particles [32]. Platinum supported on silica that was assumed to exhibit the highest electronegativity among the different supports, did not follow this trend. Presumably, to induce an electron deficiency in platinum particles, the carrier has to exhibit some Lewis acidity.

3.3 Hydrogenolysis of neopentane

The kinetics of the hydrogenolysis of neopentane was explored to investigate further the activity of platinum nanoclusters on different supports. It was noted that initially at given reaction conditions, the conversion level decreased with time on stream followed by a period of a constant conversion. Thus, an induction period in the hydrogenolysis of neopentane over every catalyst was observed. For this reason the calculation of the reaction rate had to be performed at a TOS value of more than 2 h. The typical product distribution at different conversion levels is shown in Figure 10.

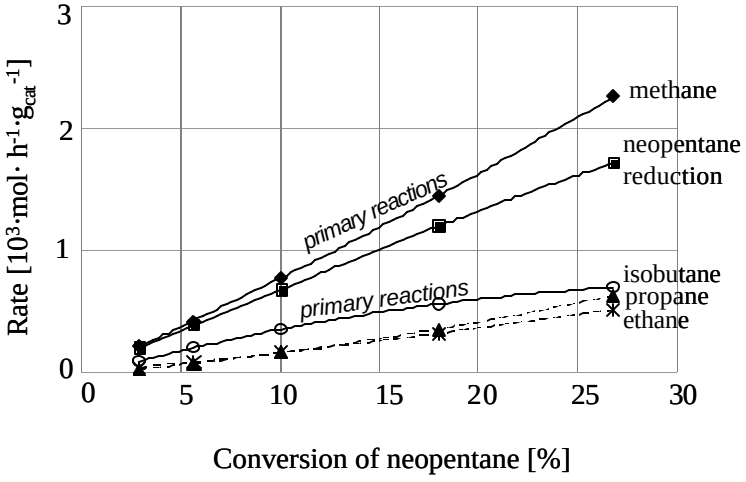

Figure 10. Product distribution (T = 588 K, WHSV = 0.5 – 2.5 h^{-1}) vs. neopentane conversion over Pt/ASA (5/95).

Over every catalyst tested the product distribution was fairly the same and included methane, ethane, propane and isobutane. Thus, only the products of hydrogenolysis were formed (i.e., no isopentane was found). The kinetic parameters of the Arrhenius equation were determined (Figure 11).

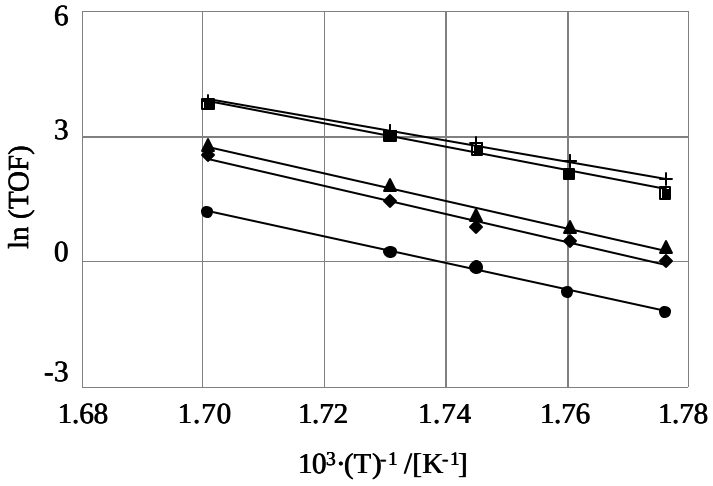

Figure 11. Arrhenius fitting obtained for the hydrogenolysis of neopentane over Pt/ASA (5/95) (+), Pt/ASA (55/45) (■), Pt/ASA (20/80) (▲), Pt/Al_2O_3 (◆), and Pt/SiO_2 (●) in the temperature range from 563 to 588 K.

The $Ea_{(exp)}$ calculated for the conversion of neopentane decreased with a dilution of the alumina content in the catalysts carriers (284, 273, 234 and 209 $kJ \cdot mol^{-1}$ for Pt/Al_2O_3, Pt/ASA (55/45), Pt/ASA (20/80) and Pt/ASA (5/95), respectively). A significant reduction in the energy of activation between the alumina and ASA (5/95)-supported platinum (i.e., $\Delta Ea_{(exp)}$ = 76 $kJ \cdot mol^{-1}$), was observed. Apparently, the activity of platinum nanoclusters was enhanced by a metal-support interaction. Similar observations in the hydrogenolysis of neopentane have been reported for different metals supported on acidic carriers [33]. The Pt/SiO_2 catalyst with $Ea_{(exp)}$ = 265 $kJ \cdot mol^{-1}$ was outside the discussed trend. Figure 12 compares the TOF of the neopentane hydrogenolysis (588 K) with the changes in energy of activation over the different Pt-supported catalyst.

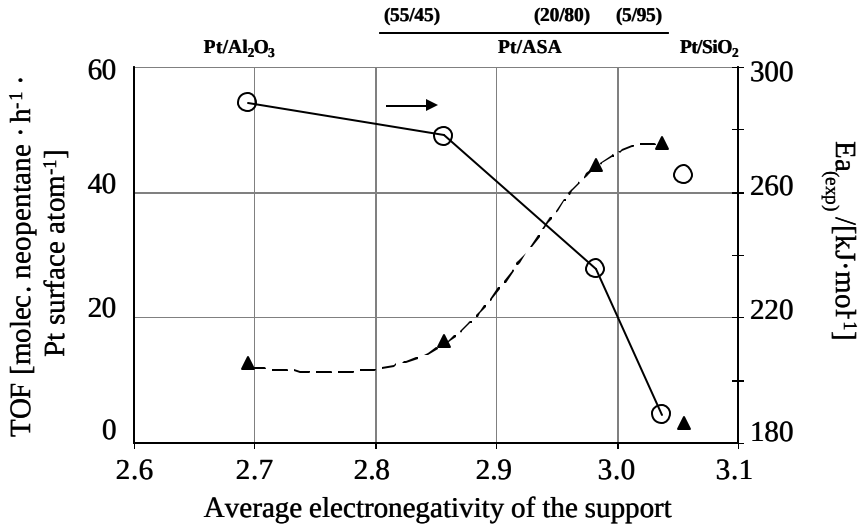

Figure 12. Changes in the apparent energy of activation and in the hydrogenolysis of neopentane (588 K) over Pt catalyst supported on carriers exhibiting different average electronegativities (Sanderson electronegativity).

The compensation effect, that had been found in the hydrogenation of tetralin (*vide supra*) was also present in the hydrogenolysis of neopentane (Figure 13). On more electron deficient metal particles, a higher heat of adsorption together with the loss of entropy of neopentane, can explain the observed compensation effect. This effect has been regularly observed for hydrogenolysis reactions [20, 27, 34, 31].

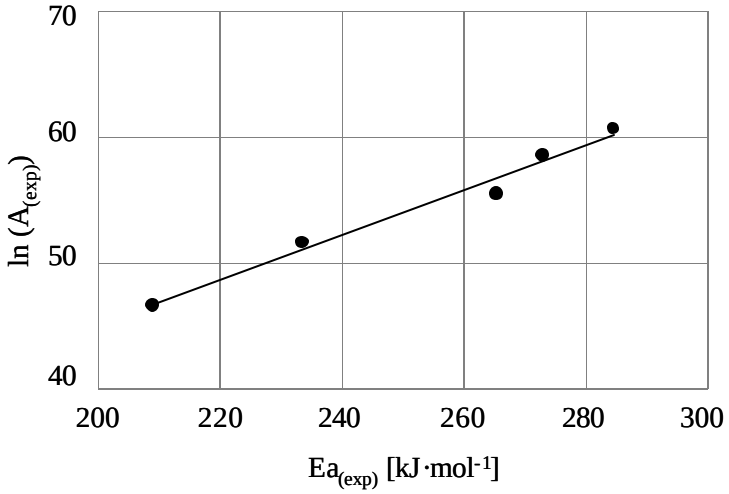

Figure 13. A Constable plot of $\ln(A_{exp})$ vs. $Ea_{(exp)}$ found for the hydrogenolysis of neo-pentane over a series of Pt-catalysts supported on alumina, ASA and silica carriers.

Figure 14 shows a correlation of the catalytic activity for the hydrogenolysis of neo-pentane versus the hydrogenation of tetralin.

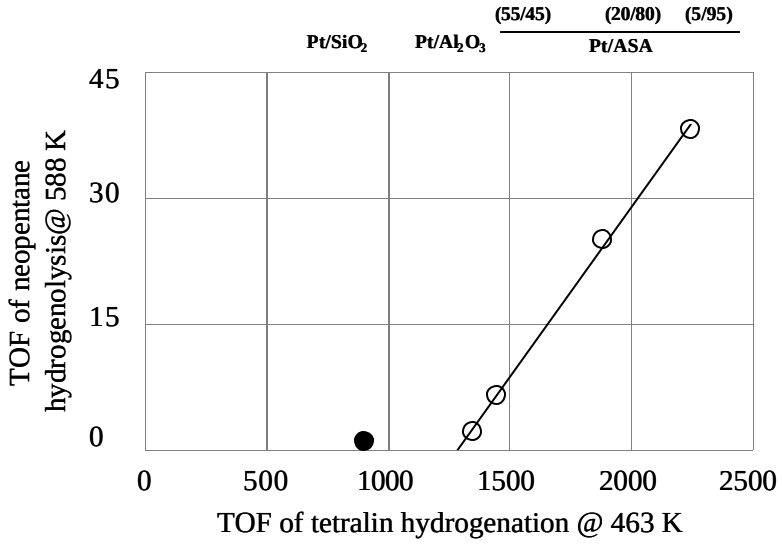

Figure 14. Rate of the hydrogenolysis of neo-pentane (T = 588 K) vs. rate of tetralin hydrogenation (T = 463 K) over different Pt-catalysts.

The rate of hydrogenolysis of neopentane increased with intermediate electronegativities of the supports in the same way observed during the hydrogenation of tetralin. This indicates that the metal-support interaction is responsible for the different Pt activities found on the various supports. It cannot be excluded, however, that the positive intercept at the x-axis indicates that a larger number of surface metal atoms are involved in hydrogenation than in hydrogenolysis or that a second pathway exists that does not follow the hydrogenation route on the metal. The rates of both reactions increased with intermediate electronegativities and, hence, with increasing covalences of the supports. This points to a higher potential acid strength of accessible Lewis acid sites with increasing concentration of silica in ASAs. Following the generally accepted interpretation that the variation in the activity for hydrogenolysis is ascribed to a stronger electron deficiency of Pt, the low activity of Pt/SiO_2 suggests that Lewis acid sites are indispensable for inducing a direct electronic effect on Pt.

3.4 Electronic structure of platinum by XANES

The electronic properties of platinum particles on the different ASA-supports were studied by X-ray absorption spectroscopy (XANES). The results are shown in Figure 15.

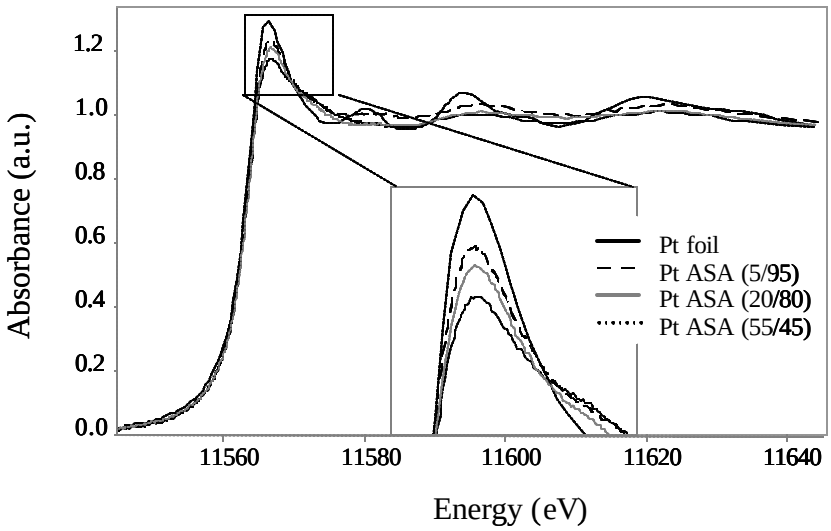

Figure 15. Normalized XANES spectra at L_{III} edge at 323 K under H_2.

The intensity of the white line in the XANES spectra at the L_{III} edge of the Pt/ASA catalysts varied for the different ASA carriers. Apparently, the electron density of platinum was dependent on the composition of the support. Further, the spectra were located below that recorded for the platinum foil. This could indicate a higher electron density on the metal nanoclusters than in the bulk (i.e. the Pt-foil). Probably, hydrogen could act as an electron donor. One of the factors affecting the intensity of the white line in the present study is the size of the metal clusters. However, Ichikuni et. al. [35] found that the effect of small platinum particles (< 1.5 nm) on the white line intensity upon hydrogen adsorption is insignificant. Another explanation includes a metal-support interaction. Figure 16 discloses a linear relationship between the area of the peak above the L_{III} edge and the composition of the ASA support.

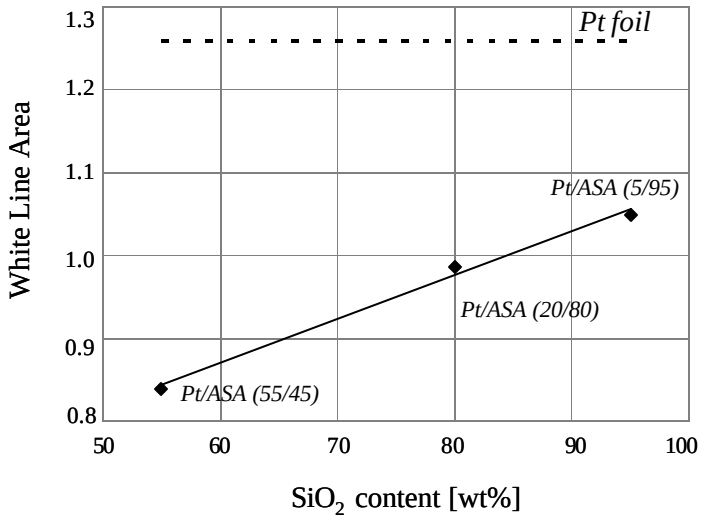

Figure 16. Area of the white line as a function of the silica content in the support.

The platinum electron density of the different ASA carriers decreased upon increasing silica content in the support (and upon increasing the electronegativity of the support). As a result of the changes in the electronic structure of Pt, the adsorption of reactants (enthalpy, concentration of surface species) is expected to be altered.

4 Conclusions

In this study, it was shown that the hydrogenation of tetralin takes place on the metal sites and therefore the main contribution to the observed reaction rate is caused by an interaction of the support with the metal. A metal-support interaction originates a change in the activity of platinum nanoparticles. The influence of the support under these conditions seems to follow the model of an electronic interaction with Lewis acid sites that are therefore necessary for materializing this effect. XANES spectra suggest that these variations in the metal properties influence the adsorption of the reactants.

Acknowledgments

Financial support of S.R.T.C. Amsterdam is gratefully acknowledged. The authors are also grateful to Dr. W. Stork for critical discussions. Andreas Marx and Xavier Hecht (TUM, TC2) are gratefully thanked for setups troubleshooting. HASYLAB, DESY is acknowledged for the beam time at the X1 experimental station.

5 References

1 European Union, E.U. Directive 98/70/EC (1998).

2 T. A. Cavanaugh, D. S. McCaffrey Jr., W. M. Gregory, Hydrocarbon Technology International, Summer (1994) 23.

3 S. A. Ali and M. A. B. Siddiqui, React. Kinet. Catal. Lett., 61(2) (1997) 363.

4 S. L. Lee, M. De Wind, Oil & Gas J., August (1992) 88.

5 J. K. minderhoud, J. Lucien, Eur. Patent, 303.332 (1998).

6 J. P. Van den Berg, J. P. Lucien, G. Germanie, G. L. B. Thielemans, Fuel Proc. Tech. 35 (1993) 119.

7 A. Stanislaus, B.H. Cooper, Catal. Rev. Sci. Eng. 36 (1) (1994) 75.

8 Pawelec B, Mariscal R, Navarro RM, van Bokhorst S, Rojas S, Fierro JLG. Appl. Catal. A General 225 (2002) 223 and references therein.

9 Navarro RM, Pawelec B, Fierro JLG, Vasudevan PT, Cambra JF, Güemez B, Arias PL. Fuel Process Technol 61 (1999) 73.

10 Reinhoudt HR, Troost R, van Langeveld AD, Sie ST, van Veen JAR, Moulijn JA. Fuel Process Technol 61 (1999) 133.

11 A. de Mallman, D. Barthomeuf, J. Chem. Phys. 87 (1990) 535.

12 P. Chou, M.A. Vannice, J. Catal. 107 (1987) 129.

13 S.D. Lin, M.A. Vannice, J. Catal. 143 (1993) 563.

14 Thermodynamic Calculation was performed in HSC Chemistry for Windows 5.1, Outokumpu Research Oy, P.O. Box 60, FIN – 28101 Pori, Finland.

15 K. Schrage, R. L. Burwell, J. Am. Chem. Soc. 88 (1966) 4555.

16 E. P. Martins, D. A. G. Aranda, F. L. P. Pessoa, J. L. Zotin, Braz. J. Chem. Eng. 17 (2000) 1603.

17 A. W. Weitkamp, Adv. Catal. 18 (1968) 1.

18 L. Fisher, V. Harlé and S. Kasztelan, Hydrotreatment and Hydrocracking of oil fractions 31 (1996) 261.

19 A. D. Schmitz, G. Bowers and C. Song, Catal. Today 31 (1996) 45.

20 H. Yoshitake, Y. Iwasawa, J. Phys. Chem 95 (1991) 7368.

21 H. Yoshitake, Y. Iwasawa, J. Catal. 131 (1991) 276.

22 H. Yoshitake, Y. Iwasawa, J. Phys. Chem 96 (1992) 1329.

23 D. R. Short, A. N. Mansour, J. W. Cook Jr., D. E. Sayers, J. R. Katzer, J. Catal. 82 (1983) 299.

24 K.V. Klementiv, VIPER for Windows, freeware: http://www.desy.de/~klmn/viper.html.

25 M.F. Williams, B. Fonfé, C. Sievers, A. Abraham, J.A. van Bokhoven, A. Jentys, J.A.R. van Veen and J.A. Lercher, Characterization of ASA-Supported Platinum Catalysts by 27Al (3Q) and 1H MAS NMR, FTIR, TPD, TEM, and EXAFS, *to be submitted*.

26 R.T. Sanderson, Polar Covalence, Academic Press, 1983.

27 X. D. Zhan and J.A. Guin, Energy & Fuels 8 (1994) 1384.

28 S. D. Lin and C. Song, Catal. Today 31 (1996) 93.

29 A. Stanislaus and B.H. Cooper, Catal. Rev. Sci. Eng. 36 (1994) 75.

30 M. Koussathana, D. Vamvouka, H. Economon, and X. Verykios, Appl. Catal. 77 (1991) 283.

31 G.C. Bond, M.A. Keane, H. Kral, J.A. Lercher, Catal. Rev. Sci. Eng. 42 (2000) 323.

32 K. E. Foger and J. R. Anderson, J. Catal. 54 (1978) 318.

33 S.T. Homeyer, Z. Karpinski, W.M.H. Sachtler, J. Catal. 123 (1990) 60.

34 A.K. Galwey, Thermochim. Acta 294 (1997) 205.

35 N. Ichikuni, Y. Iwasawa, Catal. Letters 20 (1993) 87.

Chapter 4

Mechanistic aspects of tetralin hydrogenation in the presence of poisons

A series of catalysts based on platinum nanoparticles supported on amorphous silica-alumina (ASAs) with varying amounts of alumina (100, 55, 20, 5 and 0 %) were tested for tetralin hydrogenation (T = 433 to 463 K, $p(H_2)$ = 50 bar) in the presence of either quinoline or dibenzothiophene (DBT). Quinoline neutralized every acid site and competed with tetralin for the adsorption sites on platinum, while DBT poisoned the metal sites. As a result, the observed catalytic activity was significantly reduced. The mechanistic aspects of the residual catalytic activity are discussed and a model for the hydrogenation of tetralin in the presence of poisons is proposed.

1 Introduction

To meet strict environmental and legislation standards for diesel fuels, oil industry seeks out new catalytic systems and hydrotreating processes [1]. Supported noble metal catalysts (i.e., Pt, Pd) are well known for their high hydrogenation activity for deep hydrodearomatisation. Thus, the hydrogenation is one of the best routes to reduce the aromatics concentration and to supply fuel components with high cetane numbers. The reaction can be carried out at low temperatures and moderate hydrogen pressures. However, the noble metals exhibit low resistance toward sulfur and nitrogen poisons usually present in feeds [2]. Unfortunately, there is a rather limited insight about the mechanism of nitrogen poisoning of noble metals deposited on acidic carriers under hydrotreating conditions. On the other hand it has been reported that the use of acidic supports increases the catalyst resistance towards sulfur poisoning [3]. To account for the beneficial effect of the carriers acidity on the catalyst performance it was proposed that because of the electron-deficiency of nanosized metal particles, the metal–S bond strength is altered. As a result a significant change in turnover frequency of the hydrogenation reaction can be observed [4, 5, 6, 7, 8]. Another explanation of the enhanced S-poison tolerance is based on the assumption that there are some extra hydrogenation sites at the metal particle – acidic carrier interfacial region that could contribute to the overall rate of aromatic hydrogenation [9, 10, 11].

The purpose of this study was to combine N- and S- poisons (represented by quinoline and dibenzothiophene, DBT, respectively) and to explore their effect on the activity of a series of amorphous silica alumina-supported platinum catalysts employed in the hydrogenation of tetralin (1,2,3,4-tetrahydronaphthalene).

2 Experimental

2.1 Catalytic measurement

All chemicals used in the study were obtained from commercial suppliers and used as received: tetralin (Aldrich, 99 % GC assay), hexadecane (Merck, > 99 % GC assay), n-tetradecane (Aldrich, > 99 % GC assay), *cis*- and *trans*-decalin (Aldrich, 99 % GC assay), and hydrogen (99.999 volume % Linde AG).

The hydrogenation of tetralin was carried out in a trickle-bed reactor described elsewhere [12]. A feed of 20 wt. % tetralin in a mixture with n-hexadecane and n-tetradecane was poisoned either with nitrogen (400 ppmw N as quinoline) or sulfur (100 ppmw S as DBT). Parallel supply lines and reactors were used for both types of feed. The liquid feed and hydrogen were mixed before entering the reactor. The experimental conversion values were not altered by varying the amount of catalyst and the total flow rate, maintaining constant the space velocity (i.e., negligible external transport limitations). The catalytic behavior was found to be independent of the particle diameter (i.e., no intraparticle gradients). The performance of the reactor and the accuracy of the analytical method were analyzed by feeding the organic solution to the reactor filled with SiC, operating at 463 K under 50 bar hydrogen pressure. No formation of unexpected products was detected with a recovery percentage of tetralin of 99 %.

During the experiment, a number of samples were taken for off-line GC-analyses. The analyses were carried out on an HP Gas Chromatograph 6890 equipped with an Agilent DB-1701 column. n-Tetradecane was used as an internal standard. Prior to every catalytic test, the catalysts were reduced *in situ* in hydrogen (p = 1 bar, flow rate 30 $cm^3 \cdot min^{-1}$, 2 h at 588 K). To preserve the high metal dispersion a very slow heating rate of 0.41 $K \cdot min^{-1}$ was applied to reach the temperature of reduction. The catalyst testing was carried out at 453 K and 50 bar hydrogen pressure in a weight hourly space velocity (WHSV) range comprised between 4.9 and 26.3 h^{-1} for the N-poison feed, and 1.0 and 21.6 h^{-1} for the S-poison feed. A change of the WHSV was achieved by a change in the amount of catalyst and/or the flow rate (a constant molar ratio of H_2 to tetralin of 20.5 was maintained). In order to determine the apparent energy of activation ($Ea_{(exp)}$) and compare the catalytic activity, the hydrogenation experiments were carried out at 433, 443, 453 and 463 K and

at constant WHSV of 26 h^{-1} and 10 h^{-1} for quinoline and DBT, respectively (p(H2) = 50 bar).

Based on a Langmuir–Hinshelwood (LH) model a pseudo-first order dependence on the hydrocarbon reactant was found to describe the kinetics of the hydrogenation of tetralin at steady state regardless of experimental conditions (Equation 1, where X_{tet} is the conversion of tetralin at steady state and k is the product of the surface reaction rate constant and the reactants adsorption constant).

$$-\ln(1 - X_{tet}) = \frac{k}{WHSV} \qquad (1)$$

2.2 Characterization of spent catalyst samples

The catalyst samples after the hydrogenation were washed in hexane, and sieved from SiC. Such recovered catalysts were characterized by Fourier Transformed Infrared (FTIR), Transmission Electron Microscopy (TEM) and X-ray absorption spectroscopy (XANES).

For the IR study, a Perkin Elmer 2000 spectrometer operating at a 4 cm^{-1} resolution mode was used. Prior to the IR investigation, the samples were activated in vacuum (p = 10^{-6} mbar) at 423 K over 2 h. The activated catalysts were directly examined for the surface hydroxyl groups in the stretching region of the OH (3000 – 4000 cm^{-1}). Further, pyridine and carbon monoxide as probe molecules were used.

In Py-IR experiments, activated catalyst samples were exposed to pyridine vapor (p(Py) = 10^{-2} mbar) at 423 K over 0.5 h. After removing the excess of the adsorbate (i.e., outgassing at 423 K over 1 h) the spectrum was recorded. The concentration of different Py-species on the surface was determined by a method based on the molar extinction coefficients [13].

In CO-IR experiments, the catalyst were activated in H_2 at 623K for 1 hour followed by 1h at the same temperature in vacuum (p = 10^{-6} mbar) to remove hydrogen. Then, the catalyst was cooled to 313 K. Carbon monoxide was adsorbed at the pressure of 0.005, 0.05 or 0.5 mbar until no change in the IR spectrum was noted. At the end of the experiment, the sample was evacuated for 15 minutes at 10^{-6} mbar and the spectrum was recorded.

For the TEM study a JEM-2010 Jeol transmission electron microscope operating at 120 kV was used. The recovered catalysts were grinded, suspended in ethanol and ultrasonically dispersed. Drops of the dispersions were applied on a copper grid-supported carbon film. Transmission electron micrographs were recorded at a magnification of 54,000.

X-ray absorption spectra were collected on beamline X1 at HASYLAB, DESY, Hamburg, Germany. The storage ring was operated with an electron energy of 4.5 GeV and an average current of 100 mA. The Si (311) double crystal monochromator was detuned to 60 % of the maximum intensity to minimize the intensity of higher harmonics in the X-ray beam. The recovered catalysts were prepared as self-supporting wafers reduced in situ (H_2, T = 588 K over 2 h). X-ray absorption spectra were collected at the Pt L_{III} edge (11564 eV) (T = 323 K) and analyzed with the Viper software [14]. White lines were broadened by hydrogen adsorption in relation to the metal foil and, therefore, the intensity of the Pt/ASA white lines was obtained by integration of the peak areas (using a baseline of 1 in every case).

3 Results

3.1 Characterization of supported Pt-catalysts

A detailed study of the nature, concentration, strength and origin of different types of acid sites has been reported elsewhere [15]. A summary is presented in Table 1.

Catalyst	Composition [wt. %]			Acidity [mmol·g^{-1}]		EXAFS particle model. Pt-size [nm]	S_{int}
	Pt	SiO_2	Al_2O_3	BAS	LAS		
Pt/Al_2O_3	0.78	0.0	99.3	0.00	0.14	0.6	2.70
Pt/ASA (55/45)	0.82	46.1	52.9	0.02	0.13	0.5	2.86
Pt/ASA (20/80)	0.81	78.7	20.4	0.04	0.09	0.7	2.98
Pt/ASA (5/95)	0.78	94.9	4.3	0.03	0.07	0.8	3.04
Pt/SiO_2	1.03	99.1	0.0	0.00	0.00	1.5	3.05

Table 1. Characterization of the supported Pt-catalysts: chemical composition, textural properties and intermediate electronegativity of the support according to Sanderson.

All the supports had mesoporous structure, thus, no diffusion limitations of the bulky aromatic molecules were expected. Note, that the set of catalyst studied showed a progressive modification of the acidic properties with respect to Lewis and Brønsted acidity. The silica-supported Pt-catalyst was used as a neutral reference material. Average sizes of metal clusters were small and similar for the different catalysts (except for Pt/SiO_2). Moreover, the particle size distribution was narrow as confirmed by TEM. As a result, the localized effect of the acid sites on the catalytic properties of the Pt-nanoclusters could be investigated. Further, the intermediate electronegativity of the support (i.e., the Sanderson electronegativity [16]) changed progressively among the series of catalysts and could be used to correlate its value with the catalytic behavior of Pt-nanoclusters.

3.2 Hydrogenation of tetralin in the presence of quinoline

The Pt-catalysts were tested for the hydrogenation of tetralin in the presence of quinoline to understand the N-poison effect on the catalyst performance. The main reaction products were *cis*- and *trans*-decalin. The carbon mass balance of the liquid products was close to 100% regardless the reaction conditions. Thus, no reaction products were present in the gas phase. The rate of reaction over every Pt-catalyst at different temperatures is shown as a function of the average electronegativity of the support (Figure 1).

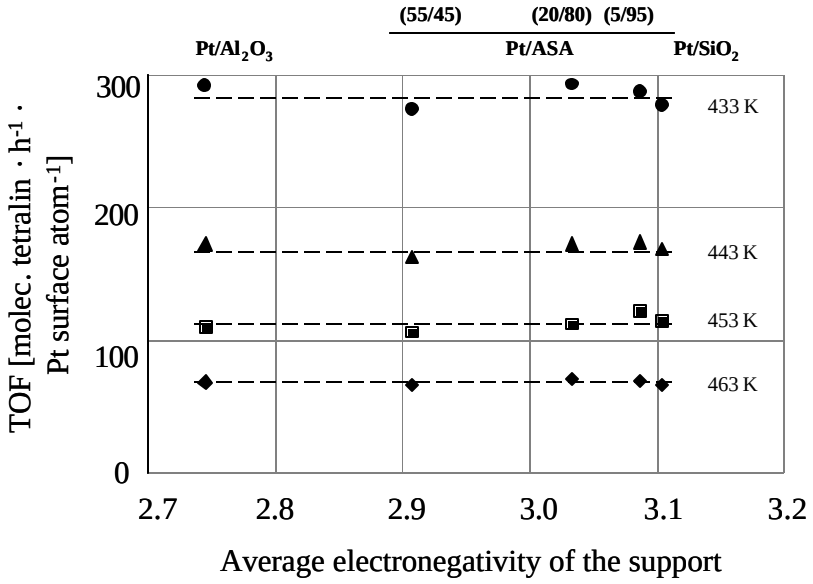

Figure 1. Rate of the hydrogenation of tetralin in the presence of quinoline over Pt-catalysts supported on carriers exhibiting different electronegativity, at 433, 443, 453 and 463 K. Hydrogen pressure, WHSV and hydrogen to feed ratio were maintained constant (50 bar, 26 h^{-1}, and 700 nl· Kg^{-1}, respectively).

At 433, 443, 453 and 463 K, the TOF values were 286, 170, 113 and 68 h^{-1}, respectively. No correlations between the catalyst activity and the composition of the support were observed. The N-poisoned feed decreased the catalytic activity in the hydrogenation of tetralin to about 10 % of that previously reported for the clean feed [12].

The Arrhenius plot (Figure 2) was used to derive the apparent energy of activation ($Ea_{(exp)}$) in the hydrogenation of tetralin over different ASA-supported Pt catalysts in the presence of quinoline.

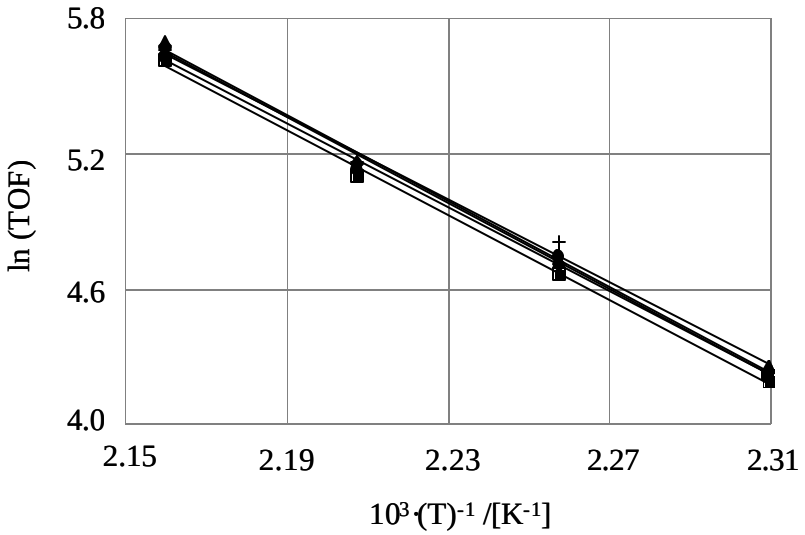

Figure 2. Arrhenius plot for the hydrogenation of tetralin over Pt/Al_2O_3 (?), Pt/ASA (55/45) (¦), Pt/ASA (20/80) (?), Pt/ASA (5/95) (+), and Pt/SiO_2 (•) in the temp. range comprised between 433 and 463 K.

The $Ea_{(exp)}$ over Pt/Al_2O_3, Pt/ASA (55/45), Pt/ASA (20/80), Pt/ASA (5/95) and Pt/SiO_2 was calculated as 80, 79, 79, 77 and 78 $kJ \cdot mol^{-1}$, respectively. Despite changes in the support composition, the $Ea_{(exp)}$ was almost constant. A different trend of $Ea_{(exp)}$ values was found when no poison was present in the feed (48, 47, 40, 35, and 57 $kJ \cdot mol^{-1}$, respectively).

Figure 3 presents the *cis* to *trans* decalin selectivity over this series of catalysts.

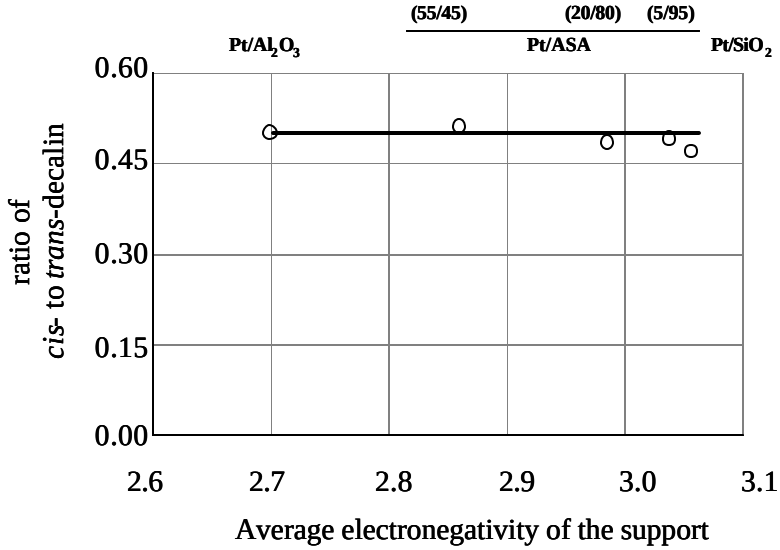

Figure 3. Dependence of cis - to trans-decalin selectivity on the electronegativity of the Pt-catalysts supports at approximately 20 % conversion level of tetralin (T = 453 K, 50 bar).

To exclude the change of the isomer ratio upon the thermodynamically driven shift of the *cis* to the *trans* product after secondary re-adsorption of decalines, a blank experiment was performed. As the isomerization of decalins was kinetically retarded it was concluded that the comparison was valid. The isomer ratio distribution was the same for all the catalysts tested (i.e., about 0.50). Thus, no correlation with the support was observed. Further, in comparison to the results obtained for the clean feed, quinoline caused a significant increase of the product selectivity to the *trans*-decalin isomer (i.e., the cis/trans ratio was reduced 3.5 times at a similar tetralin conversion level of 20 %).
The quinoline present in the feed was partially consumed leading to tetrahydroquinoline (1, 2, 3, 4 THQ) in the presence of hydrogen over the metal catalyst (Figure 4).

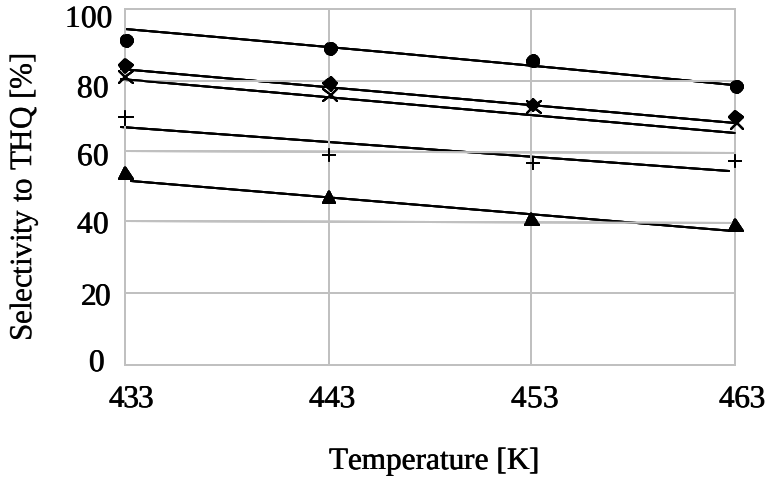

Figure 4. Selectivity to tetrahydroquinoline in the hydrogenation of quinoline over Pt/Al_2O_3 (?), Pt/ASA (55/45) (X), Pt/ASA (20/80) (?), Pt/ASA (5/95) (+), and Pt/SiO_2 (•) catalysts, in the temperature range comprised between 433 K and 463 K.

The selectivity of this reaction varied between 40 and a 100 % depending on the reaction conditions. At higher temperatures the hydrogenation of quinoline to tetrahydroquinoline was less significant but the conversion depended on the particular composition of the catalyst support. This was attributed to a promotion of the secondary reaction pathway over acid sites leading to decahydroquinoline. The secondary reaction pathway was least catalyzed over a neutral support (i.e., silica), while over acidic ASA-supports it was strongly promoted. Other reaction pathways of quinoline would lead to hydrogenolysis and scission of the C – N bond. However, no other products were detected in the liquid

phase (GC-MS), probably because the reaction temperature was too low to achieve hydrodenitrogenation.

3.3 Hydrogenation of tetralin in the presence of DBT

The Pt-catalysts were tested for the hydrogenation of tetralin in the presence of dibenzothiophene (DBT) to analyze the S-poison effect on the catalyst performance. Main reaction products were *cis*- and *trans*- decalins. The catalytic activity was very low and no correlation with the intermediate electronegativity of the support was observed. However, a change in the reaction rate over the series of Pt-catalysts could be correlated with the Brønsted acidity of the support (Figure 5).

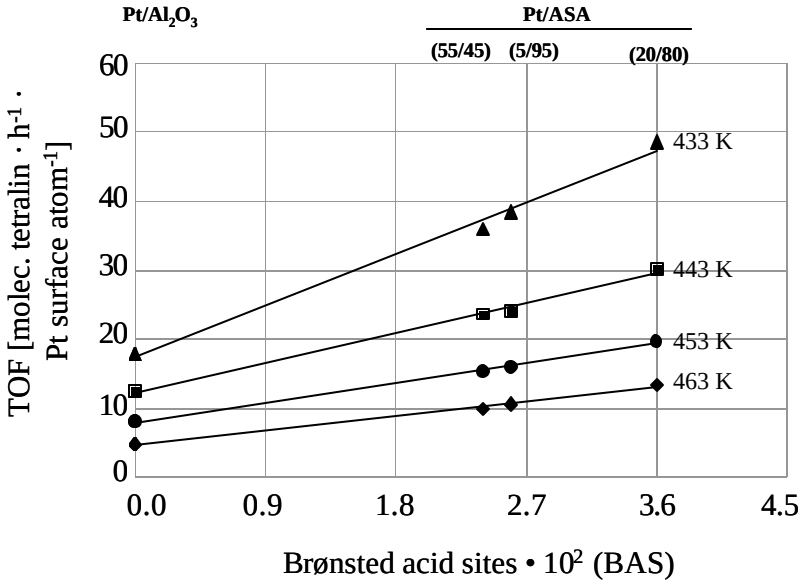

Figure 5. Rate of tetralin hydrogenation over Pt-catalyst supported on carriers exhibiting different acidity. The experimental conditions were 50 bar, WHSV = 10 h^{-1} and H_2/feed = 700 nl/Kg.

Figure 6 shows a comparison of reaction rates in the hydrogenation of tetralin over Pt/SiO_2 catalysts vs. those observed over Pt/Al_2O_3 catalysts.

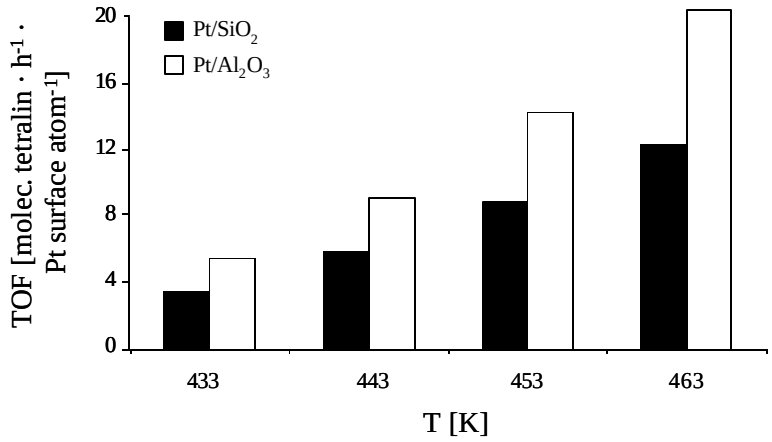

Figure 6. Rate of tetralin hydrogenation over Pt/SiO_2 and Pt/Al_2O_3 catalysts (p = 50 bar, WHSV = 10 h^{-1} and H_2 to feed ratio = 700 nl/Kg).

The activity observed for the Pt/SiO_2 catalyst (i.e., neutral support) indicated the presence of a residual activity over the metal sites. For a Pt/Al_2O_3 catalyst that exhibits only Lewis acid sites, a slightly higher catalytic activity was found. The catalyst activity increased with the concentration of Brønsted acid sites in the ASA supports. From the Arrhenius plot (Figure 7) the apparent energy of activation ($Ea_{(exp)}$) for the hydrogenation of tetralin in the presence of DBT over the different catalysts, was calculated.

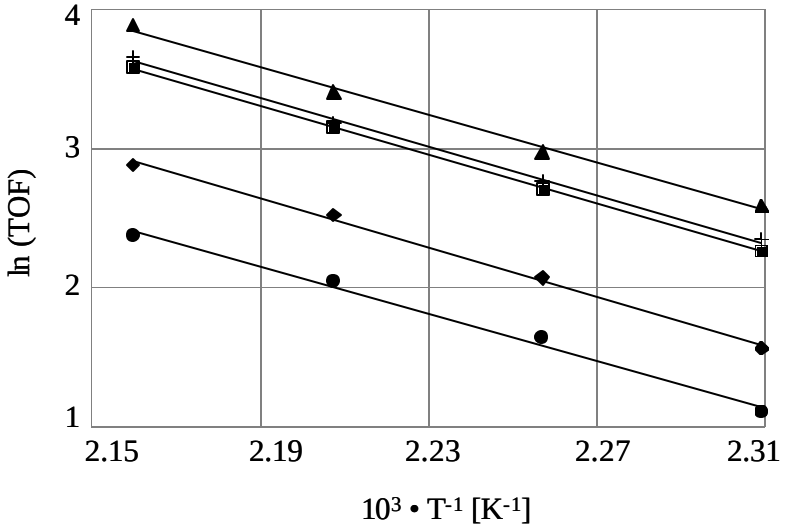

Figure 7. Arrhenius plot for the hydrogenation of tetralin in the presence of DBT over Pt/Al_2O_3 (?), Pt/ASA (55/45) (¦), Pt/ASA (20/80) (?), Pt/ASA (5/95) (+), and Pt/SiO_2 (•) catalysts, in the temperature range from 433 K to 463 K.

The $Ea_{(exp)}$ over Pt/Al_2O_3, Pt/ASA (55/45), Pt/ASA (20/80), Pt/ASA (5/95) and Pt/SiO_2 was calculated as 74, 73, 72, 72 and 74 $kJ \cdot mol^{-1}$, respectively. Note that $Ea_{(exp)}$ was almost constant for the different catalyst supports.

The isomer ratio of the *cis*- to *trans*- decalin was also calculated (Figure 8).

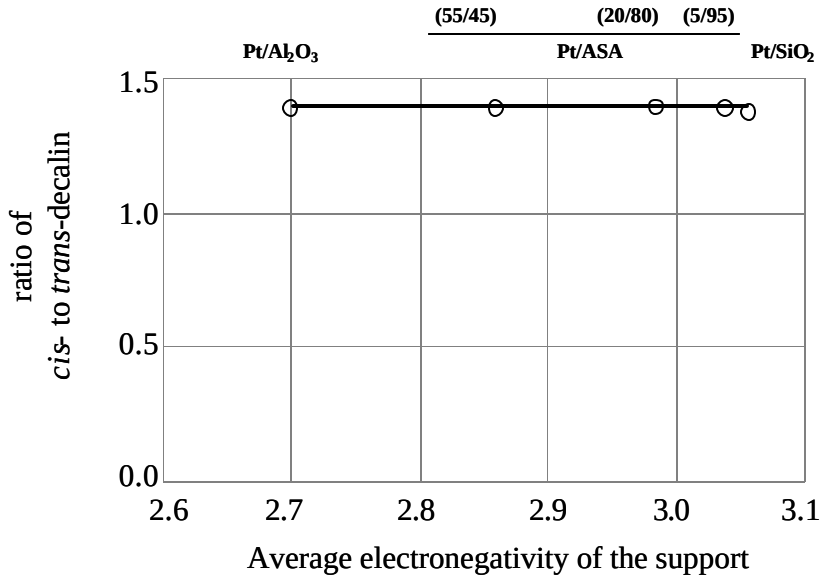

Figure 8. Dependence of cis - to trans-decalin selectivity on the intermediate support electronegativity of the Pt-catalysts at approximately 20 % conversion level of tetralin (T = 453 K, p(H2) = 50 bar).

The isomer ratio of the *cis*- to *trans*- decalin was 1.4 and no indication of the influence of the catalyst support was found. Apparently, the S-poison promoted the reaction selectivity to the *trans*-isomer.

The dibenzothiophene molecule present in the feed was partly consumed. An analysis of the liquid products showed the presence of dimethylthiophene while no other S-containing products were detected. Thus, only the hydrogenation of DBT was observed. The kinetics of the hydrogenation of DBT proceeded at higher reaction rates and led to a much higher conversion than that observed in the hydrogenation of tetralin. A general first order dependence on DBT concentration was observed (Figure 9) [17].

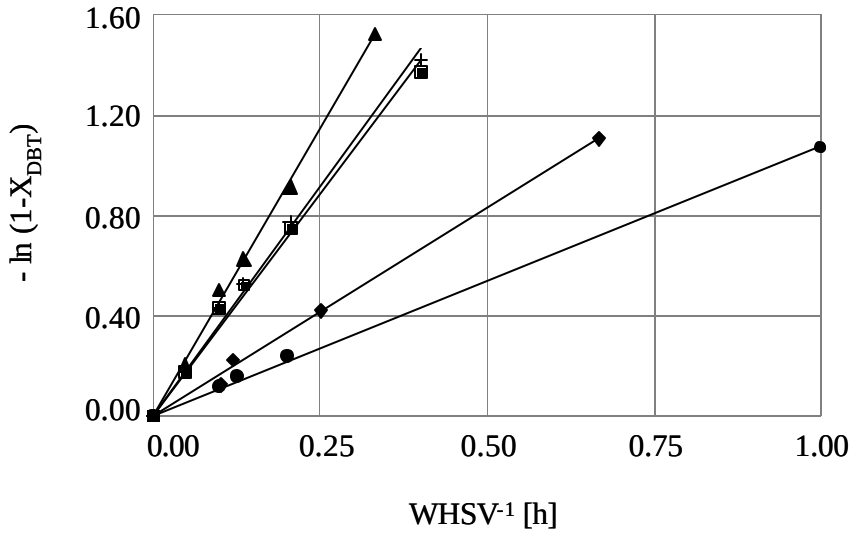

Figure 9. First order kinetic fitting of the hydrogenation of DBT over Pt/Al_2O_3 (?), Pt/ASA (55/45) (¦), Pt/ASA (20/80) (?), Pt/ASA (5/95) (+), and Pt/SiO_2 (•) catalysts, at 453 K.

The apparent energy of activation ($Ea_{(exp)}$) for the reduction of DBT over different ASA-supported Pt catalysts was calculated from the Arrhenius equation (Figure 10).

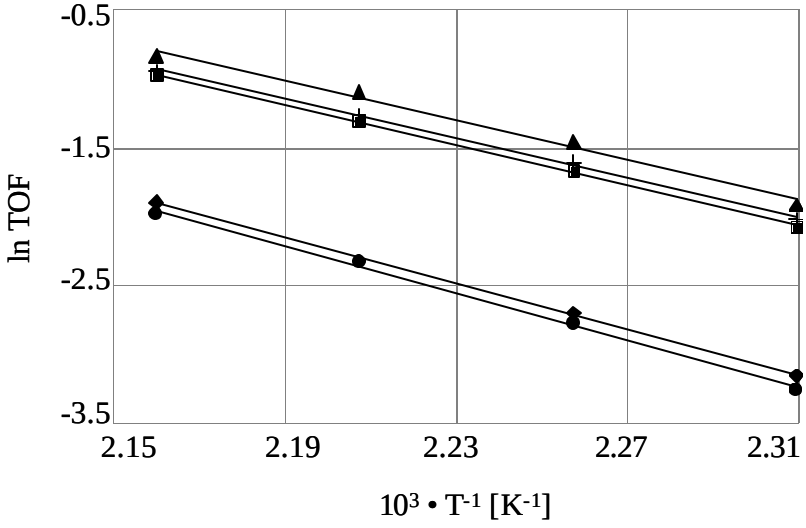

Figure 10. Arrhenius plot over Pt/Al_2O_3 (?), Pt/ASA (55/45) (¦), Pt/ASA (20/80) (?), Pt/ASA (5/95) (+), and Pt/SiO_2 (•) catalysts in the temperature range from 433 K to 463 K.

The $Ea_{(exp)}$ over Pt/Al_2O_3, Pt/ASA (55/45), Pt/ASA (20/80), Pt/ASA (5/95) and Pt/SiO_2 catalysts was calculated as 69, 61, 60, 59 and 71 $kJ \cdot mol^{-1}$, respectively. Note that (i) for the Pt/ASA catalysts the $Ea_{(exp)}$ hardly varied with the support composition and (ii) for the

Pt/SiO_2 and Pt/Al_2O_3, the $Ea_{(exp)}$ was similar and it was significantly higher than that calculated for the Pt/ASAs. The rate of DBT hydrogenation increased with the increasing concentration of Brønsted acid sites in the supports, as depicted in Figure 11.

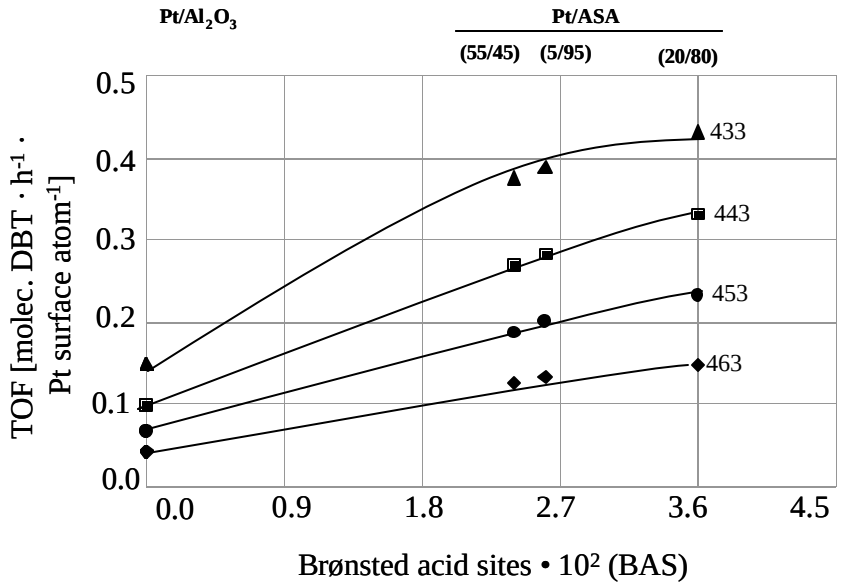

Figure 11. Rate of hydrogenation of the DBT-poison during the catalytic hydrogenation of tetralin ($p(H_2)$ = 50 bar, WHSV = 10 h^{-1} and H_2/feed = 700 nl· Kg^{-1}).

Apparently, the conversion rate of DBT increased with increasing concentration of BAS on the support. Also, a slightly higher activity from silica to alumina is observed indicating that Lewis acid sites play a role in the conversion of the S-poison (Figure 12).

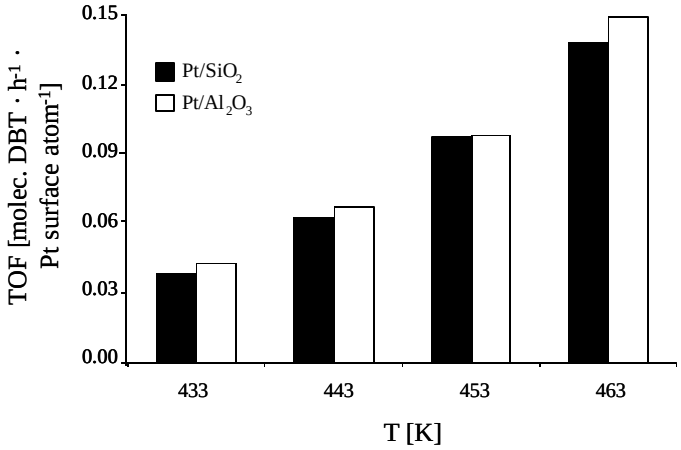

Figure 12. Rate of hydrogenation of the DBT-poison over Pt/SiO_2 and Pt/Al_2O_3 catalysts (p = 50 bar, WHSV = 10 h^{-1} and H_2 to feed ratio = 700 nl/Kg).

3.4 Analysis of the spent catalyst samples

In order to probe the effect of the N- and S- compounds on the supported-platinum catalysts during the hydrogenation of tetralin, the Py-FTIR study of the used samples was carried out. In Figure 13 the IR spectra of pyridine adsorbed over the spent Pt/ASA (55/45) catalyst are presented and compared to that recorded for the fresh catalyst.

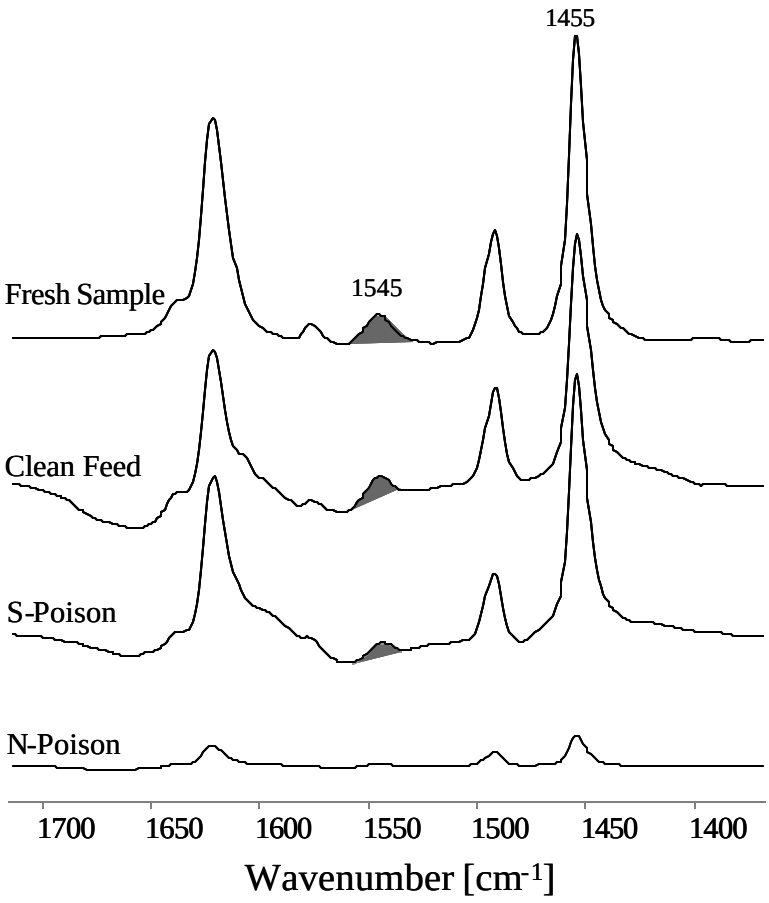

Figure 13. The Py-IR study of spent and fresh Pt/ASA (55/45) samples.

On the freshly activated catalyst, IR bands were assigned to the formation of surface pyridine species (e.g., 1545 and 1455 cm^{-1} for pyridinium ion and coordinatively-bonded pyridine, respectively) [15]. The catalyst sample used in the reaction carried out in the presence of DBT showed a very similar set of IR bands. However, the quantification of the PyH+ at 1545 cm^{-1} associated with the BAS showed that approximately 30 % less pyridine could be adsorbed on the spent catalyst compared to the amount adsorbed on the spent catalyst after clean feed. Thus, the S-poison had some, but rather moderate

hindrance effect on the adsorption properties of the ASA (55/45) support. In contrast, hardly any adsorption of pyridine was observed on the Pt/ASA (55/45) catalyst recovered after the hydrogenation of tetralin in the presence of quinoline. Apparently, the N-poison easily covered both BAS and LAS because of the basic properties of the nitrogen species. To probe accessible metal sites after the hydrogenation of tetralin in the presence of DBT or quinoline, CO adsorption was followed by IR. In Figures 14 a) and b) the IR spectra of the CO adsorption on the fresh and spent Pt/ASA (55/45) catalysts, and the adsorption capacity of the used samples, are shown.

Figure 14 a)

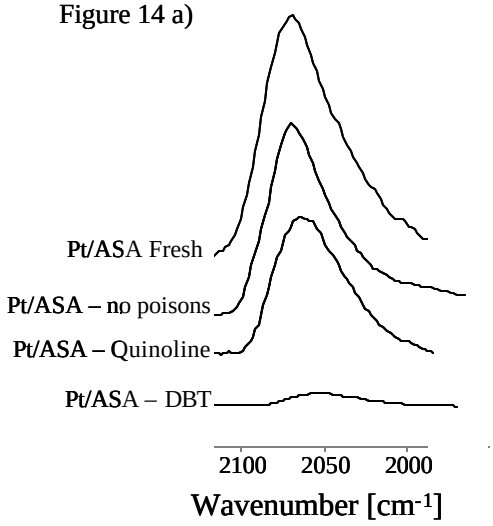

Figure 14 b)

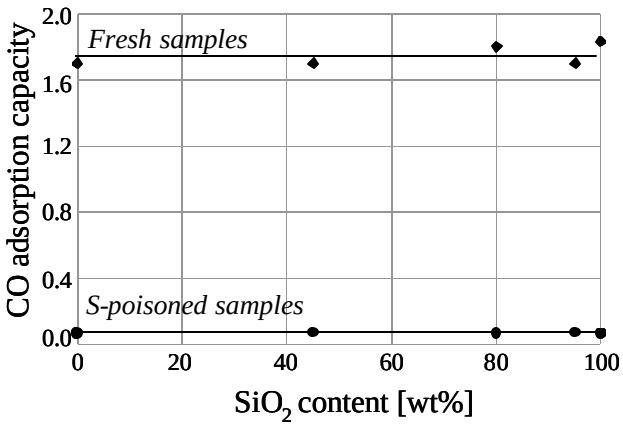

Figure 14. a) CO adsorption on the fresh and spent Pt/ASA (55/45) catalyst samples. b) Adsorption capacity of the used samples.

The adsorption capacity for CO on clean platinum sites was drastically reduced by the presence of DBT in the reaction (less than 5 % of the original Pt-surface was available for the CO adsorption). Further, the support composition had no beneficial effect on the metal resistance towards sulfur poisoning as the adsorption on Pt-particles was the same regardless the type of support. In contrast, only 40 % of the CO-accessible platinum surface sites were unavailable when quinoline was present in the feedstock. As one of the factors that could reduce the accessible surface area is the sintering of the nanosized Pt-particles, an additional TEM investigation was carried out. In Figure 15, micrographs of the fresh and spent Pt/ASA (5/95) catalysts are shown.

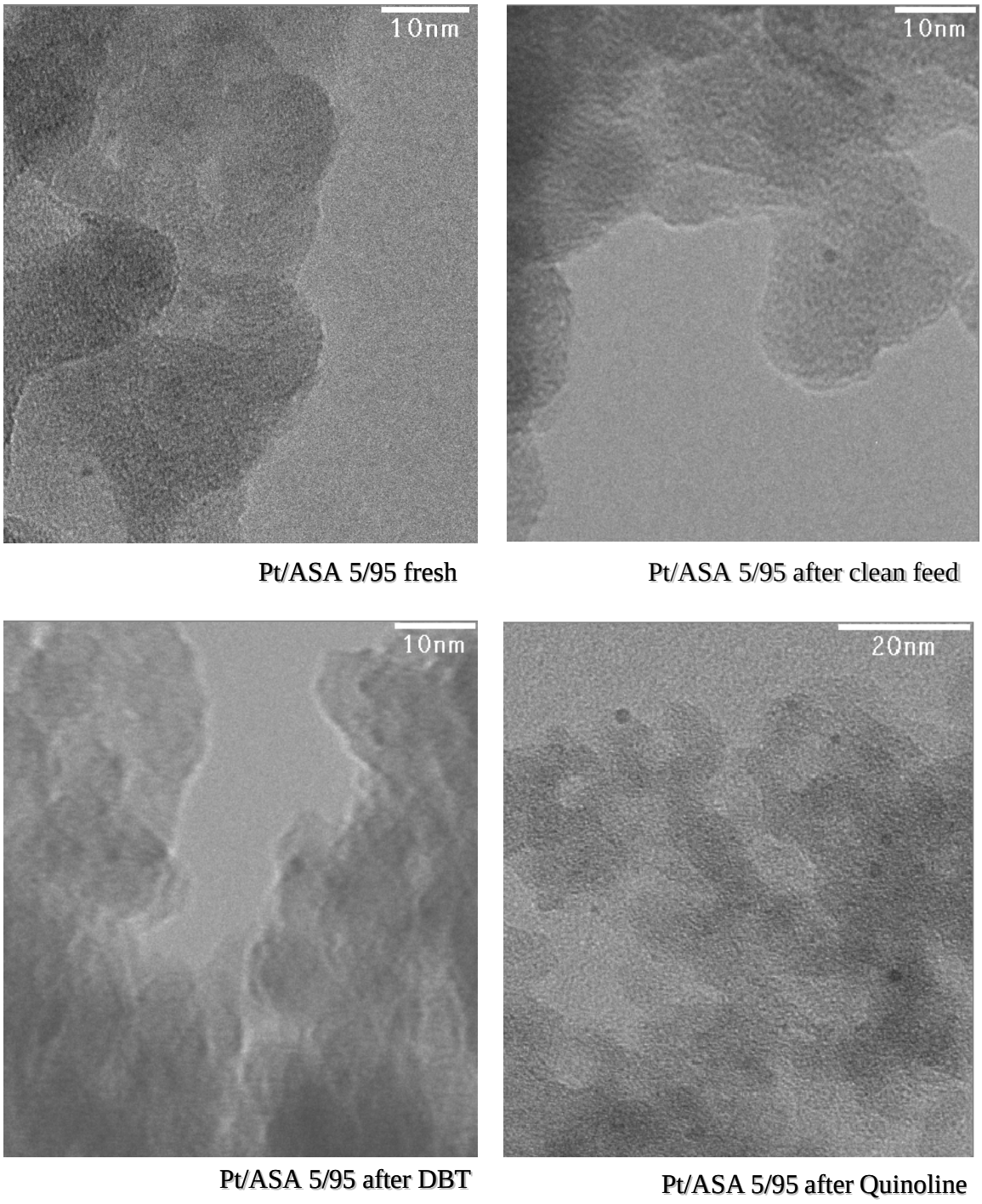

Figure 15. TEM micrographs of catalyst samples used in the hydrogenation of tetralin in the presence of DBT and quinoline.

The platinum particle size increased after the hydrogenation in the presence of DBT and quinoline, from 0.8 nm to 1.5 and 2.0 nm, respectively. Apparently, in the presence of poisons coalescence of nanosized Pt-particles was induced. Note, that N-poison promoted

this process more than the S-poison. In conclusion, the decrease of the clean Pt-surface can be ascribed to the formation of an inactive phase over the metal surface. This can be related to the transformation of platinum to Pt-S and Pt-N species or to the build-up of a coke deposit.

The electronic properties of the platinum particles on the different ASA-supports after the hydrogenation of tetralin in the presence of DBT, were analyzed by X-ray absorption spectroscopy (XANES). The results are shown in Figure 16.

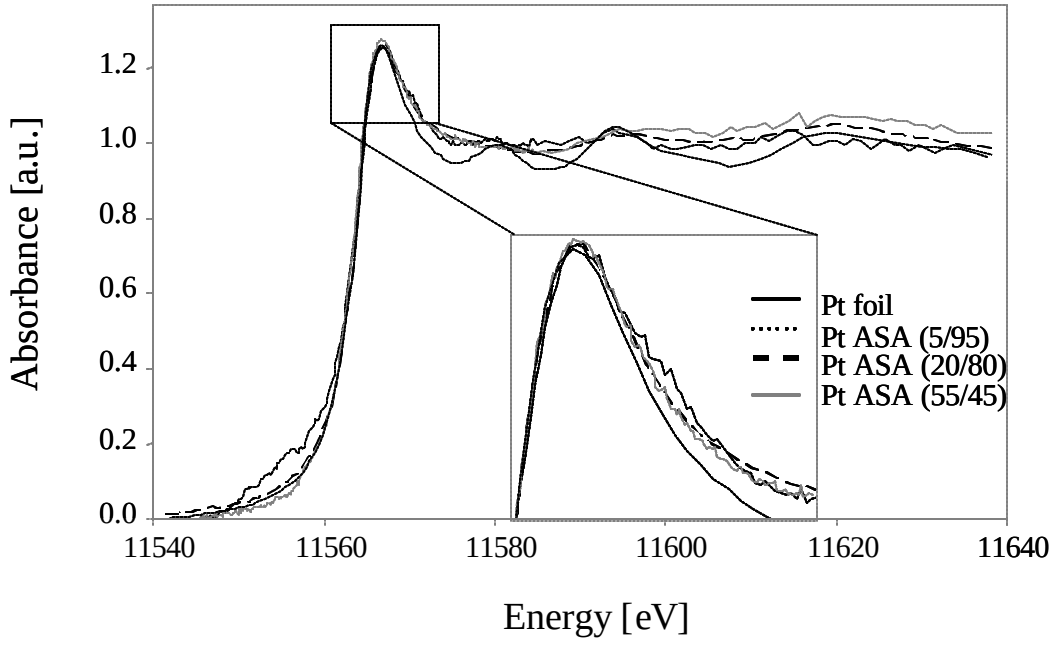

Figure 16. Normalized XANES spectra at L_{III} edge under H_2 at 323 K over Pt/ASAs catalysts after the hydrogenation of tetralin in the presence of DBT

The intensity of the white line in the XANES spectra at L_{III} edge of the Pt/ASA catalysts was comparable for all the ASA supports. Apparently, the electron density of platinum after reaction in the presence of DBT was unrelated to the composition of the support. In comparison to the platinum foil some broadening of the XANES spectra indicated the presence of pre-adsorbed hydrogen. Hydrogen acts as an electron donor, thus a higher electron density on the metal site and a decreased intensity of the white line is usually observed [12]. In our case the intensity of the spectra was located just above that recorded for the reference Pt-foil. Probably, because of the presence of S-species adsorbed on the metal surface, the level of electron density within the Pt-cluster was reduced. Other

factors that change the intensity of the white line are: i) the size of the metal clusters and ii) the composition of the support and the presence of adsorbates. The former was estimated from EXAFS data and particle modeling calculations. Apparently, the sizes of the metal clusters after the reaction in the presence of DBT were similar (i.e., around 1.5 nm for all the Pt/ASAs catalysts). CO-IR experiments proved that the sulfur coverage on the metal was uniform for different Pt/ASAs catalysts. This supports the conclusion that the position of the white line with respect to the foil depends on the amount of S- and H-species on the surface. In Figure 17 the area of the peak above the L_{III} edge of the fresh samples and after the reaction in the presence of DBT is plotted as a function of the composition of the ASA support.

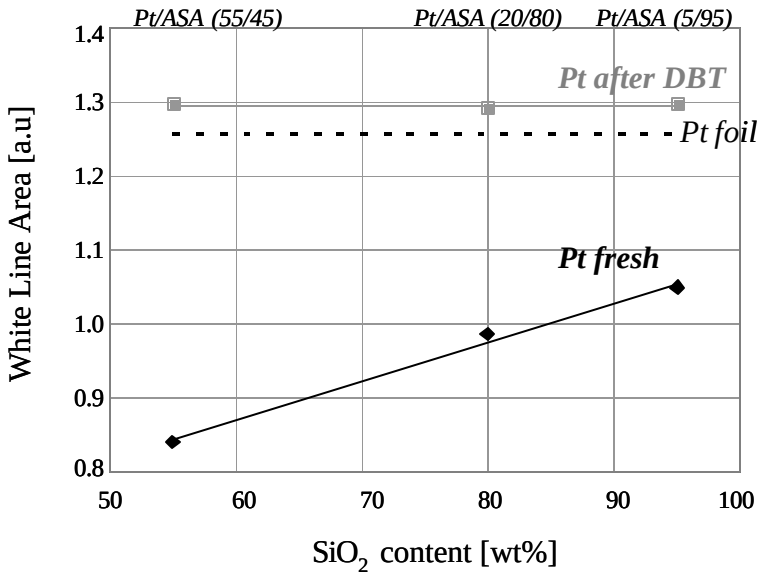

Figure 17. Area of the peak above the L_{III} edge of the fresh samples and after the reaction in the presence of DBT as a function of the silica content in the support.

In the presence of DBT no metal - support interaction could be detected as previously found for the fresh Pt/ASA catalysts. Clearly, S-poison disturbs any influence of the mesoporous oxide support on the small Pt-cluster. As a consequence migration of metal atoms and coalescence of Pt-particles became more feasible.

4 Discussion

4.1 Hydrogenation of tetralin in the presence of quinoline

In the presence of quinoline, neither the rate of hydrogenation of tetralin nor the apparent energy of activation varied with the composition of the supports. This can be explained by: i) the overall electronegativity of the support cannot exercise its influence on the metal electronic structure and/or ii) an equalization of the acidic properties of the support has occurred. The latter can be linked with the intrinsic basic properties of the nitrogen species that can neutralize both BAS and LAS present in the support [18]. The Pyd-FTIR analyses of the spent catalysts show that most of the nitrogen–containing deposit is likely located on the support. The former interaction is more complex to elucidate. One of the requirements is that metal clusters are in the nanosize range. Anderson estimated that only those Pt-particles that are not bigger than about 1 nm can be substantially influenced by the support [19]. Therefore, the coalescence of Pt-particles to a size of about 2 nm under the N-poison invalidates the explanation based on metal support - interactions. Further, the build-up of the coke on the support likely decreases a possible interaction with the Pt-cluster. Note, that in the course of the reaction the silica-alumina insulator gets covered with a carbonaceous deposit with some conducting properties; thus the support itself is transformed.

The fairly high and uniform values of $Ea_{(exp)}$ for the tetralin hydrogenation in the presence of quinoline, in comparison to the values obtained in its absence [12], can be explained taking into account the competitive adsorption of the N-poison. The heat of adsorption of tetralin is included in the energy of activation (i.e., the hydrogenation is first order in tetralin). If it is assumed that the true energy of activation of tetralin is always the same, then a change in the heat of adsorption of tetralin originates the observed differences. Likely, the N-poison adsorbs better on the Pt-surface than tetralin, thus the active sites (i.e., those exhibiting a high enthalpy of adsorption) are covered with quinoline. The residual, less active sites are available for tetralin; however, the lower heat of adsorption associated with these sites is indicated by the increase of $Ea_{(exp)}$. A slightly different scenario could be proposed considering that quinoline donates electrons to the metal

surface, reducing its electrophilicity. In consequence a higher electron density on the metal surface will weaken the adsorption of any olefinic intermediate [20, 21, 22]. The *cis* to *trans* selectivity is a good evidence for electronic effects in the catalysis on metals. According to Weitkamp the formation of *trans* decalin depends on the consecutive desorption and re-adsorption of a partially hydrogenated intermediate, ? ^{1,9} – octalin [23]. Not surprisingly, the observed isomer selectivity to *trans*-decalin in the hydrogenation of tetralin is higher when quinoline is present in the feed.

4.2 Hydrogenation of tetralin in the presence of DBT

The hydrogenation of tetralin in the presence of DBT was drastically reduced, undoubtedly due to the reaction of the S-species with platinum. It is known that the high stability of metal sulfide species is the origin of the rapid deactivation of the metallic function of the catalytic activity even at very low sulfur concentrations in the feed [24, 25]. Further, sulfur poisoning induces metal migration as it reduces the interaction of the metal with the support. Both TEM and EXAFS studies confirmed that in the presence of DBT the size of platinum clusters on ASAs increases from 0.8 nm to about 1.5 nm. Under our experimental conditions the hydrogenation of dibenzothiophene was relatively faster than that of tetralin. This illustrates further the high preference for the adsorption of DBT on platinum. Nevertheless, some residual catalytic activity for hydrogenating tetralin was observed (approximately 2 % of the rate recorded for the clean feed). A linear correlation was found of the rate of tetralin hydrogenation with the concentration of strong Brønsted acid sites in the ASA supports. On the other hand, the intermediate electronegativity (i.e., the polarity) of the support did not seem to correlate with the reaction rate. Different S-species are adsorbed on platinum depending on the starting poison and other experimental conditions. A full decomposition of the S-molecules could also lead to a sulfur deposit on the Pt-surface. Consequently, some electron transfer from the metal to the non-metal occurs, due to the difference in electronegativity between the elements. On the other hand, DBT and tetralin are actually hydrogenated, thus, the activation of the hydrogen molecule is still feasible. From the XANES data it has been evidenced that the hydrogen molecule can still be adsorbed on the poisoned metal cluster.

4.3 Proposed hydrogenation model

To account for those findings we propose a model for the hydrogenation of tetralin on the perimeter of the S-poisoned Pt-cluster. The tetralin molecule, anchored on the Brønsted acid sites, is saturated upon reaction with the hydrogen activated on the Pt-S cluster. Tentatively, also a strong Lewis acid site could serve as a similar adsorption site for tetralin (see activity on alumina). The reaction pathways on the active and S-poisoned platinum cluster are shown in Figure 18.

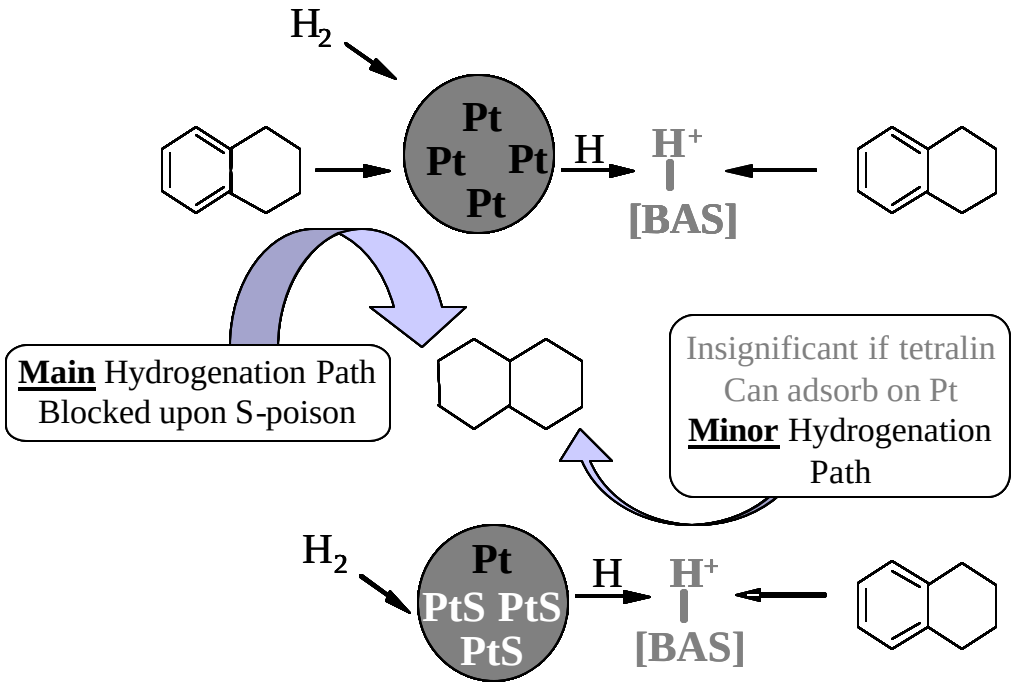

Figure 18. Reaction pathway for the hydrogenation of tetralin in the absence and presence of DBT.

5 Conclusions

The catalytic hydrogenation of tetralin over Pt/ASA catalysts has been studied in the presence of N- and S-poisons. Two types of active sites for catalytic hydrogenation were identified: (1) those on the metal particle and (2) those on the perimeter of the metal particle where an acid site anchors the aromatic molecule to be further hydrogenated by the hydrogen activated on platinum. The former pathway generates the high catalytic activity of the supported platinum catalysts in the hydrogenation of aromatics. The metal-support interaction can be used to tune the catalytic activity of nanosized Pt-clusters. However, in the presence of basic N-poisons the acid sites and a fraction of the metal sites are blocked. Further, quinoline induces metal migration and sintering. Therefore, the electronic effects are eliminated (equalized) and the strong competition between tetralin and quinoline for the metal sites leads to an increase of the apparent energy of activation for tetralin hydrogenation. The S-poison molecule first targets the metal sites inhibiting metal - support interactions. The activation of hydrogen molecules on the poisoned metal is still possible and provides hydrogen atoms for the minor hydrogenation pathway. This hydrogenation route is not significant when using a clean feed but becomes the main pathway to reduce the tetralin molecule in the presence of S-poisons. Therefore, an increase in the concentration of anchoring Brønsted acid sites in the vicinity S-poisoned Pt leads to an increase in the catalytic activity despite the presence of DBT.

Acknowledgments

Financial support of S.R.T.C. Amsterdam is gratefully acknowledged. The authors are also grateful to Dr. W. Stork for critical discussions. Andreas Marx and Xavier Hecht (TUM, TC2) are gratefully thanked for setups troubleshooting. HASYLAB, DESY is acknowledged for the beam time at the X1 experimental station.

6 References

1 B. H. Cooper, B. L Donnis, Appl. Catalysis A 137 (1996) 203.

2 J. Barbier, E. Lamy-Pitara, P. Marecot, J.P. Boitiaux, J.Cosyns, F. Verna, Adv. Catal. 37 (1990) 279.

3 A. Stanislaus, B. H. Cooper, Catal. Rev. Sci. Eng. 36(1) (1994) 75.

4 P. Gallezot, Catalysis by Zeolites (B. Imelik, C. Naccache, Y. Ben Taarit, J. C. Vedrine, G. Coudurier, and H. Praliaud, Eds.), Vol. 5, Elsevier Science, Amsterdam (1980) 227.

5 M. T. Tri, J. Massardier, P. Gallezot, B. Imelik,B , Metal-support and Metal Additives Effects in Catalysis (B. Imelik, C. Naccache, G.Coudurier, H. Praliaud, M. Meriaudeau, P. Gallezot, G. A. Martin,and J. C. Vedrine, Eds.), Vol. 11, Elsevier, Amsterdam (1982) 141.

6 F. Figueras, R. Gomez, M. Primet, Adv. Chem. Ser. 121 (1973) 480.

7 T. T: Phuong, J. Massardier, P. Gallezot, J. Catal. 102 (1986) 456.

8 R. Szymanski, H. Charcosset, P. Gallezot, J. Massardier, J, L.Tournayan, J. Catal. 97 (1986) 366.

9 P. Chou, M.A. Vannice, J. Catal. 107 (1987) 129.

10 S.D. Lin, M.A. Vannice, J. Catal. 143 (1993) 563.

11 M. V. Rahaman, M. A. Vannice, J. Catal. 127 (1991) 251 and 267.

12 M.F. Williams, B. Fonfé, C. Woltz, J.A.R. van Veen and J.A. Lercher, Metal support interaction- Influence of the support on the catalytic activity of Platinum for Deep Hydrotreating. *to be submitted.*

13 C.A. Emeis, J. Catal., 141 (1993) 347.

14 K.V. Klementiv, VIPER for Windows, freeware: http://www.desy.de/~klmn/viper.html.

15 M.F. Williams, B. Fonfé, C. Sievers, A. Abraham, J.A. van Bokhoven, A. Jentys, J.A.R. van Veen and J.A. Lercher, Characterization of ASA-Supported Platinum Catalysts - ^{27}Al (3Q) MAS NMR, ^{1}H MAS NMR, FTIR, TPD, TEM, and EXAFS, *to be submitted.*

16 R.T. Sanderson, Polar Covalence, Academic Press, 1983.

17 H. R. Reinhoudt, R. Troost, S. Van Schalkwijk, A. D. Van Langeveld, S. T. Sie, J.A.R. van Veen, J. A. Moulijn, Fuel Processing Technology 61 (1999) 89.

18 M. J. Girgis, and B. C. Gates, Ind. Eng. Chem. Res., 30 (1991), 2021.

19 J. R. Anderson, Structure and properties of small particles, Academic Press, London, 1975.

20 G. Leitz, J. Volter, Mechanism of Hydrocarbon reactions, Elsevier, Amsterdam, 1975, 151-162.

21 J. J. Rooney, G. Webb, J. Catal., 3 (1964) 488.

22 J. J. Rooney, J. Mol. Catal., 31 (1985) 147.

23 A. W. Weitkamp, Adv. Catal. 18 (1968) 1.

24 C. H. Bartholomew, P. K. Agrawal, J.R. Katzer, Adv. Catal., 31(1982)135.

25 J. Barbier, E. Lamy- Pitara, P. Marecot, J. P. Boitiaux, J. Cosyns, F. Verna, Adv. Catal., 37(1990) 279.

Chapter 5

Summary

1 Summary

This thesis addresses the mechanistic aspects of the hydrogenation of aromatics in the presence of S- and N-poisons over noble metal catalysts supported on acidic carriers.

Projected environmental regulations limit the aromatic contents of diesel fuels. The hydrogenation process of aromatic hydrocarbons over supported noble metals (e.g., Pt, Pd) fails to deliver high yields of refined petroleum distillates because of their low tolerance towards S- and/or N-poisons. One promising technology to improve the performance of catalysts to meet the tight limits fixed for the aromatics contents is based on the use of acidic carriers that increase the noble metal resistance towards sulfur poisoning. However, the reaction mechanisms that are operative in these catalysts, the role played by a different kinds of acid sites (i.e., Brønsted or Lewis), and their optimal concentration and strength have not been unambiguously explained. Further, the process has not been adequately studied in the presence of basic N-compounds that are always present in the feedstock. The aim of this study was to elucidate some of these questions.

To explore the possibility of tailoring an optimal acidic carrier reinforcing platinum resistance to the S-poisons, a series of Pt-catalysts supported on amorphous silica-alumina (ASA) was prepared and thoroughly characterized. ASA supports were synthesized with different proportions of silica, alumina and aluminosilicate phases. The concentrations of alumina and aluminosilicate domains were quantified using ^{27}Al MAS NMR spectroscopy. Up to 40 % of aluminum atoms could be incorporated into the aluminosilicate phase (i.e., the Pt/ASA (20/80) catalyst). The ^{1}H MAS NMR revealed that only a small fraction of the AlO_4^- tetrahedra within the aluminosilicate phase were compensated by protons leading to Brønsted acid sites (BAS). Most of the AlO_4^- tetrahedra were presumably neutralized by cationic alumina species. Lewis acid sites (LAS) were formed in the alumina clusters present in the support. The nature and concentration of different acid sites were determined in sorption studies using pyridine as a probe molecule (infrared spectroscopy and temperature programmed desorption studies), and compared with the ^{1}H MAS NMR results. Weak and strong LAS were detected and BAS could be also differentiated as either weak or strong. Weak BAS emerge from interacting Al-O(H)-Si sites of the aluminosilicate phase. These clusters of

hydroxyl groups are polarized via hydrogen bonding. Strong BAS are associated with isolated Al-O(H)-Si sites.

H_2 chemisorption, TEM and EXAFS supported by particle modeling, were applied to characterize platinum sites of the catalyst. Very small Pt particles were found, with average sizes in the range of 0.6 to 0.8 nm and narrow size distributions. XANES spectra demonstrated the presence of metal-support interactions that affected the electronic structure of the platinum particles.

The catalytic activity of the set of synthesized catalysts was determined in the hydrogenation of a model polycyclic aromatic molecule (1, 2, 3, 4-tetrahydronaphthalene or tetralin). The heat of adsorption of the reactants on the metal sites increased with the average electronegativity of the support and the corresponding decrease of the electron density on platinum. An electronic interaction with the Lewis sites was inferred from these results.

Finally, the catalysts were tested for the hydrogenation of tetralin in the presence of quinoline and/or dibenzothiophene (DBT) as nitrogen and sulfur poisons, respectively.

The rate of hydrogenation of tetralin was reduced by one order of magnitude when quinoline was added to the feedstock. Neither the rate nor the apparent energy of activation calculated for the hydrogenation of tetralin varied with the composition of the catalyst support. Analysis of the spent catalyst showed that most of the nitrogen-containing deposit was located on the acidic support and only a small fraction was retained on the metal. To account for these observations it was proposed that quinoline adsorbs on the metal and in a parallel process the N-poison (quinoline or products of its hydrogenation) neutralizes the acidic sites of the supports. Eventually, this leads to a competitive adsorption of tetralin and quinoline on platinum and to the cancellation of any metal-support interaction. As a result of this process and the decrease in the enthalpy of adsorption, apparent activation energies, $E_{a(exp)}$, for the hydrogenation of tetralin in different supports were fairly uniform and higher than those observed for feedstocks devoid of the N-poison.

The hydrogenation process in the presence of DBT occurred at an even lower rate than in the presence of the nitrogen poison. The rate of the hydrogenation of tetralin was about 2 % of that of the poison-free reaction. In contrast, DBT could be hydrogenated at a higher

rate. This means that the poisoned catalyst was able to activate hydrogen molecules. The FTIR-CO study of the spent catalyst samples showed a nearly completely blockage of platinum, explained by the high affinity of DBT adsorption over Pt. The very small rate of tetralin hydrogenation could be enhanced with an increase in the concentration of the strong Brønsted acid sites in the ASA support. The hydrogenation rate was not affected by the polarity of the support (intermediate electronegativity). A mechanism was suggested to explain the fact that tetralin hydrogenation did occur even when metal sites were blocked by the S-poison. As S-poisoned metal sites exhibited the capacity to activate hydrogen molecules, tetralin must be adsorbed over Brønsted acid sites of the support in the vicinity of the metal particle. This brings together both reactants and enables the reaction to occur.

In this study two types of active sites were identified for the catalytic hydrogenation of aromatics over nanosized platinum particles supported on amorphous silica-alumina: (1) the metal particles and (2) the perimeter of the metal particles where an acid site anchors the aromatic molecule to be subsequently hydrogenated by the hydrogen activated on platinum. The first pathway generates the high catalytic activity of the supported platinum catalysts for the hydrogenation of aromatics. The second reaction pathway is not significant when using clean feeds but becomes the only possible route to hydrogenate the tetralin molecule in the presence of S-poisons. Consequently, an increase in the concentration of anchoring Brønsted acid sites in the vicinity of S-poisoned Pt particles leads to an increase in the catalytic activity.

2 Zusammenfassung

In der vorliegenden Doktorarbeit wurde der Mechanismus der katalytischen Hydrierung von Aromaten in Gegenwart und Abwesenheit von schwefelhaltigen und stickstoffhaltigen Katalysatorgiften an geträgerten Platinkatalysatoren untersucht. Die verwendeten Aluminosilikat-Träger unterschieden sich in ihrem Al/Si-Verhältnis und in ihrer Azidität.

Geplante Umweltauflagen sehen eine strenge Limitierung des Aromatengehalts in Dieselkraftstoffen vor. Der Hydrierungsprozess von aromatischen Kohlenwasserstoffen an geträgerten Edelmetallkatalysatoren (Pt, Pd) scheitert dabei an der hohen Empfindlichkeit gegenüber schwefel- und/oder stickstoffhaltigen Katalysatorgiften. Eine vielversprechende Möglichkeit zur Verbesserung der Katalystorperformance ist die Verwendung von sauren Trägern, die die Beständigkeit von Edelmetallen gegenüber Schwefelvergiftung erhöhen. Der zugehörige katalytische Reaktionsmechanismus, die Rolle von Brønsted und Lewis sauren Zentren und deren optimale Konzentration und Stärke wurden bisher nicht eindeutig beschrieben. Außerdem wurde der Prozeß bisher nicht ausführlich genug in der Anwesenheit von im Dieselkraftstoff vorkommenden basischen, stickstoffhaltigen Komponenten untersucht. Das Ziel dieser Arbeit war es einigen der Unklarheiten auf den Grund zu gehen.

Zur Untersuchung des Trägereinflusses wurde eine Serie von an aziden Aluminosilikaten (ASA) geträgerten Platinkatalysatoren synthetisiert und charakterisiert. Die ASA-Träger unterschieden sich in ihrem Anteil an Siliziumdioxid-, Aluminiumoxid und Aluminosilikatphase. Die Aluminiumoxid- und Aluminosilikatkonzentrationen wurden mit ^{27}Al MAS NMR Spektroskopie quantifiziert. Es konnten bis zu 40% der Aluminiumatome (Pt/ASA (20/80) Katalysator) in die Aluminosilikatphase eingegliedert werden. Mit ^{1}H MAS NMR konnte gezeigt werden, dass nur ein kleiner Teil der AlO_4^- Tetraeder in der Aluminosilikatphase durch Protonen kompensiert wurden und sich so Brønsted saure Zentren (BAS) bildeten. Der Großteil der AlO_4^- Tetraeder wurde wahrscheinlich durch kationische Aluminiumoxidspezies neutralisiert. Lewis saure Zentren (LAS) wurden in den Aluminumoxidclustern gebildet. Die Art und Konzentration der verschiedenen sauren Zentren wurde durch Sorptionsuntersuchungen

mit Pyridin als Probemolekül bestimmt (IR-Spektroskopie und TPD) und mit den ^{1}H MAS NMR Resultaten verglichen. Es wurden schwache und starke LAS identifiziert. Die BAS konnten ebenfalls in schwache und starke BAS unterteilt werden. Schwache BAS treten bei sich gegenseitig beeinflussenden Al-O(H)-Si Zentren in der Aluminosilikatphase auf. Diese aus Hydroxylgruppen bestehenden Cluster werden durch Wasserstoffbrückenbindungen polarisiert. Starke BAS wurden isolierten Al-O(H)-Si Zentren zugeordnet.

Die Platinzentren der Katalysatoren wurden mit H_2- Chemisorption, TEM, EXAFS und Partikelmodellierung charakterisiert. Dabei wurden kleine Platinpartikel mit einer gemittelten Größe im Bereich von 0.6 bis 0.8 nm bei einer engen Größenverteilung identifiziert. Metall-Träger-Wechselwirkungen, die eine verminderte Elektronendichte der Platinpartikel verursachen, konnten durch XANES-Spektren nachgewiesen werden.

Die katalytische Aktivität der synthetisierten Katalysatoren wurde mittels der Hydrierung des polyzyklischen aromatischen Probemoleküls 1, 2, 3, 4-Tetrahydronaphthalin (Tetralin) untersucht. Die Adsorptionswärme der Reaktanden auf den Metallzentren stieg mit der mittleren Elektronegativität des Trägers und der entsprechenden Abnahme der Elektronendichte des Platins an. Die Ergebnisse lassen auch auf eine elektronische Wechselwirkung mit den Lewis sauren Zentren schließen.

Schließlich wurden die Katalysatoren bezüglich der Hydrierung von Tetralin in Anwesenheit von Katalysatorgiften getestet. Dabei dienten Chinolin und/oder Dibenzothiophen (DBT) als stickstoff- bzw. schwefelhaltige Katalysatorgifte. Die Hydrierungsrate von Tetralin wurde durch die Zugabe von Chinolin um eine Größenordnung reduziert. Weder die für die Hydrierung von Tetralin berechnete Rate, noch die scheinbare Aktivierungsenergie variierten in diesem Fall mit der Zusammensetzung des Katalysatorträgers. Die Analyse der Katalysatoren nach der Reaktion zeigte, dass sich der Großteil der stickstoffhaltigen Ablagerungen auf dem aziden Träger befand, und nur ein geringer Anteil auf dem Metall verblieb. Gemäß diesen Beobachtungen wurde vorgeschlagen, dass Chinolin auf dem Metall adsorbiert, und dass das stickstoffhaltige Katalysatorgift (Chinolin oder dessen Hydrierungsprodukte) parallel dazu die aziden Zentren des Trägers neutralisiert. Dies führt schließlich zu einer konkurrierenden Adsorption von Tetralin und Chinolin am Platin und zur Aufhebung

jeglicher Metall-Träger-Wechselwirkungen. Die hier beobachteten nahezu identischen scheinbaren Aktivierungsenergien ($E_{a(exp)}$) ergeben sich als eine Folge der konkurrierenden Adsorption. Aufgrund der Abnahme der Adsorptionsenthalphie ist $E_{a(exp)}$ in diesem Fall höher verglichen zu $E_{a(exp)}$ für die Reaktion in Abwesenheit des stickstoffhaltigen Katalysatorgifts.

In Anwesenheit von DBT wurde eine geringere Hydrierungsrate beobachtet als in Anwesenheit des stickstoffhaltigen Gifts. Die Hydrierungsrate von Tetralin war ungefähr 2 % der Rate der unvergifteten Reaktion. DBT wurde mit einer höheren Rate als Tetralin hydriert. Dies bedeutet, dass der vergiftete Katalysator in der Lage war Wasserstoffmoleküle zu aktivieren. Die FTIR-CO Untersuchungen der Katalysatoren nach der Reaktion offenbarten eine nahezu vollständige Blockierung des Platins, was auf eine hohe Affinität von Platin zu DBT schließen läßt. Die sehr kleine Rate der Tetralinhydrierung konnte durch die Erhöhung der Konzentration von starken Brønsted sauren Zentren des ASA-Trägers gesteigert werden werden. Die Hydrierungsrate wurde durch die Polarität des Trägers (mittlere Elektronegativität) nicht beeinflusst. Folgender Mechanismus beschreibt die Hydrierung von Tetralin, wenn die Metallzentren durch Schwefel blockiert sind. Schwefelvergiftete Metallzentren besitzen weiterhin die Fähigkeit Wasserstoffmoleküle zu aktivieren. Durch die Adsorption von Tetralin an Brønsted sauren Zentren des Trägers in Nähe der Metallpartikel werden die beiden Edukte zueinander gebracht und somit die Reaktion ermöglicht.

In dieser Arbeit wurden zwei Arten von aktiven Zentren für die Hydrierung von Aromaten an Platinnanopartikeln auf amorphen Aluminosilikat-Trägern identifiziert. Es handelt sich hierbei um (1) den Metallpartikel und (2) den unmittelbaren Umkreis des Metallpartikels, wo das aromatische Molekül an einem sauren Zentrum adsorbiert und anschließend durch den am Platin aktivierten Wasserstoff hydriert wird. Der erste Reaktionsweg ist verantwortlich für die hohe katalytische Aktivität der geträgerten Platinkatalysatoren für die Hydrierung von Aromaten. Der zweite Reaktionsweg ist unbedeutend wenn reine Edukte verwendet werden, stellt allerdings die einzig mögliche Route dar, um Tetralin in Gegenwart von schwefelhaltigem Katalysatorgift zu hydrieren. Folglich führt eine Erhöhung der Konzentration von Brønsted sauren Zentren in

unmittelbarer Nähe der schwefelvergifteten Platinpartikel zu einer Erhöhung der katalytischen Aktivität.